2012

Characterization of the Central Cavity of a Potassium Channel: Helix Dipoles, Conformational Plasticity and Inhibition

Disan Schold Davis

CHARACTERIZATION OF THE CENTRAL CAVITY OF A POTASSIUM CHANNEL: HELIX DIPOLES, CONFORMATIONAL PLASTICITY, AND INHIBITION

A Thesis Presented to the Faculty of

The Rockefeller University

in Partial Fulfillment of the Requirements for

the degree of Doctor of Philosophy

by

Disan Schold Davis

June 2012

CHARACTERIZATION OF THE CENTRAL CAVITY OF A POTASSIUM CHANNEL: HELIX DIPOLES, CONFORMATIONAL PLASTICITY, AND INHIBITION

Disan Schold Davis, Ph.D.

The Rockefeller University 2012

Potassium channels are important for regulating the flow of potassium ions across semi-permeable cell membranes in an efficient and selective manner. Potassium channels form a conduction pore comprised of a selectivity filter responsible for the strong preference for potassium, and a water-filled central cavity that contributes to rapid conduction by lowering the energy barrier for potassium ions to cross the low dielectric membrane environment. In the high resolution structure of the potassium channel KcsA, a hydrated potassium ion was observed in the central cavity. It was proposed that some electrostatic stabilization for this potassium ion may come from the backbone of nearby α-helix C-termini, through the helix dipole effect. We studied the role of helix dipoles in KcsA using protein semisynthesis in order to modify the backbone of KcsA and reduce the dipoles of the implicated helix termini. The modified protein was studied by both X-ray crystallography and electrophysiology, demonstrating that the pore helix dipoles may play an important role in potassium conductance. In the course of these experiments, a new conformation for the KcsA cavity was discovered: a phenylalanine (Phe) from each subunit flipped into the center of the

cavity, the cavity ion was no longer observed, and a new non-peptidic density extended into the cavity through lateral openings exposed by the conformational change of the Phe. Subsequent structural studies identified conditions that induce or prevent this conformational change. In particular, mutations were incorporated into KcsA that make the protein less likely to enter the alternative conformation, while not greatly affecting potassium conductance. Crystal structures of KcsA in complex with cavity blocking small molecules revealed that certain inhibitors bind to the cavity in its alternative conformation, and electrophysiology confirmed inhibition by one such molecule in the membrane environment. A sequence alignment between KcsA and several human potassium channels identified a subset of channels where this mode of cavity block may be conserved, including BK and HERG channels. Thus, this new conformation of block could have important implications for the pharmacology of human potassium channels. This work furthers our understanding of electrostatic interactions, structural plasticity, and a new mode of action for a family of inhibitors, within the cavity of KcsA. The study of helix dipoles has relevance for the function of a wide range of proteins, and characterization of conformational-dependent cavity block has particular relevance to some pharmacologically relevant human potassium channels.

To Mom and Dad, for your unwavering love and encouragement

ACKNOWLEDGMENTS

First and foremost, thank you to Dr. Tom Muir for the opportunity to work in such a stimulating lab environment, for sharing with me his enthusiasm for science, and, in particular, for his relentless drive to see this project through. A sincere thank you also to Dr. Rod MacKinnon, for sharing his passion and profound understanding of potassium channels, and for welcoming me into his lab.

Thank you to everyone in both the Muir and MacKinnon labs for their help and support. I have been blessed to have the opportunity to work so closely with two wonderful labs. Special thank you's to Drs. Miquel Vila-Perello, Silvia Frutos, and Peter Moyle for teaching me to become a peptide chemist, and so much more; to Drs. Champak Chatterjee and Steve Lockless for starting me off on my work with KcsA; to Dr. Deena Oren for everything crystallography; to Dr. Beat Fierz for his thorough feedback on this manuscript; to the MacKinnon lab 'crystallography crew' for teaching me X-ray crystallography and making the best of long days in Long Island; to the Muir lab c. 2010 for great memories and support at a much needed time in my graduate work; and to Matt Holt for maintaining a little Muir lab spirit with me at Rockefeller this past year.

Thank you to my Faculty Advisory Committee, Drs. Howard Hang and Brian Crane, for their determination in the success of this project and support along the way. A special thank you also to Dr. Gary Yellen, of Harvard Medical School, for participating as an external examiner for my defense.

Thank you to the TPCB Program and to Rockefeller University, with a special thank you to the RU Dean's Office.

This work would never have been completed without the tremendous support of my parents, my close family and friends, and my loving boyfriend. I extend my warmest gratitude and love to all of them.

TABLE OF CONTENTS

LIST OF FIGURES

Chapter 5

LIST OF TABLES

LIST OF ABBREVIATIONS

ATP, adenosine triphosphate
Ba^{2+}, barium ion
CBD, chitin binding domain
Cs^{+}, cesium ion
CD, circular dichroism
CHAPS, 3-[(3-cholamidopropyl)dimethylammonio]-1-propanesulfonate
Co^{2+}, cobalt ion
DM, n-decylmaltoside
DTT, dithiothreitol
ELISA, enzyme-linked immunosorbent assay
EM, electron microscopy
EPL, expressed protein ligation
ESI, electrospray ionization
FAB, fragment antigen binding
GST, glutathione-S-transferase
HEPES, 2-[4-(2-hydroxyethyl)piperazin-1-yl]ethanesulfonic acid
IR, infrared spectroscopy
ITC, isothermal calorimetry
K^{+}, potassium ion
K2P, two-pore potassium channel
KCl, potassium chloride
K_{ir}, inward rectifier potassium channel
K_{v}, voltage-gated potassium channel
MALDI, matrix-assisted laser desorption/ionization
MES, 2-(N-morpholino)ethanesulfonic acid
MESNA, 2-mercaptoethanesulfonic acid
Na^{+}, sodium ion
NaCl, sodium chloride
NCL, native chemical ligation
NH_4^{+}, ammonium ion
NMR, nuclear magnetic resonance
PAGE, polyacrylamide gel electrophoresis
PBS, phosphate buffered saline
PDB, protein data bank
PE, phosphatidylethanolamine
PG, phosphatidylglycerol
POPA, 1-palmitoyl-2-oleoyl phosphatidic acid
POPC, 1-palmitoyl-2-oleoyl-sn-glycero-3-phosphatidylcholine
POPE, 1-palmitoyl-2-oleoyl-sn-glycero-3-phosphatidylethanolamine
POPG, 1-palmitoyl-2-oleoyl-sn-phosphatidylglycerol
PPA, dioctanoyl glycerol pyrophosphatidic acid
QA, quaternary ammonium
Rb^{+}, rubidium ion

RP-HPLC, reverse phase high performance liquid chromatography
RT, room temperature
SEC, size exclusion chromatography
SPPS, solid phase peptide synthesis
SDS, sodium dodecyl sulfate
TAA, tetraalkylammonium
TBA, tetrabutylammonium
TCEP, tris(2-carboxyethyl)phosphine
TEA, tetraethylammonium
TFA, trifluoroacetic acid
TFE, trifluoroethanol
THA, tetrahexylammonium
Tl^+, thallium ion
TMA, tetramethylammonium
TOA, tetraoctylammonium
TPA, tetrapentylammonium
TPrA, tetrapropylammonium
Tris, 2-amino-2-hydroxymethyl-propane-1,3-diol
VSD, voltage sensor domain
WT, wild-type

CHAPTER 1: INTRODUCTION

A semipermeable hydrophobic barrier defines the boundary of every cell. This barrier is formed by a bilayer of lipid molecules, known as the cell membrane. The middle of the membrane is oily and prohibits the exchange of charged ions and molecules between the cell and its environment. Embedded in the membrane are proteins that facilitate the transfer of ions, molecules, and other indirect signals from one side to the other. Together, these components of the cell membrane provide protective and regulatory functions that facilitate cell survival and proliferation.

Cell membranes are important for regulating the inherent gradient between the dense biological matter in the cytoplasm and the surrounding extracellular environment. Most cells maintain gradients of the common signaling ions—sodium, potassium, calcium, and chloride—in order to regulate cellular homeostasis. This results in a negatively charged environment in the cell and an electrical potential across the cell membrane. The net electrical potential and the concentration gradient of a particular ion combine to create an electrochemical gradient for each ion. These gradients form the driving force for inter- and intra-cellular communication in many types of cells. The most well studied system is the electrical activity of neurons that allow for complex and efficient transmission of information.

The seminal work of Hodgkin and Huxley began to expose the molecular basis of neural signaling by looking at discrete electrical pulses known as action potentials that are responsible for the function of most neurons (Hodgkin and

Huxley, 1952a; 1952b; 1952c; Hodgkin et al., 1952). An action potential is initiated by a strong, transient flood of sodium (Na^+) into the cell to depolarize the membrane potential, followed by a rapid release of potassium (K^+) to the environment to repolarize the membrane and again build up negative charge inside the cell. This work led to the first characterization of proteins that can allow a specific ion, such as K^+, to cross the membrane while excluding all others, such as Na^+.

Membrane-embedded proteins are responsible for regulating and facilitating the movement of these (and other) charged species across membranes by stabilizing their transition through the low dielectric membrane environment. The passive movement of ions along their electrochemical gradients is facilitated by transmembrane channels. Active transport of ions is also needed to maintain the cell potential and is accomplished by moving ions against their electrochemical gradients using cellular energy (such as adenosine triphosphate (ATP)) or by coupling this process to the energetically favorable diffusion of another ion. Channels and transporters can be opened and closed by a variety of signals including changes in membrane potential and the concentrations of other ions. Thus, channels and transporters create favorable environments for ions to cross the membrane in specific, regulated ways.

My work focuses on the bacterial potassium channel, KcsA. To preface my work, I will introduce potassium channels in the context of some important functional studies, followed by advances achieved through high resolution structural information. I will also introduce protein chemistry as a powerful tool for

modifying proteins in specific ways. Together, electrophysiology, structural biology, and protein chemistry have provided the tools for me to study a component of KcsA conduction, to characterize a new conformation of KcsA, and to look at some of the implications of this work for potassium channels more broadly.

1.1 Features of Potassium Channels

Functionally, potassium channels are a set of transmembrane proteins that exhibit exquisite sensitivity for potassium over other relevant cations. Early identification of potassium channel genes revealed a highly conserved sequence of amino acids—the signature sequence TVGYG—that was demonstrated to play a role in potassium selectivity and conduction (Heginbotham et al., 1992; 1994). Alignments and hydrophobicity plots of potassium channel genes suggested that all of the proteins in this family share a core domain with two predicted transmembrane segments and a shorter reentrant loop containing the signature sequence (Figure 1.1). Most potassium channels assemble as homotetramers. Initial studies on channel assembly demonstrated tetramerization through mixtures of channel subunits that were sensitive or insensitive to block, where the fraction of block was correlated with the probability of a channel containing a sensitive subunit (MacKinnon, 1991). Subsequent studies confirmed this with other potassium channels using a variety of methods including mass tagging and cross-linking (Cortes and Perozo, 1997; Heginbotham et al., 1997).

Through these and several other biochemistry and electrophysiology

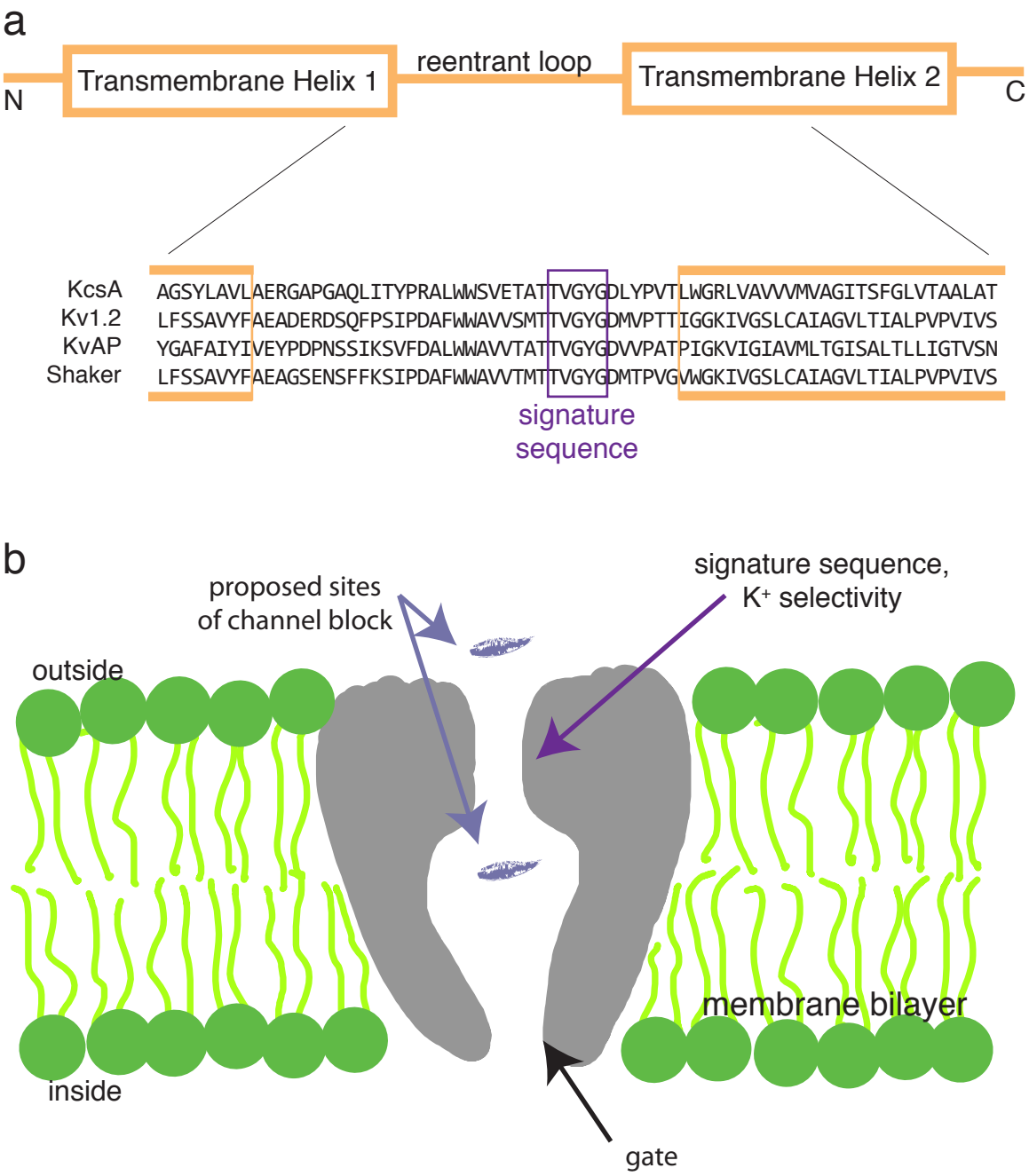

Figure 1.1: Sequence and structural features of potassium channels. (a) Alignment of a few notable potassium channel sequences, with predicted hydrophobic α-helical segments designated by the bars below the sequences and the signature sequence marked by a box. (b) Schematic of a potassium channel (gray) based on initial biochemical and electrophysiology data. The protein is shown as a cross section through the membrane (green) and the middle of the channel, to highlight the conduction pore. The proposed region imparting potassium selectivity (purple) and the channel gate (black) are marked. Areas proposed to be susceptible to channel block are marked in blue.

experiments, scientists established a very compelling model for the general potassium channel architecture, prior to obtaining any structural information. Potassium ions traverse the membrane along the fourfold axis of the tetramer. From the intracellular side, the ion must first past through the open channel gate into a wide cavity before entering a narrow potassium-selective pore in the outer leaflet of the membrane and final release into the extracellular solution (Figure 1.1).

1.1.1 Potassium Channel Gating

On the most basic level, a channel contains a pore for conducting ions across the membrane and a gate to regulate when the ions have access to the pore. All potassium channels contain a gate; however, the means of regulating this gate vary widely between different proteins. Some channels respond to primarily one signal, while others integrate several components into a complex network that affects channel opening. These activities correspond to the function of the channels and allow for precisely executed gating in complex environments.

The broadest families of potassium channels consist of two groups differentiated by their topology and gating properties: channels that are voltage gated and others that respond to a variety of ligands (Miller, 2000; Hille, 2001). Many proteins in the voltage-sensing family are also regulated by ligands. Ligand-gated channels can respond to G-proteins, specific lipids, intracellular ion concentration, and other small molecules. Ligands often interact with soluble regulatory domains that assemble on the intracellular face of the membrane

protein (Choe and Roosild, 2002; Dart, 2010; Luescher and Slesinger, 2010). Members of the ligand-gated inward rectifier (K_{ir}) family of proteins consist of the transmembrane pore domain, constructed from subunits with two transmembrane-spanning helices, as well as intracellular regulatory domains (Bichet et al., 2003). One type of ligand-gated channel exists as dimers of concatenated dimers and is referred to as the two-pore (K2P) channel (Enyedi and Czirják, 2010).

Voltage gated channel (K_v) subunits contain six transmembrane segments: four helices that make up the voltage sensing domain (VSD) followed by the two helices of the conserved pore domain (Yellen, 2002). The mechanism of voltage gating is still being studied, but we do know that the VSD responds to changes in membrane potential through movement in the membrane, largely guided by a series of positively charged arginine residues (Bezanilla and Armstrong, 1974; Jiang et al., 2003a; 2003b; Long et al., 2007; Tao et al., 2010)). Many channels in this family integrate voltage sensing and ligand sensitivity to produce highly tunable channels (Yellen, 2002).

Early studies of potassium channels suggested that the physical gate to the channel sits on the intracellular side of the membrane. The most convincing studies applied blocking molecules to the intracellular side of the membrane and observed inhibition of K^+ current only when the channels were in the open state (Armstrong and Hille, 1972; Liu et al., 1997). These experiments will be discussed in more detail in Section 1.1.3.

1.1.2 Potassium Channel Selectivity

All potassium channels have a similar trend for the selectivity of various cations. Most notably, these proteins are over 1,000-fold selective for potassium over sodium and no conductance of pure Na^+ or Li^+ can be measured. Larger monovalent cations are conducted similarly to potassium, including rubidium (Rb^+), Thallium (Tl^+), and ammonium (NH_4^+), while cesium (Cs^+) conducts about two orders of magnitude more slowly (Heginbotham and MacKinnon, 1993). This trend in selectivity, usually stated as K^+, $Rb^+ > Cs^+ >> Na^+$, is often used to identify a protein in the potassium channel family (Hille, 2001).

Potassium selectivity has long been proposed to arise from a narrow region of the conduction pore (Hodgkin and Keynes, 1955). It was suggested that potassium ions could be coordinated by protein oxygen atoms in this narrow channel, as if to mimic the K^+ hydration shell using a mechanism similar to known ionophores (Mullins, 1959; Hille, 1973; Eisenman and Dani, 1987).

Electrophysiology studies provided initial evidence for a “long pore” channel, where multiple ions must interact in the pore in a cooperative fashion for optimal conductance. Several experiments helped to form this model: the nonlinear dependence between the potassium concentration gradient and ion flux; careful analysis of block by monovalent cations; and the potassium concentration dependence for relieving block, among other studies (Hodgkin and Keynes, 1955; French and Adelman, 1976; Hagiwara et al., 1977; Yellen, 1984a; 1984b; Schumaker and MacKinnon, 1990). This interaction between potassium ions in the pore is referred to as “coupling,” where the conductance of one ion will

be enhanced by the presence of nearby potassium ions moving in the same direction.

Cloning and mutagenesis techniques initiated the identification of residues important for selectivity or that border this narrow pore. These experiments revealed that the narrow potassium-selective region consists of a short peptide that includes the potassium channel signature sequence (MacKinnon and Yellen, 1990; Yellen et al., 1991; Heginbotham et al., 1994).

1.1.3 Potassium Channel Block

Consistent with the hypothesis of a narrow pore, molecules much larger than a dehydrated potassium ion are prohibited from crossing the membrane through this pore. Some molecules close in size to K^+ could enter the conduction pathway and get stuck—or block—the narrow pore. For example, barium, Ba^{2+}, is only slightly larger than K^+ but its greater charge makes it an efficient blocker of potassium channels (Armstrong and Taylor, 1980; Neyton and Miller, 1988a; 1988b; Zhou et al., 1996; Vergara et al., 1999). Small molecule and peptide toxins isolated from venomous animals have also been very useful tools for studying the architecture, conduction properties, and physiology of various potassium channels because of their high specificity for particular channel types (Hille, 2001). Because of its relevance to the work in this thesis, the review of other blocking molecules will focus specifically on the quaternary ammonium (QA) ion class of inhibitors.

QA ions were discovered during early work on neural signaling, where tetraethylammonium (TEA) was an effective blocker of potassium current in the squid giant axon (Tasaki and Hagiwara, 1957; Armstrong and Binstock, 1965). QA ions inhibit all potassium channels that have been tested, suggesting that they interact with a conserved feature of potassium channel structures (French and Shoukimas, 1981; Swenson, 1981; MacKinnon and Yellen, 1990). These ions played important roles in characterizing the physiology and general architecture of potassium channels.

QA ions consist of a quaternary substituted amine, holding a formal positive charge, and decorated with four alkyl substituents. These inhibitors are more effective at inhibiting potassium channels from the intracellular side of the membrane (Armstrong and Hille, 1972); however, millimolar concentrations of some QAs can block from the extracellular side in certain channels (MacKinnon and Yellen, 1990). For intracellular inhibition, these ions can only block channels in the open state (Armstrong, 1966; 1969). Relief of block is enhanced by hyperpolarization or a high concentration of extracellular potassium, suggesting that these molecules bind to a space along the ion conducting pathway that is competitive with potassium (Armstrong, 1971; French and Wells, 1977).

Intracellular inhibition has been particularly important for studying the character of the potassium conducting pathway between the gate and the narrower selectivity filter. QAs with longer alkyl chains or optimally spaced benzene rings were superior inhibitors with stronger binding affinities and slower off-rates than TEA (Armstrong, 1971; Swenson, 1981). A few mutations on the

inner helix of the cavity more strongly affect the inhibition of larger, hydrophobic blockers (Choi et al., 1993). In contrast, a mutation near the signature sequence reduced TEA affinity such that shorter alkyl chain inhibitors are more strongly affected (Yellen et al., 1991). These observations suggest that QA ions can make interactions both near the selectivity filter and in the surrounding hydrophobic cavity.

Careful study of the interaction between blocking molecules and potassium channels also provided information on the overall architecture of the conduction pore (Figure 1b). The portion in the inner leaflet includes the channel gate, and can open to allow blocking molecules access to a wide cavity between the gate and the narrow, potassium-selective pore (Bezanilla and Armstrong, 1972; Armstrong, 1975). Specific interactions in the cavity account for the strong inhibition by QA ions (Choi et al., 1993; del Camino et al., 2000). Asymmetric, lower affinity block from the extracellular side of the membrane was consistent with the narrow pore opening directly to the extracellular solution (MacKinnon and Yellen, 1990). Additionally, the distance between mutations that affect intracellular or extracellular QA ion block is only 8 residues, leading to hypotheses that the potassium selective region could be a short, extended peptide (Guy and Seetharamulu, 1986; Yellen et al., 1989). These experiments produced a remarkably accurate model for potassium channels that can only be fully appreciated in light of more recent high resolution structures.

1.2 Potassium Channel Structure

Electrophysiology, biochemistry, and genetics provided an impressively detailed picture of the function and structural organization of potassium channels; however, the introduction of structural biology has provided a surge in our understanding of the atomic level interactions essential for their activity. Electron microscopy (EM), nuclear magnetic resonance (NMR), and X-ray crystallography have all been useful tools for studying membrane protein structure (Minor, 2007; McDermott, 2009; Raunser and Walz, 2009; Patching, 2011). While X-ray crystallography was first successfully applied to soluble biological macromolecules, membrane proteins have become common crystallography targets through advances in techniques for identifying promising candidates, working with these proteins in detergent, and optimizing crystallization conditions for membrane proteins (Minor, 2007; Hunte and Richers, 2008).

1.2.1 The First Potassium Channel Structures

The first crystal structure of a potassium channel was of the stable, pore forming domain of a bacterial protein homologous to the rest of the potassium channel family. This protein, KcsA, came from *Streptomyces lividans*, and was identified through the highly conserved signature sequence (Schrempf et al., 1995). KcsA shows similar potassium selectivity and toxin block (MacKinnon et al., 1998) to other potassium channels; however, the protein requires intracellular acidification for activation (Cuello et al., 1998; Heginbotham et al., 1999; Meuser et al., 1999). A comprehensive set of electrophysiology experiments confirmed

that KcsA behaves like known eukaryotic potassium channels (LeMasurier et al., 2001).

The initial X-ray crystal structure, to 3.2 Å, provided the first view of the potassium channel architecture and the mechanism of potassium selectivity (Figure 1.2) (Doyle et al., 1998). The structure was achieved in part by using a truncated form of the protein, consisting of only the stable transmembrane core. As predicted, the potassium conduction pathway is formed at the intersection of four identical subunits. Looking from the side, the protein forms an ice-cream-cone shape assembled from the two transmembrane helices of each subunit. The narrow opening at the intracellular side of the membrane is likely too small for hydrated K^+ to move through, so this is proposed to be the closed state of the channel.

Between the transmembrane helices of each subunit, there is a reentrant loop coming from the outer leaflet of the membrane. It comprises an α-helix pointing into the pore followed by an extended loop back to the extracellular surface. Potassium selectivity arises through this extended loop, named the selectivity filter. This region includes the signature sequence and forms a narrow channel for binding potassium ions, just as predicted (Hodgkin and Keynes, 1955). The helices behind the selectivity filter—named the pore helices—are positioned with their C-termini angled so that vectors running along the length of the helices would intersect at a potassium ion in the middle of a widened cavity through the inner membrane leaflet. The second—or inner—transmembrane helix contains hydrophobic residues that line this water-filled cavity. Thus,

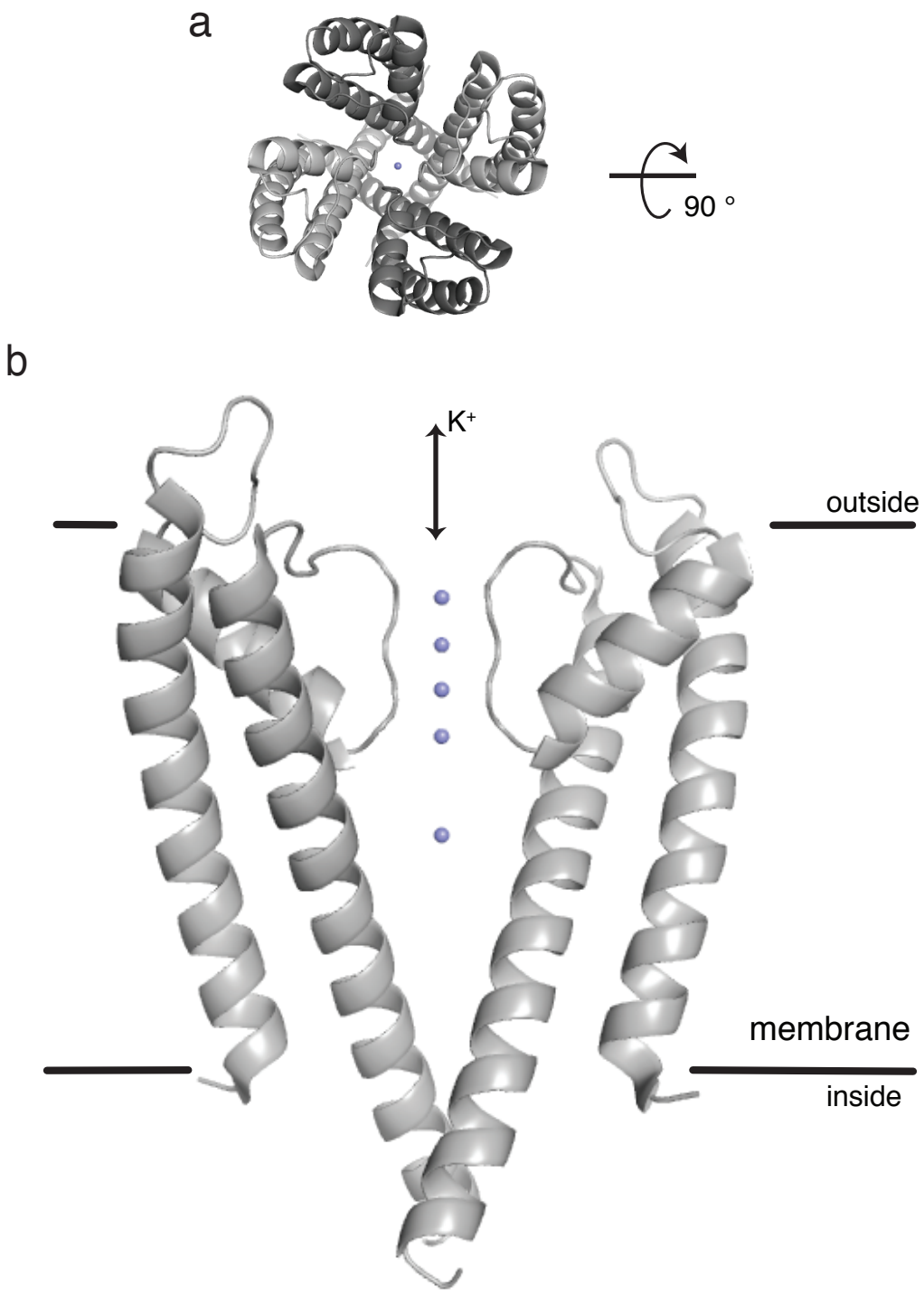

Figure 1.2: High resolution structure of KcsA (1k4c). (a) Tetrameric channel shown from the plane of the membrane from the extracellular side. The subunits are colored in alternating dark and light gray with a blue potassium ion in the center. (b) A 90 ° rotation and removal of the dark gray subunits shows the side-view of the channel and the length of the conduction pore. The approximate membrane boundaries are marked.

electrostatic charge to stabilize the cavity ion was proposed to come from the carbonyls of the pore helices through the helix dipole effect (Doyle et al., 1998; Roux and MacKinnon, 1999).

A subsequent structure to 2.0 Å provided atomic-level resolution of the channel (Zhou et al., 2001b). This high resolution structure was achieved by raising antibodies to the tetrameric channel and isolating the fragment of antigen binding (FAB). The FAB was specific to the extracellular loops of KcsA and aided in crystallization by providing the lattice contacts in the high resolution crystals, thus leaving the protein and its detergent micelle largely unperturbed.

This complex produced complementary structures in both high- and low-potassium conditions, elucidating a precise role for potassium in ion conduction (Figure 1.3). There are four potassium ion binding sites formed by oxygen atoms from the protein, with each site mimicking the octahedral hydration shell of a potassium ion (Figure 1.3b). These sites have been named S1 through S4, starting from the extracellular side. S1 through S3 are formed only from backbone carbonyl oxygens, but S4 is formed by carbonyls as well as a threonine sidechain hydroxyl from each subunit. Potassium ions were proposed to move through the filter in a mostly dehydrated state, but with potassium ions being conducted alternately with water molecules. Thus at any given time, two of the observed binding sites will be occupied (S1 and S3, or S2 and S4). Without sufficient potassium, the selectivity filter of the channel collapses into a conformation that closes the conduction pore (Figure 1.3c). Because the conductive conformation can only be accessed in the presence of potassium, the

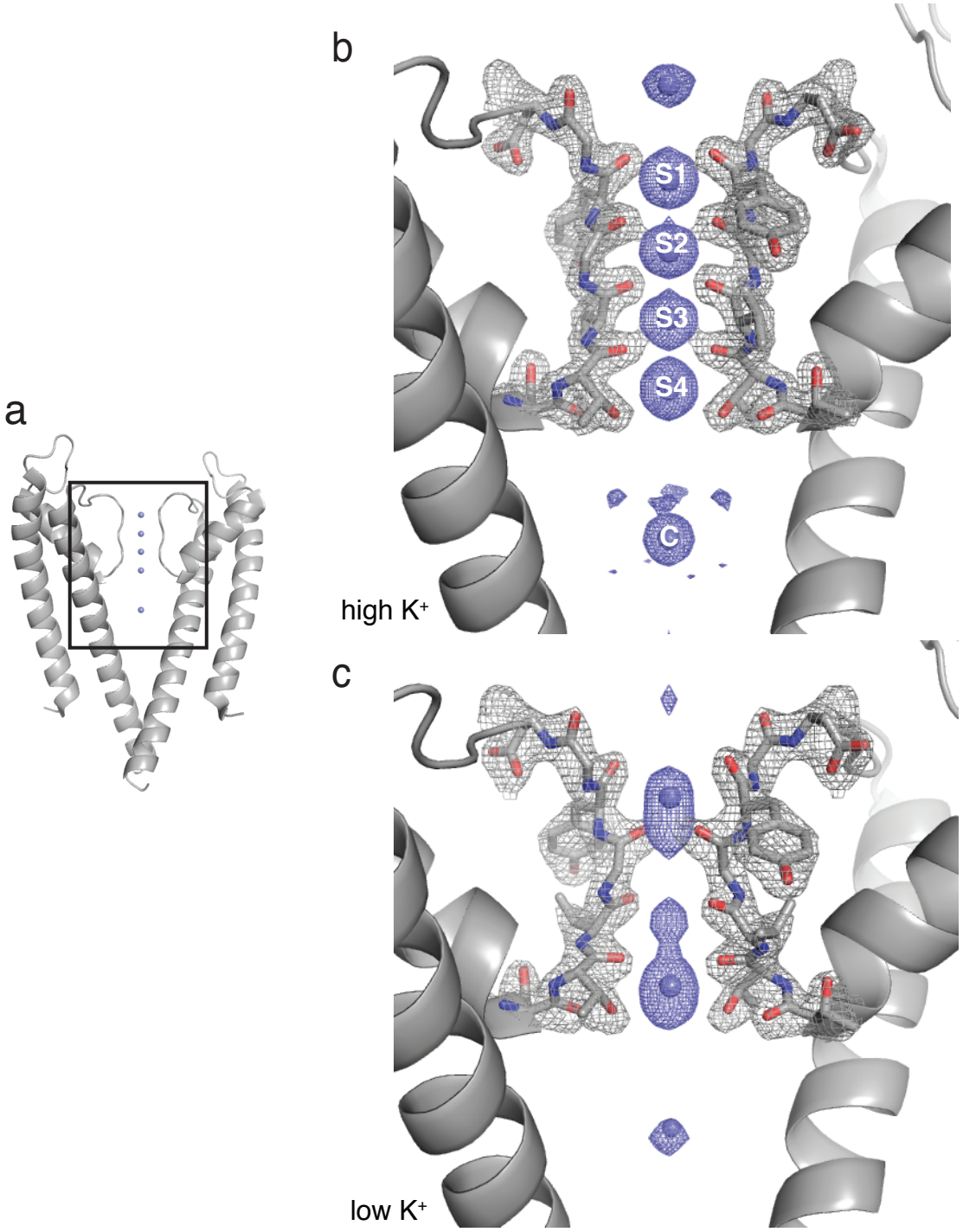

Figure 1.3: Structures of the KcsA selectivity filter and cavity. (a) The close-up region of the selectivity filter is defined. (b) The high potassium KcsA (1k4c) structure. The selectivity filter ions are labeled S1-S4 and the cavity ion is marked with a C. The ordered water shell is somewhat visible around C at this contour level. (c) The low potassium (1k4d) structure. The pore region is shown with the selectivity filter residues drawn in stick and colored by atom and the potassium ions shown in blue. $2F_o$-F_c density maps for the protein are shown in gray at 2 σ and F_o-F_c omit maps for the ions are shown in blue at 5 σ.

protein is able to be strongly selective for potassium over other ions (Morais-Cabral et al., 2001).

In this structure, an ordered lipid molecule was observed between subunits in the intracellular leaflet. Subsequent work identified this lipid as phosphatidylglycerol (PG) (Valiyaveetil et al., 2002b). This high resolution structure also showed an octahedral hydration shell around the cavity potassium ion (Zhou et al., 2001b). The backbone carbonyls and a threonine hydroxyl in the selectivity filter mimic the arrangement of the hydration shell. It is interesting to consider that the nearby electrostatic interactions and cavity geometry must be optimized for potassium in order to produce the precisely ordered hydration shell that is observable by X-ray crystallography.

1.2.2 Electrostatics and Dynamics of KcsA

With a high resolution structure of a potassium channel available, several groups set out to study the mechanisms by which KcsA (or membrane proteins in general) can stabilize cations as they move through the low dielectric membrane environment. Initial electrostatic calculations demonstrated stabilization of potassium ions by the carbonyl and hydroxyl oxygens in the selectivity filter. From these calculations, the helix dipoles were estimated to contribute significantly to ion stabilization in the cavity (Chung et al., 1999; Roux and MacKinnon, 1999). A more comprehensive review of helix dipoles will be presented in Chapter 2.

Additional studies used computational methods to explore the details of potassium conductance, stability, and selectivity; protonation of acidic residues behind the filter; and binding of other small molecules such as QA ions in KcsA (Allen et al., 1999; Aqvist and Luzhkov, 2000; Bernèche and Roux, 2001; Luzhkov and Aqvist, 2001; Mashl et al., 2001; Ranatunga et al., 2001; Noskov et al., 2004; Faraldo-Gómez et al., 2007; Jensen et al., 2010). Crystal structures have provided highly informative, static views of potassium channels; however, computational techniques have used this information to explore a variety of questions beyond the scope of the structures themselves, including the study of mechanisms of conduction or gating, or the modeling of a protein ortholog to study other types of potassium channels (Sansom et al., 2002; Roux, 2005).

1.2.3 Related Protein Structures

Crystallization of KcsA in the presence of the FAB is robust and has allowed for a variety of potassium channel features to be examined crystallographically. Barium block was observed structurally in KcsA, where Ba^{+} binds in the most intracellular ion binding site of the selectivity filter (S4) (Jiang and MacKinnon, 2000). Conducting cations with slightly larger atomic radii (Rb^{+} and Cs^{+}) were observed with only three ions in the selectivity filter rather than four, suggesting that their lower conduction rates may be due in part to a mechanism for conductance without ion coupling (Zhou and MacKinnon, 2003).

Several structures have looked specifically at the central cavity. KcsA was crystallized in the presence of tetrabutylammonium (TBA), showing that the ion

binds in the center of the cavity, replacing the cavity potassium ion, but causing no other structural changes to the protein (Figure 1.4). The four alkyl chains of TBA extend laterally toward each of the four subunits, but other structural arrangements may not be observed due to fourfold averaging in the protein structure (Zhou et al., 2001a; Faraldo-Gómez et al., 2007; Yohannan et al., 2007). Competition between Na^+ and Tl^+, as a K^+ surrogate, suggests that the cavity ion binding site has 5-fold selectivity for K^+ over Na^+ (Zhou and MacKinnon, 2004). Various ions also bind differently in the cavity: conducting ions (K^+, Rb^+, and Tl^+) all showed similar binding, while Na^+ showed weaker binding, and Cs^+ showed binding in two positions, with one quite close to the intracellular mouth of the filter (Zhou and MacKinnon, 2004).

Mutation of threonine 75 in KcsA was used to explore the role of its sidechain hydroxyl in potassium ion coordination at site S4 in the selectivity filter. Upon mutation of the Thr75 to cysteine, occupancy of the S4 binding site was significantly reduced along with some reduction of occupancy in the second position (S2). Correspondingly, conduction of this mutant channel was reduced; however, conduction and ion binding for Rb^+, which may not follow the coupled conduction mechanism, was not similarly affected. These findings support the model that potassium ions are coupled while moving through the channel pore (Zhou and al, 2004). Related experiments have been performed using chemically modified channels and will be discussed after an introduction to the semisynthesis of those proteins in Section 1.3.

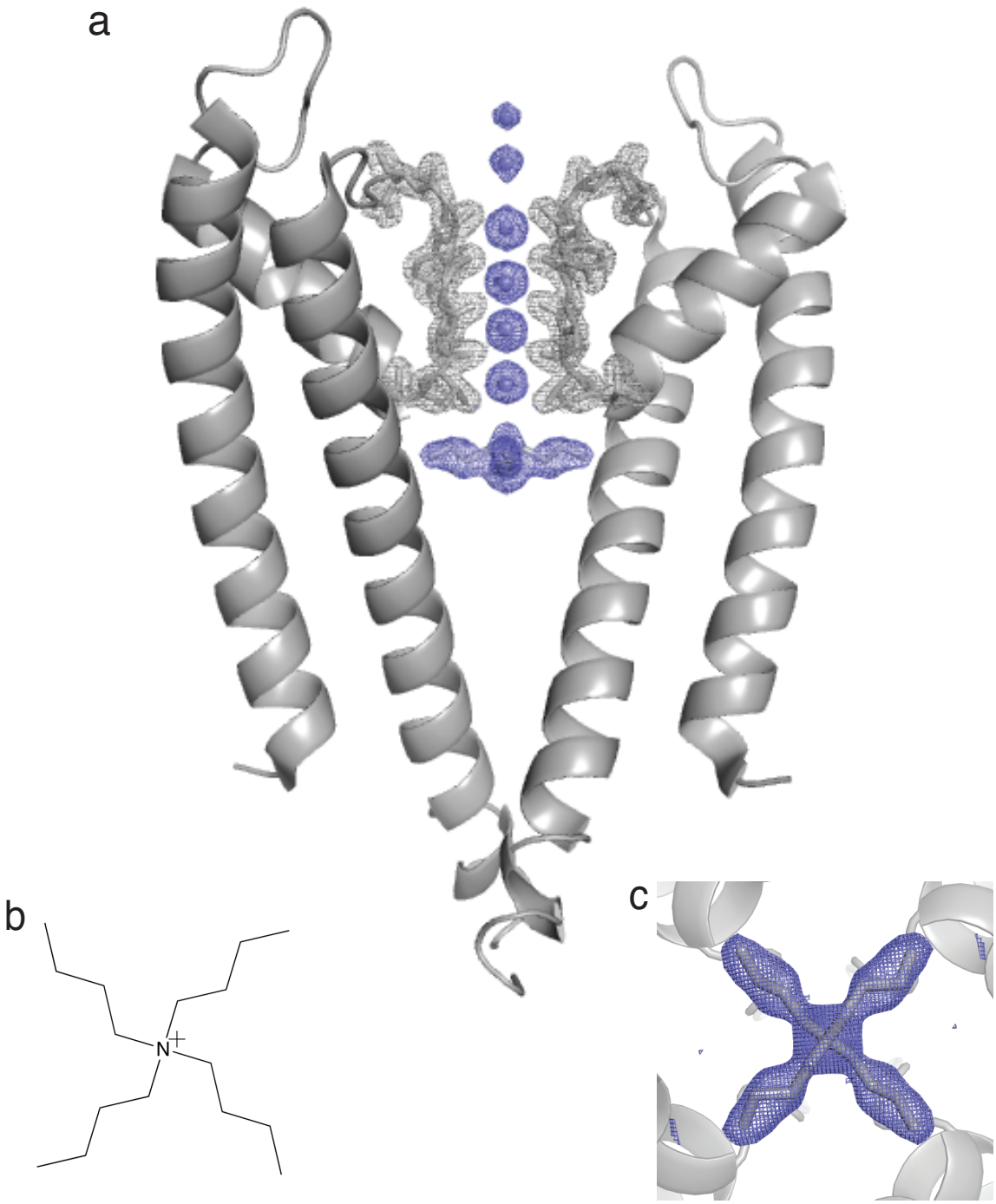

Figure 1.4: Structure of KcsA with TBA in the central cavity (2hvk). (a) Two subunits with TBA are shown. The selectivity filter is shown in stick, with a $2F_o$-F_c density map shown in gray at 2σ. The K^+ ions are shown in blue and TBA is shown in gray sticks in the central cavity. The blue density is from an F_o-F_c omit map, with the ions contoured at 5σ, and the TBA density contoured at 2σ. (b) The chemical structure of TBA. (c) The TBA molecule in the cavity, viewed from the bottom of the conduction pore (all coloring and density contours are the same as in panel (a)).

All of these initial KcsA structures were of the truncated pore domain of the channel with a closed intracellular gate. Subsequent structures were determined for the full-length KcsA channel as well as for the related channel MthK with an open gate (Figure 1.5). The full-length channel structures confirm that the intracellular domain of KcsA forms a four helix bundle that may be involved in channel regulation, allowing the channel to be activated in circumstances other than low pH, which is unlikely to be the physiological activator (Cortes et al., 2001; Uysal et al., 2009). The crystal structure of the open MthK channel provided a model for channel opening, where the transmembrane helices hinge at a glycine residue in the inner helices to allow the helices to splay apart and expose the central cavity to the intracellular solution (Jiang et al., 2002b). Subsequently, the cation channel NaK was crystallized in both open and closed conformations (Shi et al., 2006; Alam and Jiang, 2009a; 2009b). Additional experiments have been performed to visualize the open conformation of KcsA, but an open, conductive conformation has not yet been realized (Uysal et al., 2009; Cuello et al., 2010b; 2010c).

These crystal structures of KcsA have allowed us to understand potassium channel structure and function to a new level of detail. KcsA crystallography has also paved the way for structural studies of other potassium channels, channels of other types, and other transmembrane proteins such as transporters and receptors (Tate, 2001).

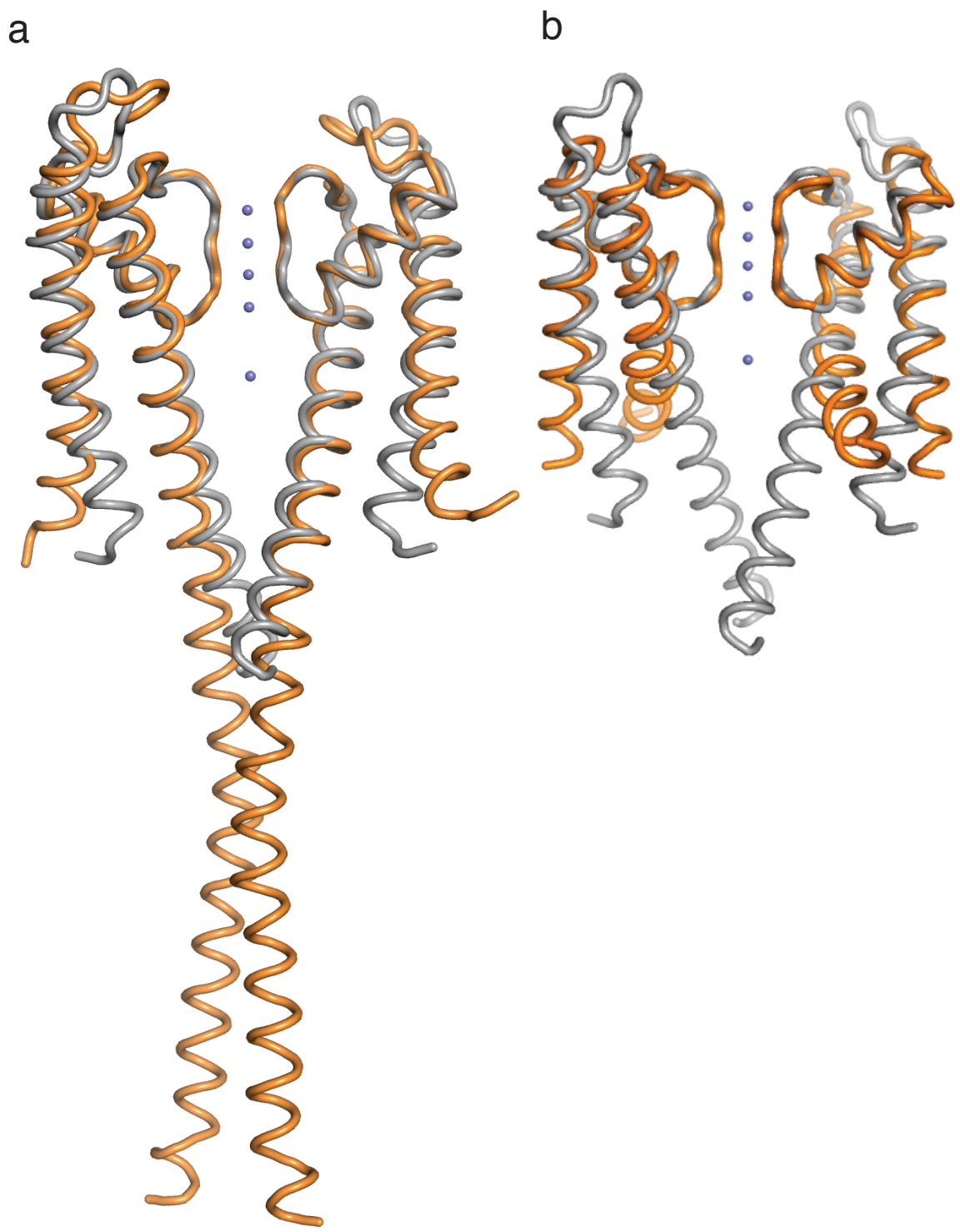

Figure 1.5: Structures of full-length KcsA and a related channel in the open conformation. (a) The high resolution structure of KcsA (1k4c, shown in gray) is overlayed with the structure of full-length KcsA (3eff, orange). (b) The high resolution structure (1k4c, gray) is overlayed with the open structure of MthK (1lnq, orange). Potassium ions from the 1k4c structure are shown in blue for reference.

1.2.4 Recent Structures with New Information on the Central Cavity

While a comprehensive discussion of the discoveries made on ion channels using structural biology is beyond the scope of this work, a few recent structures will be mentioned for their relevance to the potassium channel cavity and the research that will be presented. The structures are of the first putative voltage gated sodium channel, NavAb, and the first two-pore (K2P) potassium channels, TRAAK and TWIK-1 (Figure 1.6). Each of these structures shows a new non-peptidic density in the cavity of the channel, intruding from the surrounding lipid environment into the cavity through lateral openings in the peptide wall. NavAb shows density that extends between the center of the cavity and the outer walls in all four directions (Payandeh et al., 2011). Since the K2Ps are dimeric channels, the new density in these channels is also dimeric, extending through the lateral openings between the dimer interfaces (Brohawn et al., 2012; Miller and Long, 2012). In NavAb and TWIK-1, these densities are proposed to be occupied by alkyl chains from the lipid environment. It is even suggested that these openings could be places where small hydrophobic molecules could enter the cavity (Zamponi et al., 1993; Payandeh et al., 2011). Finally, these structures also have in common an aromatic residue (phenylalanine or tyrosine) nearby that may control access to the lateral openings.

These particular examples highlight the importance of structural biology to understanding the complex interactions between protein structure and function—

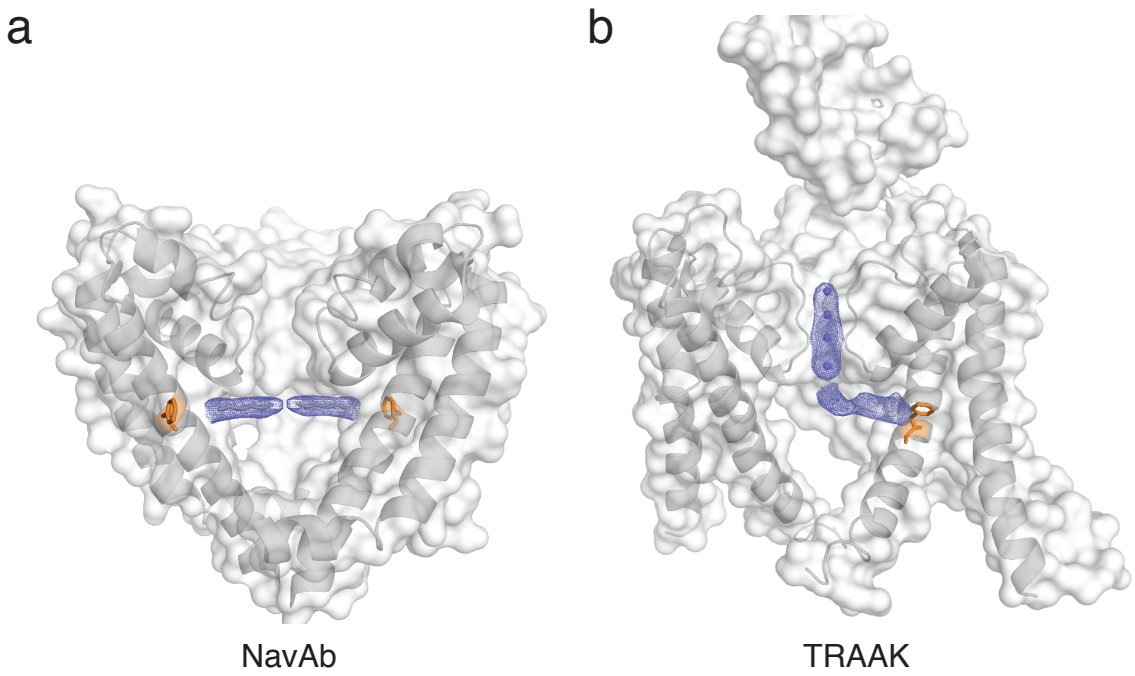

Figure 1.6: Examples of structures with non-peptidic density in the cavity. These structures are shown as a surface with the front subunit removed. Two opposing subunits are shown in cartoon. F_o-F_c omit maps for the ions are shown in blue at 5 σ and for the cavity density at 2 σ. An aromatic residue hypothesized to interact with the modeled density is shown in each structure in orange. (a) NavAb (3rvy), showing the density corresponding with the two opposing subunits shown. (b) TRAAK (3um7), showing the asymmetric density in only its strongest direction.

and in such cases they provide new information and perspectives for studying potassium channels.

1.3 Chemical Biology Tools for Studying Potassium Channels

Chemistry provides powerful tools for dissecting and understanding biology through the manipulation of biological molecules or the addition of new chemical functionality to manipulate biological systems in subtle ways. Such tools are also useful across the growing field of neurobiology (Dougherty, 2008; Ahern and Kobertz, 2009; Focke and Valiyaveetil, 2010; Grosse et al., 2011). The roles of small molecules—including pharmacological agents, endocannabinoids, and neuropeptides—have been influenced heavily by chemical modifications including the addition of reactive groups orthogonal to the biology of the cell (Trauner, 2008). The use of light has been particularly transformative for neurobiology, from the use of voltage or light sensitive small molecules to photo-emitting or photo-activatible proteins (Knopfel et al., 2006; Fehrentz et al., 2011; Miesenböck, 2011).

Proteins have been fascinating molecules to chemists. They are polymers of precise sequences of 20 amino acid building blocks, connected to each other through amide bonds, that can fold into complex and dynamic three-dimensional structures with a wide array of functions. Traditionally, protein function has been studied through amino acid mutagenesis, replacing an amino acid with one of the other 19 to see how this affects function; however, this technique is limited to the scope of the natural amino acids and lacks finer variations in side chain

functionality or variations in backbone electrostatics and conformational properties. To circumvent these limitations, chemists have created several novel tools for studying and modifying proteins of interest. These techniques include the introduction of modifications during ribosomal protein synthesis—nonsense suppression—and the chemical synthesis of modified protein molecules—protein semisynthesis. Both have proven to be very powerful techniques and have made contributions to our understanding of potassium channels and other membrane proteins.

1.3.1 Nonsense Suppression

Nonsense suppression uses the native biological machinery to incorporate modified or novel amino acids into proteins in living cells.

1.3.1.1 Nonsense Suppression Methodology

Several chemical biologists, led by Dr. Peter Schultz, have set out to hijack the protein synthesis machinery to incorporate additional, unnatural amino acids (Wang and Schultz, 2005). From their work, tRNAs and aminoacyl tRNA synthetases that are orthogonal to the host's synthetic machinery have been identified and optimized in order to deliver a desired unnatural amino acid to a repurposed stop codon or four base pair codon in a protein sequence. Nonsense suppression is still being optimized and expanded, but a wide array of unnatural amino acids have been introduced into proteins using this methodology. These unnatural amino acids include fluorophores, chemical cross-linkers, and amino

acids modified in length, shape, charge, fluorination, or chemical reactivity (Wang and Schultz, 2005).

1.3.1.2 Nonsense Suppression Applied to Membrane Proteins

Nonsense suppression has been applied to the study of several membrane proteins. The Dougherty lab has made extensive use of nonsense suppression to study the strength of cation-π interactions in the context of several membrane proteins including the nicotinic acetylcholine receptor, 5-HT (serotonin) receptor, NMDA receptor, and potassium channels (Dougherty and Stauffer, 1990; Ma and Dougherty, 1997; Dougherty, 2008). Potassium channels with high affinity for extracellular TEA accomplish this through cation-π interactions (Ahern et al., 2006). A recent study looked at whether an aromatic binding site in the potassium channel voltage sensor domain interacts with voltage-sensing arginine or lysine residues on the voltage sensor paddle (Tao et al., 2010). Nonsense suppression was also used to study potassium conduction and barium block through perturbation of the selectivity filter of a K_{ir} channel using an amide-to-ester backbone modification (Lu et al., 2001), and azido amino acids were incorporated into rhodopsin to observe conformational changes of protein activation by infrared (IR) spectroscopy (Ye et al., 2009).

Several proteins have been studied using nonsense suppression, but this methodology still has its limitations. Nonsense suppression requires that the desired modification be tolerated by the biological machinery, which often involves a selection process to optimize the orthogonal tRNA and synthetase pair

for a particular modified amino acid, if it can be tolerated at all. It also requires that the gene for the protein of interest be modified to incorporate the unnatural codon at the desired location. The efficiency of incorporating multiple copies of an unnatural residue into a protein is low, and incorporation of several different modifications in one protein is an ongoing challenge. Finally, the yield of modified protein is limited, and limits the types of experiments that can be done. Despite these limitations, this is a useful methodology for introducing unnatural modifications into proteins in living cells and the incorporation of modifications into new proteins is becoming much easier.

1.3.2 Protein Semisynthesis

In contrast to nonsense suppression, peptide synthesis, together with protein ligation strategies, can be used to directly incorporate a wide variety of chemical modifications, and combinations thereof, into proteins.

1.3.2.1 Protein Semisynthesis Methodology

Expressed protein ligation (EPL) allows a recombinant protein and a synthetic peptide to be linked together under mild aqueous conditions (Evans et al., 1998; Muir et al., 1998). The process involves a chemoselective reaction that yields a final protein with a native peptide bond between the two building blocks (Figure 1.7). The synthetic nature of one of the fragments enables the site-specific introduction of almost any chemical modification into that part of the protein, including fluorophores, caging groups, crosslinkers, backbone

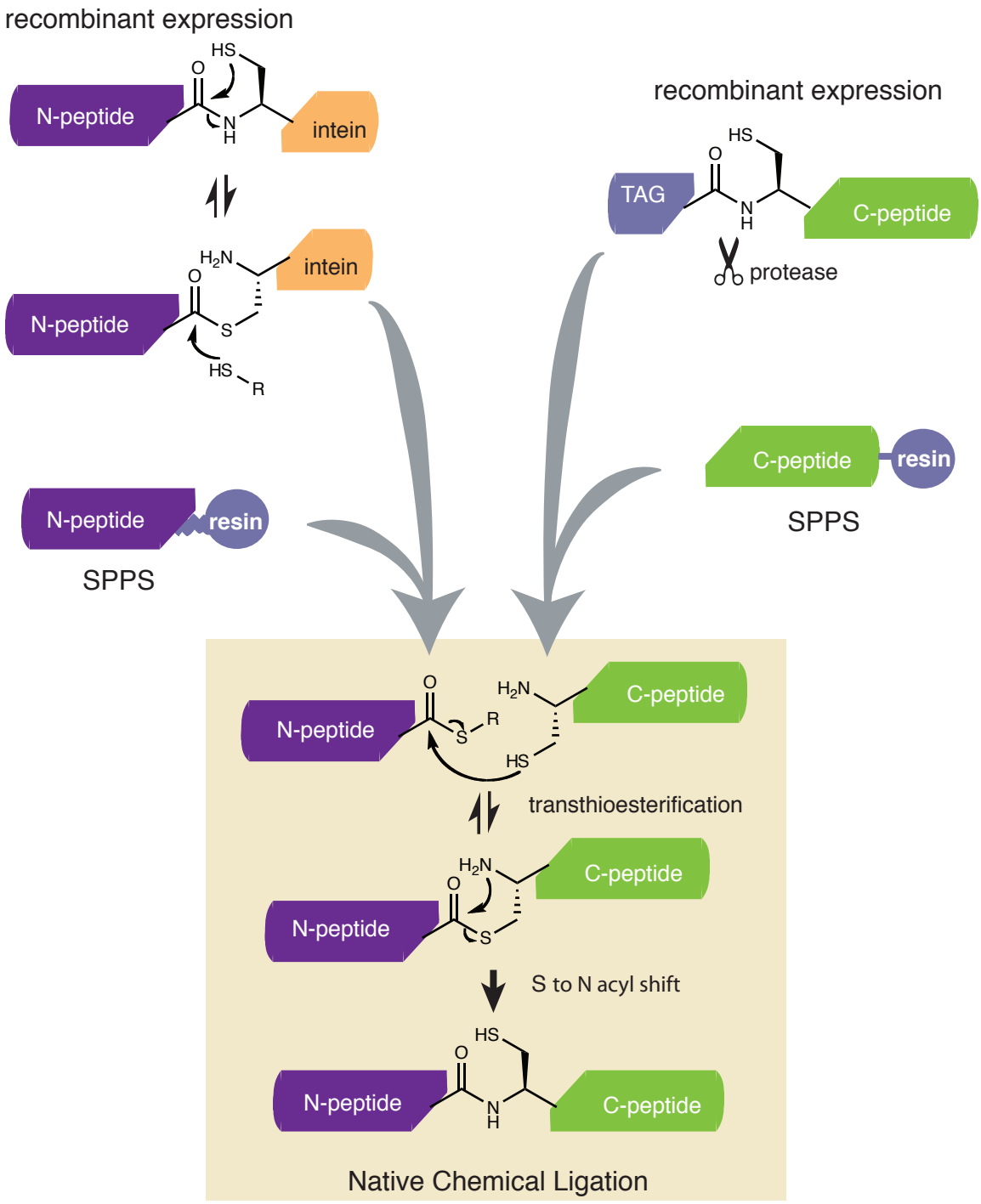

Figure 1.7: Expressed protein ligation (EPL) scheme. The top left quadrant depicts the preparation of a peptide with a C-terminal α-thioester (N-peptide; purple) from a recombinant intein (orange) fusion or synthetically by SPPS. The top right depicts preparation of an N-terminal cysteine containing peptide (C-peptide; green) either recombinantly, using proteolysis to expose the N-terminal cysteine, or synthetically by SPPS. The steps for ligating these two peptides together by native chemical ligation (NCL) are shown in the beige box.

modifications, and other analogs, as well as almost any combination of these modifications. At the same time, the recombinant nature of the other fragment allows for ligations involving a large protein segment.

EPL is based on the well-known reaction between a peptide bearing a thioester at its C-terminus (α-thioester) and a peptide with an N-terminal cysteine residue. This reaction, termed native chemical ligation (NCL), has proven to be extraordinarily powerful for the total synthesis of small proteins and their analogs (Dawson and Kent, 2000; Kent, 2009). However, NCL of synthetic fragments is limited to the use of peptides with fewer than 60 amino acids, due to the constraints of solid phase peptide synthesis (SPPS) (Kent, 1988).

One solution to this size problem is to employ recombinant polypeptide building blocks in the process. This technique involves the use of a class of auto-processing proteins called inteins (Noren et al., 2000; Paulus, 2000). Several engineered inteins have been developed that allow access to recombinant protein α-thioester derivatives by thiolysis of the corresponding C-terminal intein fusions (Muralidharan and Muir, 2006). N-terminal cysteine containing peptides can also be produced using engineered inteins or by fusion of the N-terminus to a protein tag that can be selectively cleaved during purification (Erlanson et al., 1996; Evans et al., 1999). More sophisticated approaches are available for ligating together three building blocks in a regioselective fashion, thereby permitting internal regions of proteins to be specifically modified (Kawakami and Aimoto, 2003; Bang and Kent, 2004; Dirksen and Dawson, 2008; Lee and Bang, 2010). Access to reactive proteins, without any size restriction for the expressed

protein fragment, suddenly enabled the application of NCL to the modification of a much larger fraction of the proteome. Indeed, the approach has been used to generate semisynthetic derivatives of members of essentially every major class of protein including integral membrane proteins (Muir, 2003; Muralidharan and Muir, 2006; Vila-Perello and Muir, 2010).

1.3.2.2 Protein Semisynthesis Applied to Membrane Proteins

To generate semisynthetic proteins that contain a ligation junction in the middle of a folded domain, it is essential that the protein subsequently be folded *in vitro*. In many cases, the *in vitro* folding conditions must be determined for a particular protein prior to developing a semisynthetic strategy. The folding of transmembrane proteins has been more difficult than that of soluble proteins and created an initial barrier to the application of protein chemistry in these systems. The first transmembrane peptides to be synthesized and refolded were all short, single helix segments (Montal et al., 1993; Iwamoto et al., 1994; Oblatt-Montal et al., 1995). Rhodopsin was the first multi-helix transmembrane protein to be refolded (Huang et al., 1981). Influenza protein M2 was the first transmembrane protein to be made by total synthesis using protein ligation, followed by protein folding (Kochendoerfer et al., 1999). Together, the Muir and MacKinnon labs were the first to apply the EPL technology to a transmembrane protein—specifically to look at the chemistry of potassium selectivity and conduction in KcsA (Valiyaveetil et al., 2002a). Strategies have since been developed for synthesizing the mechanosensitive channel MscL, the cation channel NaK, and

the porin OmpF for mechanistic and protein engineering studies (Clayton et al., 2004; Reitz et al., 2009; Linn et al., 2010).

1.3.2.3 Protein Semisynthesis Applied to KcsA

In order to perform semisynthesis of KcsA, with a ligation junction in the middle of the pore helix, a refolding protocol was first established; unexpectedly, the first challenge was to develop methods to unfold this stable tetrameric protein. Unfolding of KcsA requires harsh conditions such as boiling in 1% sodium dodecyl sulfate (SDS) for 30 minutes or a 50:50 trifluoroethanol (TFE):water mixture acidified with trifluoroacetic acid (TFA). Upon unfolding, it was determined that lipids are required for the refolding of KcsA; however, there are no requirements for particular lipids at this step as long as they form bilayers (Valiyaveetil et al., 2002b).

As KcsA can be folded *in vitro*, a strategy was devised for protein semisynthesis in order to explore specific properties of the selectivity filter (Figure 1.8). The strategy was designed to provide synthetic access to the selectivity filter (residues 75-79), where a ligation junction had to be positioned such that the synthetic fragment be less than 60 amino acids. For this purpose, the semisynthetic protein contains only the transmembrane core up to residue Arg122, similar to the truncated protein used for crystallography. This allows for a synthetic peptide to be synthesized between the C-terminus and Ser69 in the pore helix, where this serine tolerates mutation to cysteine (S69C) for the ligation junction and the final peptide is a long but feasible 54 amino acids. The first 68

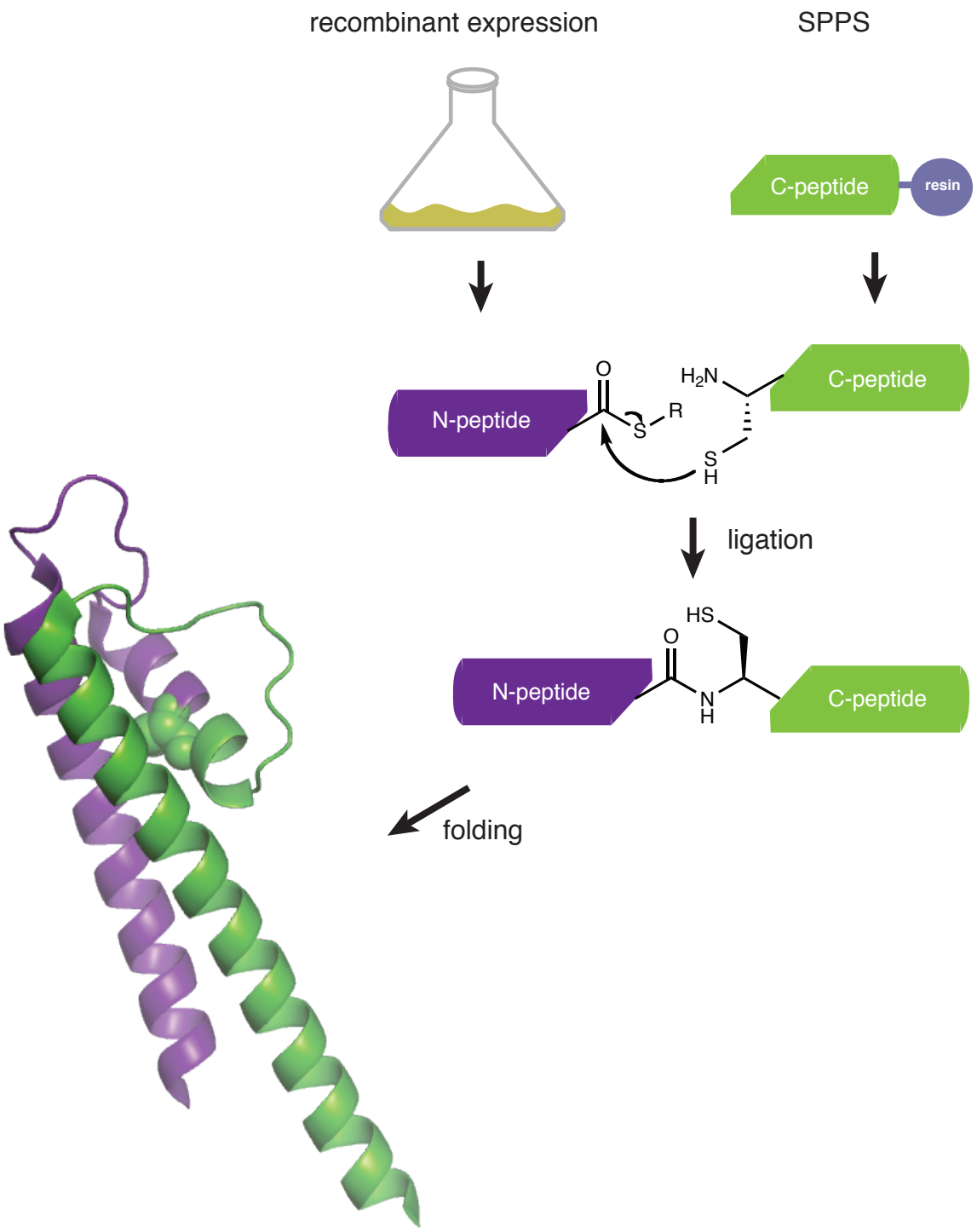

Figure 1.8: The EPL strategy for KcsA. Recombinant N-terminal peptide (purple) is expressed in *E. coli*, and a synthetic C-terminal peptide (green) is produced through Boc-SPPS. These two peptides are then ligated together by NCL. The regions corresponding to the peptide fragements are colored accordingly onto one folded subunit of KcsA. The ligation junction (S69C) is shown as spheres.

residues are expressed recombinantly in *E. coli*, in a sandwich fusion between a glutathione-S-transferase (GST) domain for solubility and the Gyr A intein to produce the C-terminal thioester. These peptides can then be ligated together in good yield in the presence of SDS for solubility and thiophenol for activation of the thioester (Valiyaveetil et al., 2002a).

With this semi-synthetic strategy in hand, two elegant experiments were performed to better understand the chemistry of the selectivity filter—each one studied using both electrophysiology and X-ray crystallography. The first semisynthetic modification targeted a ubiquitously conserved glycine in the selectivity filter in order to study the importance of its conformational freedom (Figure 1.9a). Specifically, it was hypothesized that the conformation of the conductive filter required a backbone conformation not accessible to L-amino acids; however, glycine as well as D-amino acids would tolerate this position and only glycine would be able to undergo the necessary conformational change to the low K^+ collapsed state. Thus, D-Alanine was substituted at this position, locking the selectivity filter into the conductive conformation. As expected, this channel maintained conductance and selectivity for potassium; however, it could conduct Na^+ in the absence of K^+ by lacking the ability for the filter to collapse (Valiyaveetil et al., 2004b; 2006a). The second semisynthetic modification of KcsA was an amide-to-ester substitution in the protein backbone in order to reduce the peptide bond dipole at that position. The ester modification was introduced at Gly79 to reduce the partial charge of the top set of carbonyls that coordinate potassium ions in the selectivity filter. This resulted in a reduction in

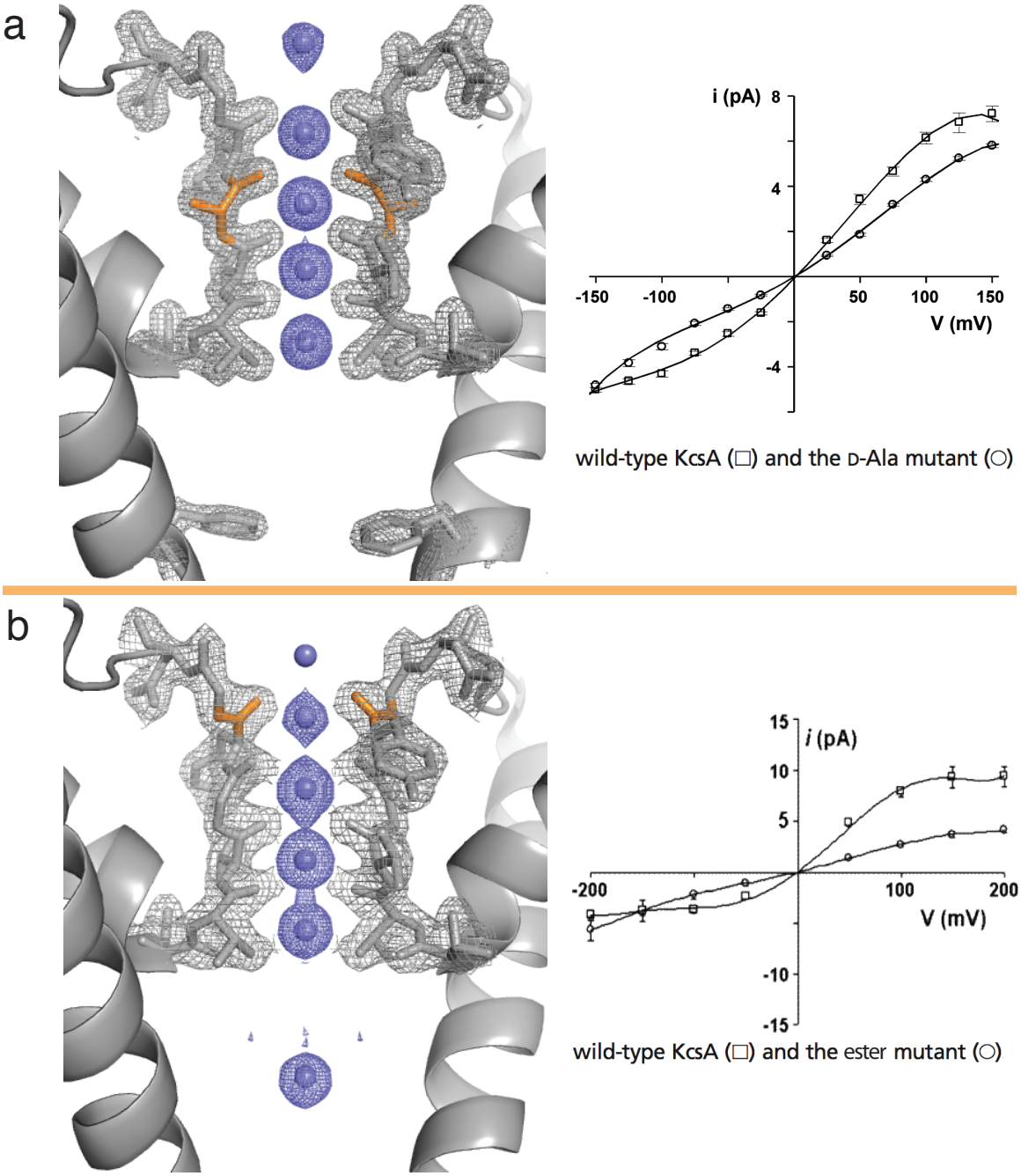

Figure 1.9: Structures of semisynthetic KcsA. Particular sites of modification are highlighted in orange. (a) Structure of D-Ala incorporated at Gly77 to lock the selectivity filter in the conductive conformation (2ih3). An I-V curve for this modification, compared to WT, is shown at right. (b) Structure of the ester incorporated at Gly79 to modulate the backbone dipole for the first set of carbonyls (2h8p). An I-V curve for this modification, compared to WT, is shown at right. The selectivity filter residues are shown in stick and the potassium ions are shown in blue. $2F_o$-F_c density maps for the protein are shown in gray at 2 σ and F_o-F_c omit maps for the ions are shown in blue at 5 σ. Electrophysiology data are from (Valiyaveetil et al., 2006a; Valiyaveetil et al., 2006b)

ion occupancy at the corresponding S1 position (Figure 1.9b) (Valiyaveetil et al., 2006b). Both of these experiments nicely demonstrate the extent of optimization in the selectivity filter in order for potassium channels to simultaneously exhibit exquisite selectivity and rapid rates of conduction.

Subsequent to this work, another synthetic strategy was devised for KcsA as well as strategies for studying other membrane proteins. KcsA semisynthesis was redesigned as a three-piece ligation such that the full-length protein could be synthesized while providing synthetic access to either the selectivity filter or the pore helix by this method (Komarov et al., 2009a). In a similar strategy to the initial KcsA semisynthesis, the nonselective cation channel NaK was synthesized with a ligation junction in the pore helix between a recombinant N-terminal fragment α-thioester and a C-terminal synthetic peptide. This work also demonstrated that purification of a hydrophobic, difficult to purify peptide could be improved through incorporation of a tri-arginine tag branching off of the N-terminal cysteine thiol until reduction prior to ligation (Linn et al., 2010). Together, these experiments demonstrate the growing interest in studying membrane protein structure and function using protein chemistry tools.

1.4 Overview

Potassium channels are a fascinatingly complex and highly evolved class of proteins. KcsA is a small, stable representative of the potassium channel family that is highly amenable to structural studies by X-ray crystallography as well as modification through protein synthesis. The work in this thesis focuses on

the potassium channel central cavity which has provided interesting and unexpected results.

Our initial work on the central cavity was inspired by the proposed helix dipole effect—where the pore helices behind the selectivity filter direct their helix C-termini toward the hydrated potassium ion in the cavity. In order to study the helix dipole effect, KcsA was synthesized with a modified helix backbone. This protein was characterized by electrophysiology and X-ray crystallography.

In the process of this study, it was revealed that the present conditions for folding KcsA *in vitro* produce an altered structure in the central cavity. These folding conditions were then studied using lipids, mutations, and QA ions with the goal of finding ways to prevent this conformational change. X-ray crystallography was used to study structures of KcsA in these various conditions to try to better understand the new conformation.

Subsequent studies provided new information on QA ion binding in the central cavity. The structures and implications of this work will be discussed in detail.

CHAPTER 2: THE HELIX DIPOLE EFFECT IN KcsA

The original crystal structures of KcsA revealed a precise mechanism for potassium selectivity and coordination in the selectivity filter, as well as a hydrated potassium ion in the central, water-filled cavity. However, the mechanism for stabilizing this hydrated ion was less clear. It was proposed that the pore helices behind the selectivity filter direct their helix C-termini toward this ion to confer stabilization through the helix dipole effect (Doyle et al., 1998). Helix dipoles have been studied using spectroscopic techniques and computational methods; however, they have not been studied through precise modulation of the backbone. Thus, we developed a methodology and applied it to studying the role of helix dipoles in KcsA. KcsA is a useful system because of its accessibility for chemical modification, as well as ease of analysis using both electrophysiology and crystallography experiments. We performed these experiments in KcsA in order to gain insight into the role of the helix dipole effect in this channel, and to establish this methodology as a way to study helix dipoles in proteins more generally.

2.1 Introduction

An alpha helix aligns peptide bonds along the length of the helix axis, through internal hydrogen bonding, but exposes free amide N-H groups at the N-terminus and C=O groups at the C-terminus. This arrangement aligns the dipoles of the peptide bonds, such that the exposed termini build up partial positive and negative charge respectively (Wada, 1976). The helix dipole effect was first

postulated based on observations of the aligned orientation of the peptide bonds and the resulting hydrogen bonding network formed in α-helices (Wada, 1976). For an individual peptide bond in solution, the dipole moment is ~3.5 D and these dipoles are aligned within 5 ° of the axis of the helix (Hol et al., 1978). Through the central region of the helix, a carbonyl oxygen at position *i* forms a hydrogen bond with the amide proton at residue *i*+4, creating a connected network of hydrogen bonding through the length of the helix. Helix dipoles are postulated to enhance the net positive charge on the amide N-H groups exposed at the helix N-terminus and the net negative charge on the carbonyl oxygens at the C-terminus (Figure 2.1).

2.1.1 The Proposed Helix Dipole Effect in Peptides and Proteins

Helix dipole effects were first proposed in proteins with structures determined by X-ray crystallography including enzyme active sites, especially phosphate binding sites, that often included helix N-termini (Hol et al., 1978; Hol, 1985). Correlations were observed for negatively charged amino acids near helix N-termini and positively charged amino acids near C-termini (Blagdon and Goodman, 1975). Later, statistics on proteins in the Protein Data Bank (PDB) also supported similar trends for charged amino acids hydrogen bonding with helix termini, referred to as helix capping (Baker and Hubbard, 1984; Richardson and Richardson, 1988).

Various studies have examined parameters that affect the magnitude of the helix dipole effect. Dielectric measurements of model peptides, as well as

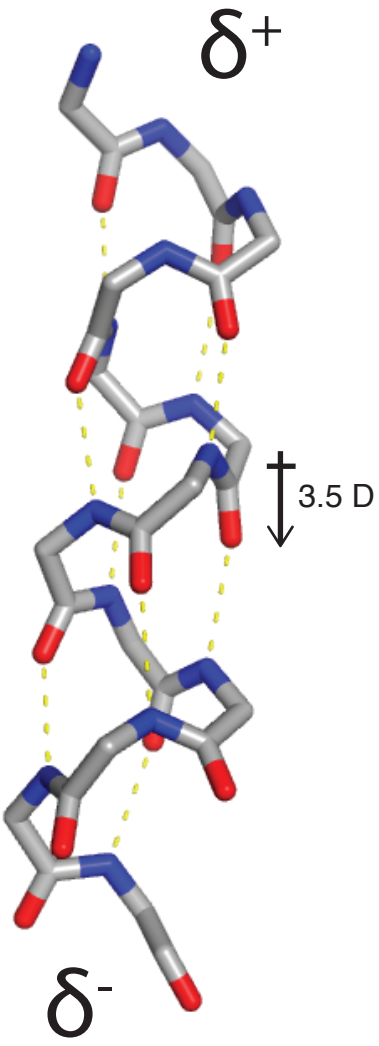

Figure 2.1: Characteristics of an α-helix implicated in the helix dipole effect. An example α-helix showing the amide nitrogens in blue and carbonyl oxygens in red. The hydrogen bonding between them is depicted by yellow dashed lines. Each peptide bond has a dipole moment of at least 3.5 D in an α-helix. These dipoles lead to a partial positive charge (δ^+) at the N-terminus and partial negative charge (δ^-) at the C-terminus.

quantum mechanical calculations, have proposed that individual peptide bond dipoles within an α-helix could increase to as much as 5 D (Applequist and Mahr, 1966; Wada, 1976; van Duijnen et al., 1979; Mehler, 1980). Electrostatic calculations were performed suggesting that the strength of a helix dipole increases with the length of the helix, up to ten residues or three turns of the helix (Hol et al., 1978; Sheridan and Allen, 1980). The results of several studies suggest that this will amount to a net charge stabilization of approximately 0.5 *e*, or one half of an elemental charge, on each terminus (Wada, 1976; Sheridan and Allen, 1980; Warwicker and Watson, 1982). As expected, this electrostatic effect is also sensitive to the dielectric environment, where helix dipoles are strongest in low dielectric media such as a lipid bilayer or the hydrophobic interior of a protein (Rogers and Sternberg, 1984; Lockhart and Kim, 1993; Sengupta et al., 2005). Microscopic electrostatic calculations have clarified that the perceived helix dipole effect actually arises from two independent partial charges, one on each end of the helix, that sufficiently account for the experimentally observed effects (Aqvist et al., 1991). For the sake of consistency with the literature, this will continue to be referred to as the helix dipole effect in this study, though referring to these as helix end-charges may be more accurate.

Model peptides have been used to study the properties of helix dipoles using spectroscopic techniques such as nuclear magnetic resonance (NMR) and circular dichroism (CD). The interactions between charged amino acids and the helix dipole can have significant effects on α-helix stability (Shoemaker et al., 1987; Huyghues-Despointes et al., 1993) and may explain differences in stability

between α- and 3(14)-helices, from β-peptides (Allison et al., 2010). There is a correlation between protein stability and helix capping, as observed through shifts in the pKa of capping residues by helix dipoles (Armstrong and Baldwin, 1993). Dipoles at helix N-termini were shown to be less sensitive to solvent screening than conventional electrostatics would predict, suggesting that the size and shape of α-helices may enhance the effect of helix dipoles in significant, biologically relevant ways (Lockhart and Kim, 1992; 1993). A statistical mechanics model for helix dipoles was constructed (by analyzing several parameters from hundreds of proteins) that effectively predicted helicity and helix stability for a set of designed peptides (Muñoz and Serrano, 1994; 1995).

Helix dipole effects have also been analyzed in the context of protein domain stability and protein function. Helix dipoles may affect helix-helix interactions such as in the electrostatic interactions of antiparallel four-helix bundles (Sheridan et al., 1982; Presnell and Cohen, 1989) and can, in certain cases, contribute to optimal protein folding and stability (Hol et al., 1981; Perutz et al., 1985; Serrano and Fersht, 1989; Nicholson et al., 1991; Bjornholm et al., 1993; Zhang et al., 2009). Various experiments have analyzed shifts in pKa at titratable capping residues at either end of the α-helix, or even both ends of the same helix. These studies demonstrate that charged residues at helix N-termini exhibit a lower pKa, compared to the amino acid on its own, while at C-termini they result in higher pKa (Sali et al., 1988; Lodi and Knowles, 1993; Miranda, 2003). In some cases, these pKa shifts are important for ligand binding and enzyme catalysis (Doran and Carey, 1996). Examples of proteins where α-helix

dipole effects have been implicated through structural arrangement, biophysical measurements, or computational analysis are summarized in Table 1. Of particular relevance to the current work, the helix dipole model even caused some scientists to propose mechanisms for ion conduction and gating aided by such dipole effects before crystal structures of any channels were determined (Boheim et al., 1983; Edmonds, 1985). Since then, several membrane protein crystal structures have revealed helices positioned appropriately to contribute to the electrostatic environment around a binding site or ion conduction pore within the membrane (Doyle et al., 1998; Dutzler et al., 2002).

2.1.2 The Proposed Helix Dipole Effect in KcsA

The first crystal structures of KcsA illuminated a structural arrangement of helix C-termini pointing to a hydrated potassium ion in the central cavity of the protein in the membrane. This arrangement was proposed to impart a helix dipole effect to help stabilize the cavity ion (Doyle et al., 1998). Computational and experimental studies have been carried out to try to better understand the role of helix dipoles in this system.

With structural information available and rapidly improving computational methods for performing protein electrostatic and quantum mechanical calculations, several groups studied the contribution of helix dipoles to potassium stability and conduction through the pore. Electrostatic calculations and molecular and Brownian dynamics simulations have suggested that the pore helix dipoles contribute to a broad energy well that stabilizes potassium ions as

Table 1: Examples of proteins with proposed helix dipole effects

	SIGNIFICANT FINDINGS	METHODS	REFERENCE(S)
ENZYME ACTIVITY			
rhodanese	N-termini lower active site Cys pKa	X-ray crystallography	(Ploegman, et al. 1979)
thioredoxin	catalytically active disulfide at helix N-term	X-ray crystallography	(Soderberg, et al. 1978)
FAD binding domains	orientation of the helix dipole is one of the few conserved features in the cofactor (FAD) binding site	X-ray crystallography	(Van Driessche, et al. 1996)
	a mutation repacks a helix proposed to orient its helix dipole into the cofactor (FAD) binding site	mutagenesis, kinetics, X-ray crystallography,	(Palfey, et al. 1994; Lah, et al. 1994)
isomerase	His pKa at lowered at N-term and raised at C-term (triose-phosphate)	NMR pH titrations	(Lodi and Knowles, 1993)
acyl cysteine proteases	Spectroscopy and kinetics of proteolysis correlate with the varied prominance of helix dipoles in the enzyme active sites of several proteases	Raman spectroscopy and kinetics	(Doran and Carey, 1996)
	N-term stabilizes active site transition state (papain)	Molecular Orbital theory, kinetics, and mutagenesis	(van Duijnen, et al. 1979, Menard, et al. 1995)
STABILITY			
clotting factor VWF A2 domain	domain stability for reversible folding and unfolding	X-ray crystallography	(Zhang, et al. 2009)
nucleosome	histone binding to DNA minor groove and to Mn2+	X-ray crystallography	(Harp, et al. 2000; Wu and Davey, 2010)
lysozyme	charged amino acid sidechains at helix termini affect stability	CD, thermo-denaturation, expression	(Harada et al, 2007)
	predicted mutations were shown to increase enzyme stability	X-ray crystallography, mutagenesis	(Nicholson, et al. 1988; 1991)
transcription factor Spt4	N-term forms an important binding surface for interacting with a regulator protein	X-ray crystallography, mutagenesis	(Guo, et al. 2008)
ribonuclease	C-terminal His has higher pKa	NMR pH titrations	(Sali, et al. 1988)
	N-cap residue mutagenesis (barnase)	chemical denaturation monitored by fluorescence	(Serrano and Fersht, 1989)
TRANSMEMBRANE			
alamethicin	voltage dependent helix flip-flop due to the orientation of the helix dipole	Electrophysiology	(Hall, et al. 1981; Boheim, et al. 1983)
KcsA	orientation of pore helix C-termini toward cavity potassium ion	X-ray crystallography	(Doyle, et al. 1998)
chloride channel	orientation of helix N-termini toward chloride coordination sites	X-ray crystallography	(Dutzler, et al. 2002)

they move through the central cavity (Figure 2.2) (Chung et al., 1999; Roux and MacKinnon, 1999). The helix dipoles have also been proposed to be important for polarizing water molecules within the cavity that may aid in ion conduction (Guidoni et al., 2000).

In one study, an amino acid near the helix C-terminus of an inward rectifier (K_{ir}) potassium channel was mutated and studied for changes in channel function using electrophysiology (Chatelain et al., 2005). Thr141 (analogous to Thr74 at the end of the pore helix in KcsA) was modified to several amino acids, including positively charged arginine and lysine residues, but none of the mutations had much effect on potassium conductance. From this work, it was concluded that the helix dipoles were insignificant. However, it is important to note that the sidechain of Thr74 in KcsA is oriented away from the helix terminus. Without crystal structures of these mutant proteins it is impossible to determine how the modified amino acids were arranged and thus whether the helix dipoles may have actually been affected.

2.1.3 The Proposed Backbone Modification to Study the Helix Dipole

Modification of a protein backbone specifically to study the helix dipole effect has not been reported, so we sought to establish a methodology that would be applicable to KcsA as well as generalizable to other proteins proposed to utilize the helix dipole effect.

As discussed in Chapter 1, protein semisynthesis has become a powerful tool for modifying proteins and a methodology has been developed for the

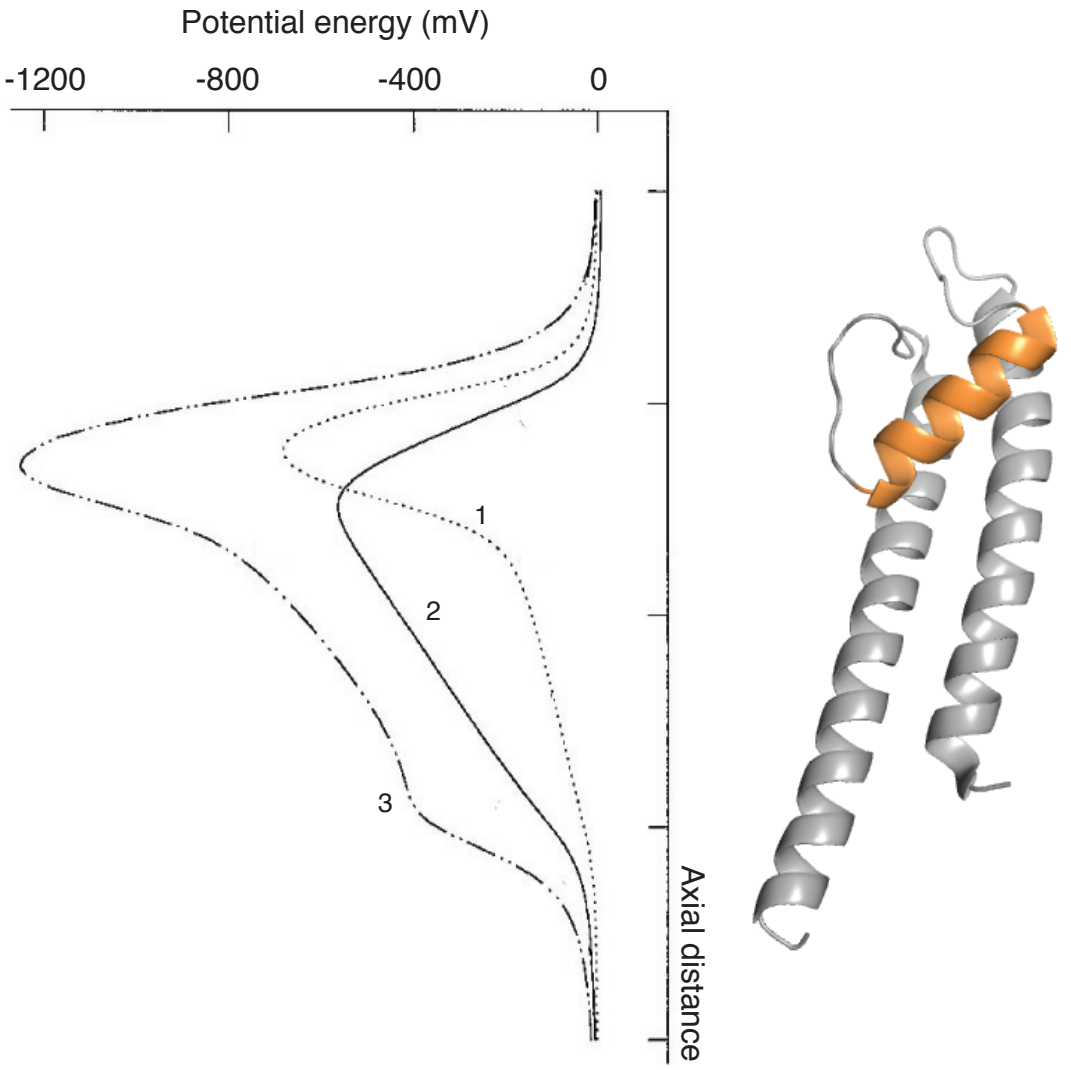

Figure 2.2: Charges important for potassium stabilization through the pore. Electrostatic calculations of the potential energy (horizontal axis) stabilizing a potassium ion as it traverses the length of the conduction pore (vertical axis). One subunit of KcsA is shown in gray cartoon, with the pore helix highlighted in orange, to provide a reference for the axial position. Independent calculations were made, taking into account electrostatic dipoles in different parts of KcsA. The dotted line (1) shows the potential energy function from dipoles in the selectivity filter region. In contrast, the solid line (2) shows the potential energy due only to the pore helix dipoles. The dot-dash line (3) shows the potential energy when all dipoles in the channel pore are incorporated, including the ones shown as well as some additional charges due to charged amino acids at the mouth of the channel. The figure was adapted from (Chung et al, 1999; Figure 3).

semisynthesis of KcsA (Valiyaveetil et al., 2002a). The C-terminus of the pore helix is chemically accessible by the current semisynthetic strategy, and an amide-to-ester backbone modification has previously been incorporated in KcsA to reduce a peptide bond dipole that coordinates a potassium ion in the selectivity filter (Valiyaveetil et al., 2006b). Based on the previous work, we hypothesized that we could reduce the pore helix dipole through incorporation of an amide-to-ester backbone modification at the end of the pore helix C-terminus.

An ester is similar in structure and conformation to an amide, though with some more rotational freedom (Brant et al., 1969; Ingwall and Goodman, 1974; Blom and Gunthard, 1981; Wiberg and Laidig, 1987). However, an ester is calculated to have a bond dipole approximately half as strong as an amide (Figure 2.3b) (Brant et al., 1969; Powers et al., 2005). Esters have been successfully incorporated once or multiple times into a protein helix (Koh et al., 1997; England et al., 1999; Lu et al., 2001), including several examples that used protein synthesis and folding to prepare ester-modified proteins (Lu et al., 1997; Beligere and Dawson, 2000; Blankenship et al., 2002; Deechongkit et al., 2004; Powers et al., 2005; Valiyaveetil et al., 2006b).

We imagined that the most C-terminal position in the pore helix would be appropriate for incorporating the ester, as it would both reduce the dipole moment at that terminal position and would also disconnect that residue from the hydrogen bonding network extending up the helix (Powers et al., 2005). Careful analysis of the KcsA structure led us to the peptide bond between alanine 73 and

threonine 74 (Figure 2.3a). This location is also synthetically tractable as discussed below.

2.2 Results

In this study, we used protein semisynthesis to incorporate an amide-to-ester backbone modification into the C-terminus of the pore helix of KcsA in order to reduce the strength of the pore helix dipoles. We analyzed the effects of this modification using electrophysiology and X-ray crystallography. These data suggest that a subtle modification in the pore helix dipoles can have a significant effect on potassium conduction without perturbation to the structure of the pore helices.

2.2.1 Semisynthesis of Helix-Dipole-Modified KcsA

We proposed to reduce the C-terminal most peptide bond dipole in the pore helix using an amide-to-ester backbone modification, through a previously established methodology (Valiyaveetil et al., 2006b). To incorporate the ester at the peptide bond between Ala73 and Thr74, Thr74 was mutated to alanine to simplify ester formation and eliminate any possible backbone rearrangements from the threonine γ-hydroxyl. The resulting modified protein will be referred to as T74Aester (Figure 2.3b).

This modification can be incorporated into KcsA through protein semisynthesis between a recombinantly expressed N-peptide fragment (residues 1-68) and a C-peptide fragment synthesized by Boc-SPPS (69-122) to include

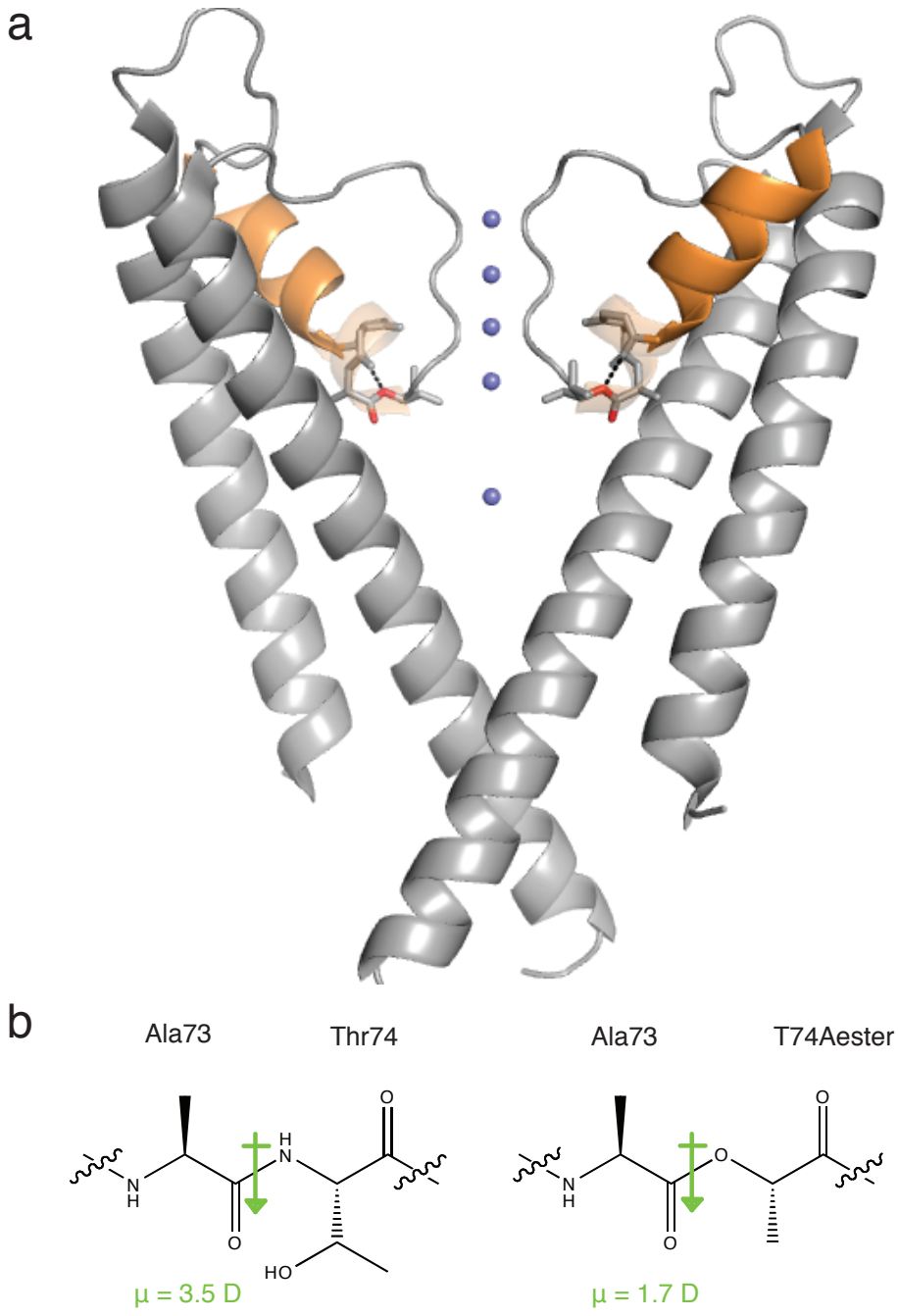

Figure 2.3: Strategy for modification of the pore helix dipole. (a) In order to modulate the dipoles at the C-termini of the pore helices (orange) in KcsA, the C-terminal most peptide bond was identified: Ala73 - Thr74. Incorporation of an ester at this position (backbone and carbonyl oxygens of this bond colored in red) will be well poised to affect interactions with the cavity ion through both reducing the bond dipole at that position as well as removing the hydrogen bond donor that would otherwise connect with the hydrogen bonding network up the length of the helix (black dashed line). (b) Molecular structures of the native, and ester-modified bond to highlight the change in backbone structure and dipoles more closely.

the amide-to-ester modification (Valiyaveetil et al., 2002a). The ligation junction is formed at S69C in the middle of the pore helix. While previous structural studies with semisynthetic KcsA used a ligation junction at Val70 (V70C) for improved ligation efficiency, all of the work for this project used the S69C ligation site to create minimal disturbances to the pore helices between experiments. Protein prepared for functional studies included the A98G mutation which is required for the function of truncated KcsA in the bilayer, while protein for structural studies contained the wild-type A98 residue at this position. The semisynthetic strategy will be covered here briefly, focusing on areas where the protocol has been modified from published methods (Valiyaveetil et al., 2002a), with more detail included in the Materials and Methods section.

The N-terminal fragment α−thioester was prepared from a recombinantly expressed fusion protein through an optimized protocol (Figure 2.4). Specifically, this hydrophobic peptide construct seems to co-purify with other contaminants that are deleterious to the RP-C4-HPLC column. Prior purification used a chitin column to selectively remove the intein-chitin binding domain (CBD) fragment away from the N-terminal fragment α-thioester (Valiyaveetil et al., 2002a); however, we hypothesized that this allowed the contaminant to be carried through the purification. Instead, a Co^{2+} column step was used to selectively bind and elute the His_6-tagged N-terminal fragment α-thioester. This protocol resulted in cleaner crude protein and less deleterious effects to the C4 purification columns in the final RP-HPLC purification step. The synthetic C-peptide fragment, including the amide-to-ester modification, was synthesized analogously

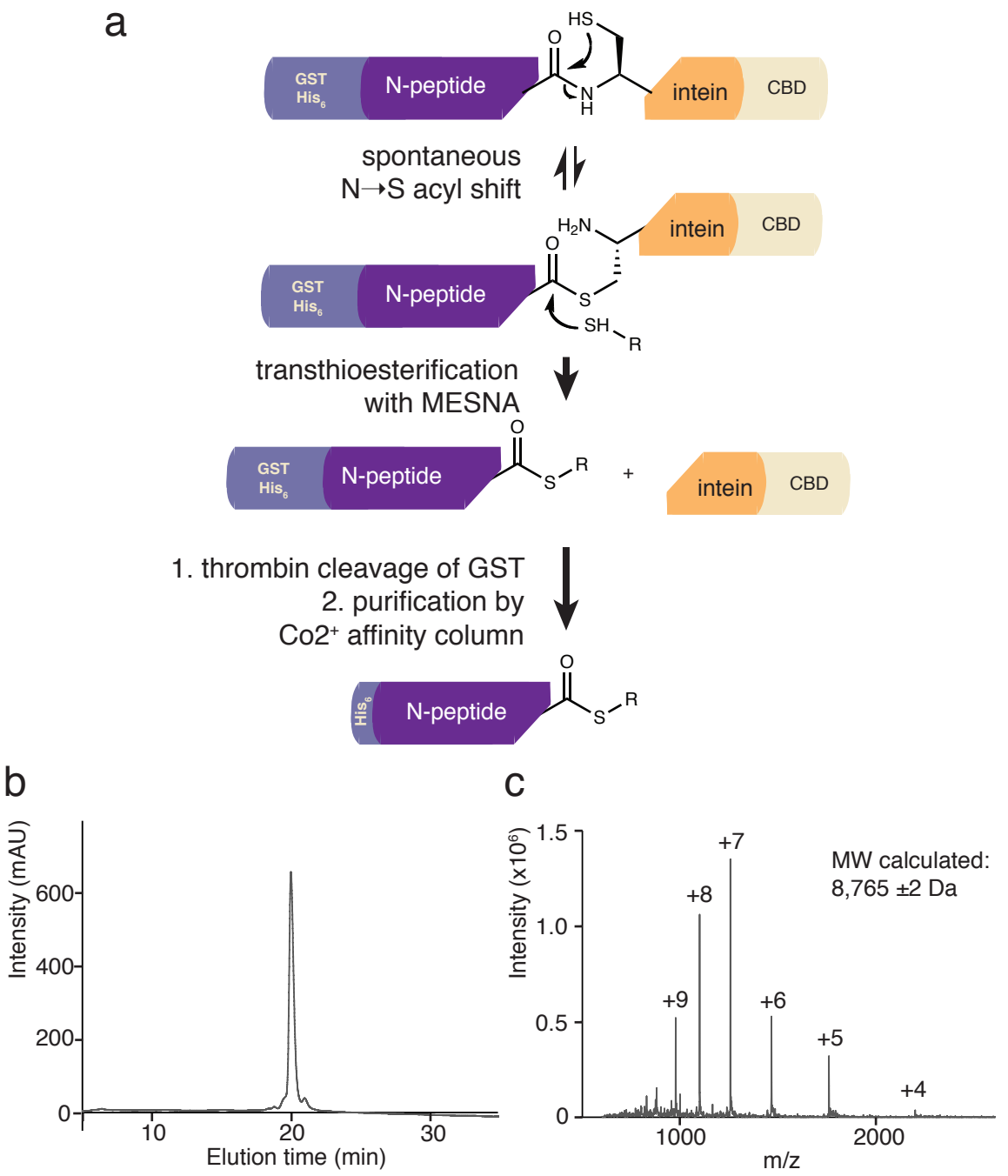

Figure 2.4: Preparation of the N-peptide α-thioester. (a) Purification scheme for recombinant N-peptide thioester: N-peptide is expressed as a sandwich fusion between GST and the Gyr-A intein-CBD. The thioester is formed by cleavage of the intein-fusion with MESNA. The GST tag is cleaved with thrombin, and the N-peptide is purified by Co^{2+} metal affinity, using the His_6 tag at its N-terminus. (b) Analytical RP-HPLC of purified N-peptide. (c) ESI-MS spectrum of purified N-peptide. Expected mass, 8,763 Da.

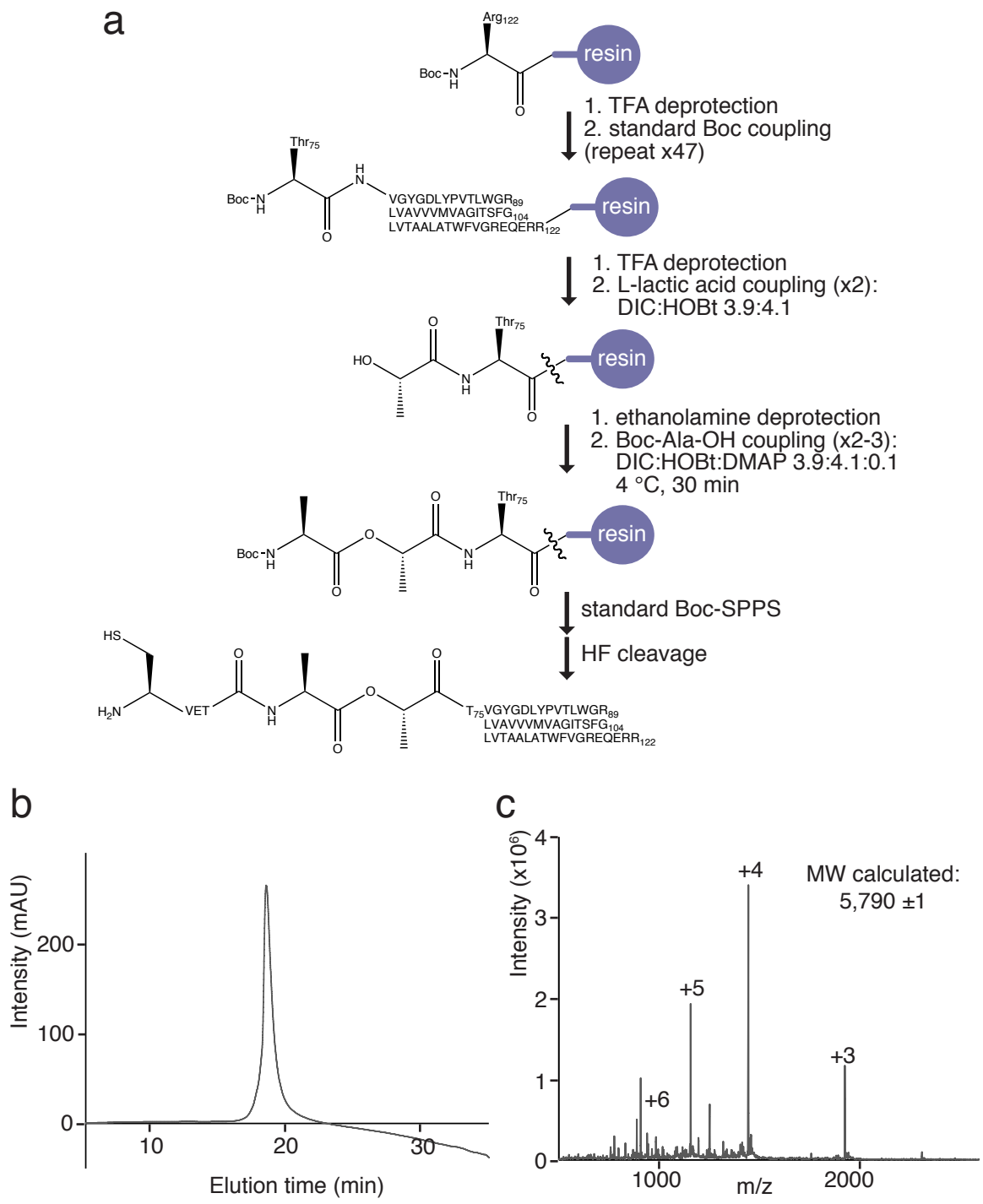

Figure 2.5: Preparation of the C-peptide. (a) The Boc-SPPS synthesis strategy: Starting with Boc-Arg(Tos)-PAM resin, 46 amino acids are coupled by standard *in situ* neutralization Boc chemistry. L-lactic acid is coupled with DIC/HOBt and Boc-Ala-OH is coupled with DIC/HOBt and catalytic DMAP, to form the ester. The final four amino acids are again coupled by the standard protocol and finally the peptide is cleaved by HF, 0 °C, 1 hour. (c) Analytical RP-HPLC of purified C-peptide. (d) ESI-MS spectrum of purified C-peptide. Expected mass, 5,789 Da.

to the previously reported Boc-SPPS strategy (Figure 2.5) (Valiyaveetil et al., 2006b)

Figure 2.6a outlines the subsequent steps for ligation and purification of the semisynthetic protein. Ligation of the purified N- and C-peptide fragments was performed in the presence of SDS for solubility and thiophenol to activate the thioester. The ligation conditions were optimized to 0.3% SDS, down from 1% SDS, and to 2.25% thiophenol, from 2% (Figure 2.6b). Upon reaction completion, the crude ligation mixture was reduced and diluted with lipids to fold the crude mixture. The folding reactions for these experiments were performed in the presence of 13.5 mg/ml soybean lipids, 25 mM MES buffer pH 6.4, 150 mM KCl, and 5 mM DTT (all final concentrations), with 0.1% SDS and 10 mM phosphate buffer present from dilution of the ligation mixture. Usually, folding progress is monitored as a shift from monomer to tetramer observed by SDS-PAGE; however, the T74Aester tetramer was not stable under the denaturing conditions of the gel. Similar behavior has been observed for other mutations in KcsA (Irizarry et al., 2002; Choi and Heginbotham, 2004; Krishnan et al., 2008). To overcome this, an enzyme-linked immunosorbent assay (ELISA) was developed to observe the presence of folded tetramer using the KcsA antibody serum that was also used to produce FAB for structural studies. The final folded protein is purified by Co^{2+} affinity purification and size exclusion chromatography (Figure 2.6c). Thin-Layer MALDI mass spectrometry was used to determine that the final protein had the expected mass (Figure 2.6d) (Cadene and Chait, 2000).

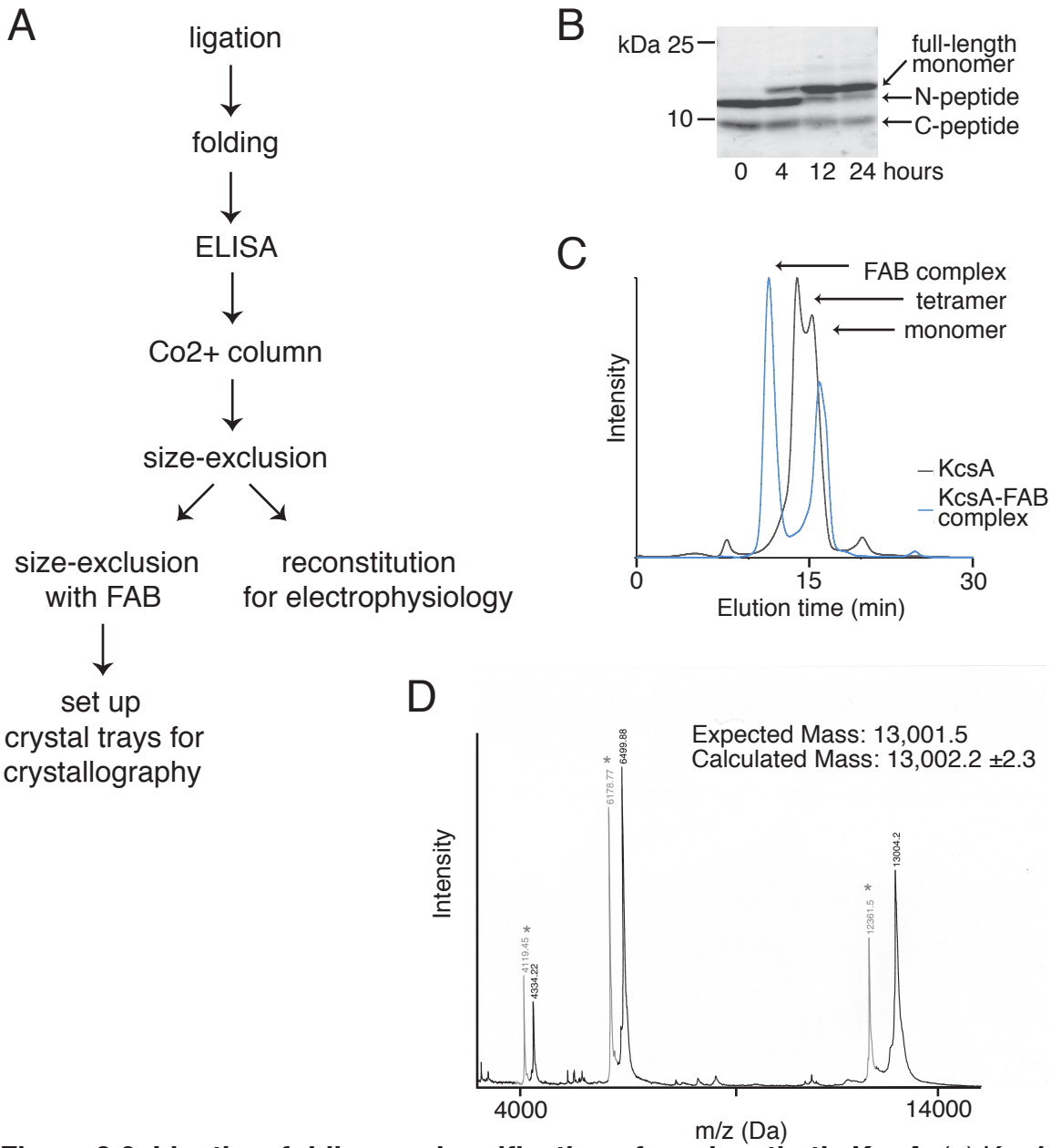

Figure 2.6: Ligation, folding, and purification of semisynthetic KcsA. (a) KcsA is ligated and immediately folded in the presence of lipid vesicles. Folded tetramer is detected by ELISA and then purified by Co^{2+} affinity column and size-exclusion chromatography. Pure protein can then be purified again as a KcsA-FAB complex and concentrated for crystal screens, or reconstituted into lipid vesicles for electrophysiology experiments. (b) Ligation progress of purified peptides in the presence of 0.3% SDS and 2.25% thiophenol shown by SDS-PAGE. (c) Overlaid size exclusion chromatograms of folded channel (gray) as well as the KcsA-FAB complex (blue). The monomer, tetramer and shifted complex peaks are labeled, and the unmarked peak is free FAB. (d) The mass of the full length protein determined by thin-layer MALDI-TOF, with the cycochrome C calibration peaks shown in gray and marked with asterisks (*).

2.2.2 Function of Helix-Dipole-Modified KcsA

We analyzed the functional implications of reduced pore helix dipoles (the presumed consequence of the amide-to-ester substitution) in the T74Aester protein by recording single-channel potassium conductance in a lipid bilayer (Figure 2.7b). T74Aester, containing the A98G mutation required for function, was reconstituted into 3:1 PE:PG lipid vesicles and recordings were made in a bilayer of the same composition, and in the presence of symmetric 150 mM KCl. The ester-containing protein showed much lower conductance than the recombinantly prepared, natively folded WT or T74A proteins. A current-voltage (I-V) curve was determined, revealing a 10-fold reduction in T74Aester channel conductance (Figure 2.7a). This change in conductance is specific to the ester containing protein, but a direct comparison of the conductance between this protein and *in vitro* refolded KcsA with a native backbone (T74Aref) is still ongoing. These results suggest that the helix dipoles may play a major role in the efficiency of ion conduction in potassium channels.

While WT KcsA shows some outward rectification, with higher conductance in the outward direction (ions that flow through the cavity and then the selectivity filter), the ester-modified protein has a linear, symmetric current-voltage relationship (Figure 2.7c). We speculate that the helix dipoles may play an important role in rehydration and especially dehydration of ions as they exit or enter the selectivity filter. It may also be the case that helix dipoles are important for aligning potassium ions to efficiently enter the filter. In the low-dielectric

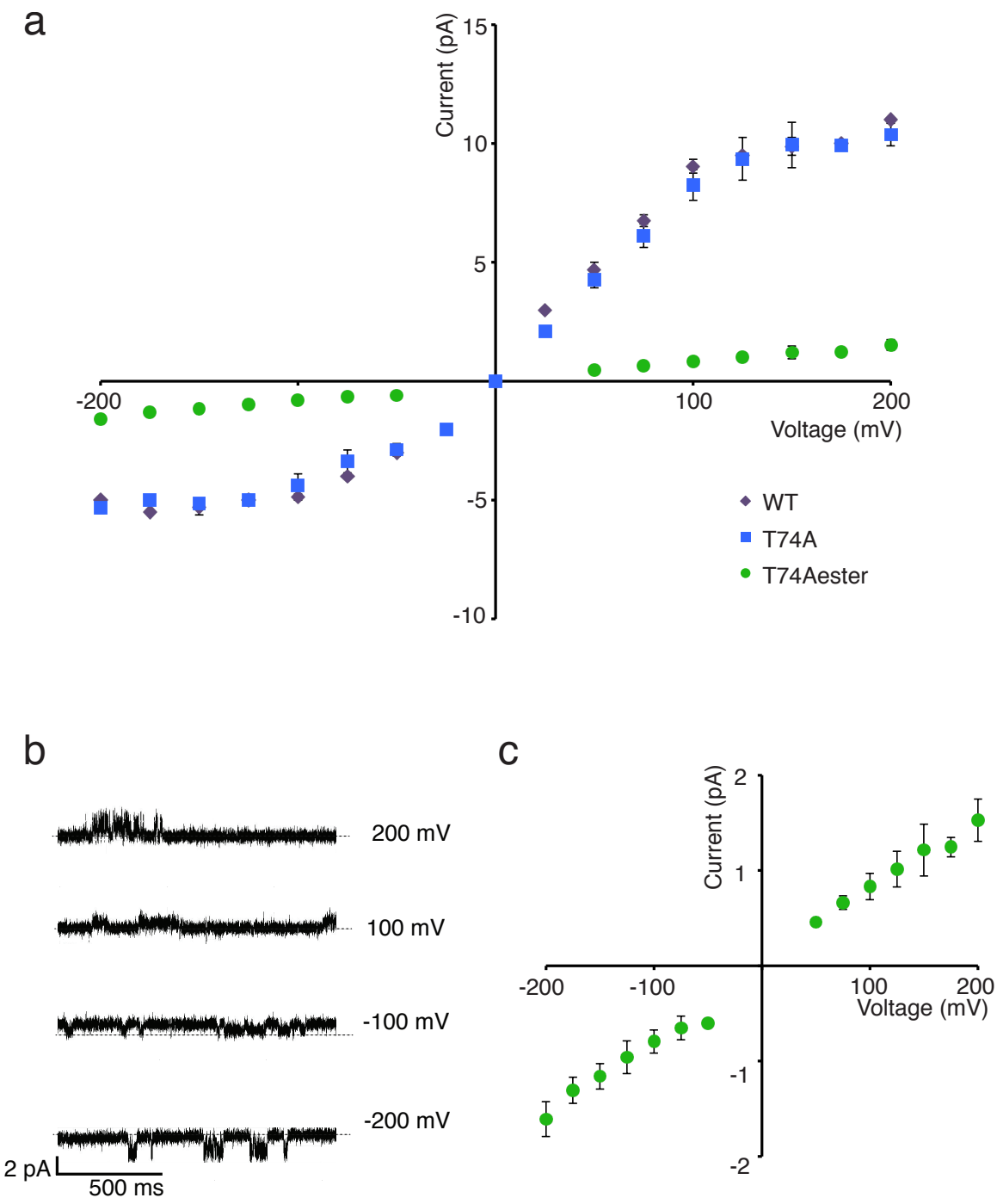

Figure 2.7: Single-channel electrophysiology of T74Aester. (a) Current-voltage (I-V) relationships for WT (purple), natively folded T74A (blue), and semi-synthetic T74Aester (green) proteins. Error bars are from an average of at least three independent bilayer recordings. (b) Single channel traces of T74Aester at various voltages. The gray dotted lines mark the closed state. (c) Zoomed in I-V curve for T74Aester only.

membrane environment, helix dipoles may contribute substantially to the high conductance observed in KcsA.

2.2.3 Structure of Helix-Dipole-Modified KcsA

We crystallized T74Aester, with wild-type Ala98, in order to asses the structural effects of the ester modification. We obtained an X-ray crystal structure of this semisynthetic protein refined to 2.3 Å resolution, using standard protocols for crystallization of the KcsA-FAB complex (Figure 2.8a). The conformation of the selectivity filter and pore helices show no perturbations relative to the WT protein (1k4c), with a C_α RMSD of 0.14 Å (Figure 2.8b); however, there was a conformational change in the cavity. Specifically, the Phe103 residues that line the cavity changed rotamer and flipped into the middle of the cavity (and will be referred to as the 'flipped' cavity conformation). Crystal structures of natively purified recombinant protein containing the T74A mutation but no ester (T74Arec, Figure 2.9a) and *in vitro* refolded recombinant protein again with T74A and no ester (T74Aref, Figure 2.9b) were both obtained for comparison. Statistics for these structures are summarized in Table 2. The native structure had a WT-like cavity conformation, but the refolded structure produced the flipped conformation, similar to T74Aester. From these structures as well as more data presented in Chapter 3, we concluded that the conformational change in the cavity of T74Aester was due to the requisite folding step for preparation of this semisynthetic protein, and unrelated to protein mutations or modifications. While we cannot analyze the effects of the ester on the cavity ion due to the

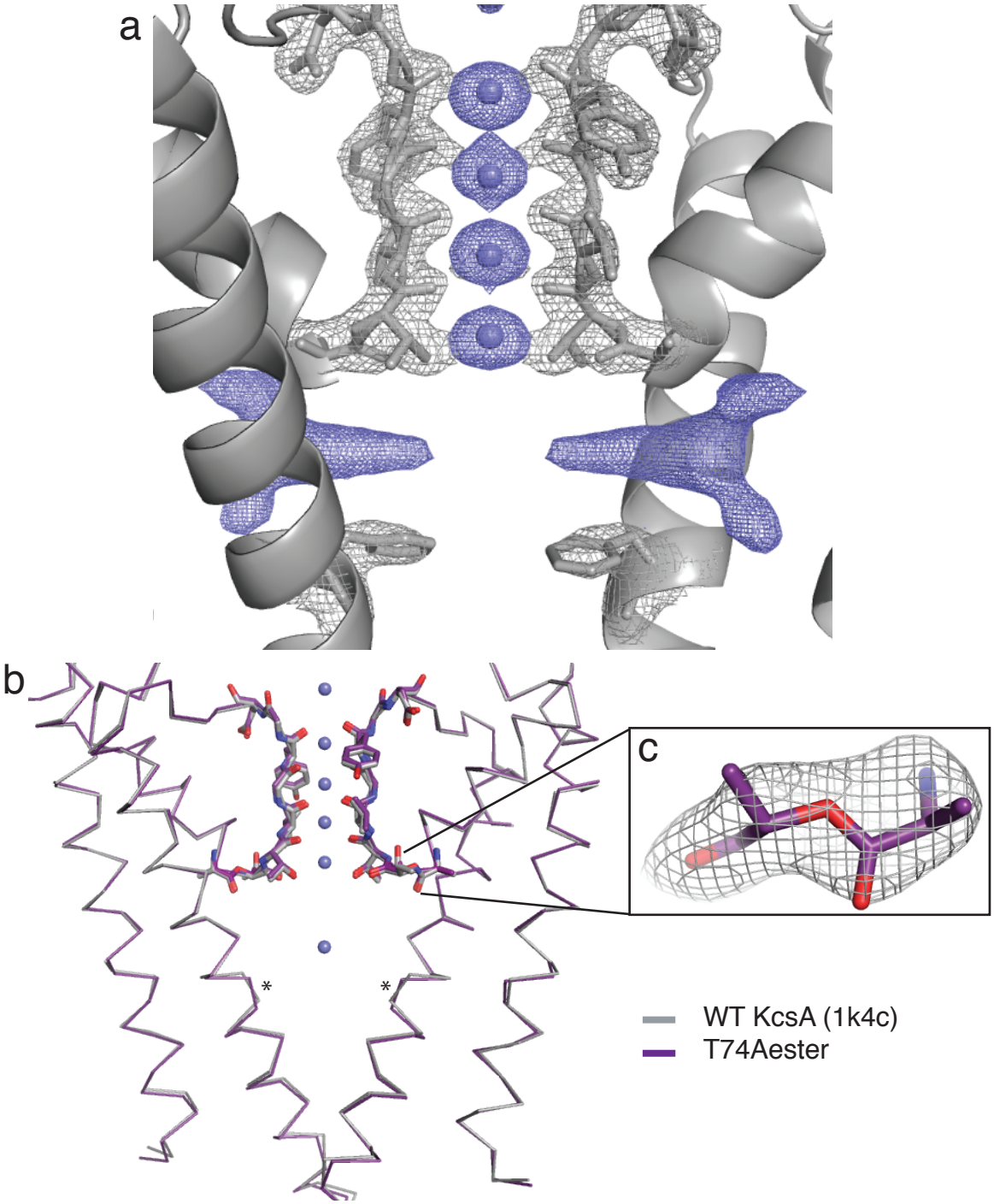

Figure 2.8: Crystal structure of T74Aester. The structure was refined to 2.3 Å resolution. (a) Selectivity filter and cavity. The selectivity filter residues and Phe103 are shown in stick and the potassium ions are shown in blue. $2F_o$-F_c density maps for the protein are shown in gray at 2 σ. F_o-F_c omit maps for the ions are shown in blue at 5 σ and for the unmodeled density at 2 σ. (b) T74Aester (purple) overlaid with WT KcsA (1k4c, gray) to show backbone agreement, with C-α RMSD of 0.14 Å. The locations of Phe103 are marked (*) (c) The inset shows the density around the ester bond with a $2F_o$-F_c map at 2 σ.

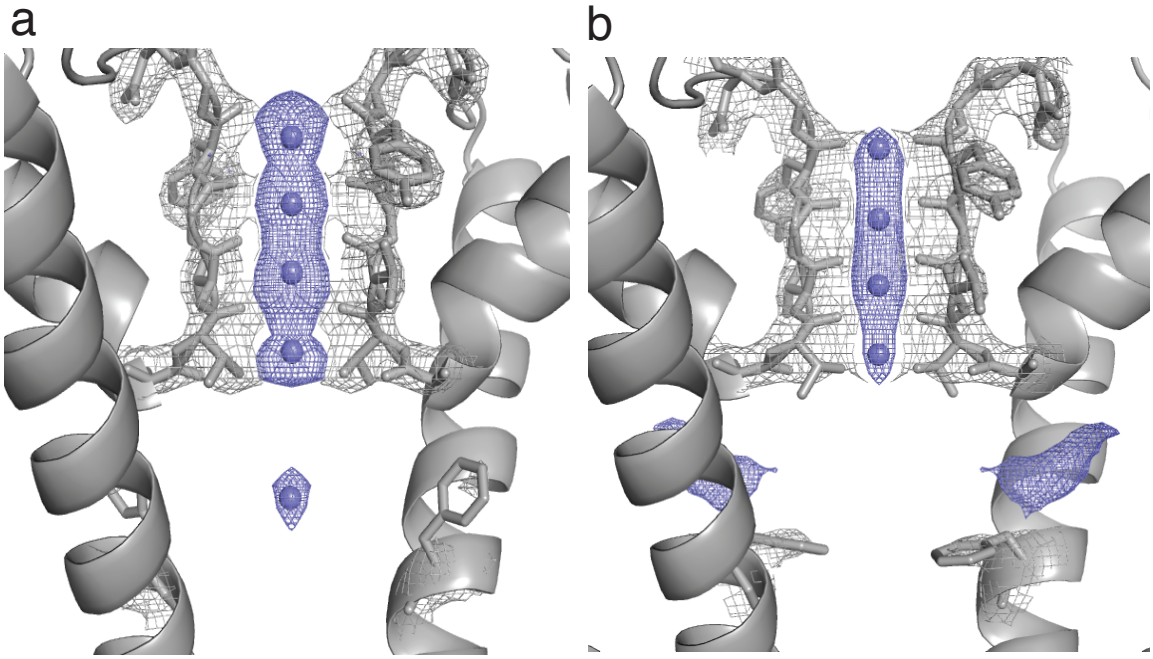

Figure 2.9: Control structures for the T74A sidechain mutant. (a) The structure of recombinant T74A KcsA, refined to 2.9 Å resolution and (b) the structure of T74A KcsA that was made by unfolding and refolding the recombinant protein *in vitro*, refined to 3.05 Å resolution. The selectivity filter residues and Phe103 are shown in stick and the potassium ions are shown in blue. $2F_o$-F_c density maps for the protein are shown in gray at 2 σ. F_o-F_c omit maps for the ions are shown in blue at 5 σ and for the unmodeled density at 2 σ.

conformational change in these structures, structure alignments with WT KcsA clearly demonstrated that the ester did not cause global structural perturbations to the protein, such as unwinding or misalignment of the pore helices.

2.3 Conclusions

The perturbation of an amide to an ester changed only two atoms in each monomer, or a total of eight atoms in the protein. In doing so, the ester modification reduced the amide bond dipole at each helix C-terminus and removed its connection to the hydrogen bonding network up the pore helix. The conductance of the ester containing protein was 10-fold reduced from natively folded KcsA, and we confirmed that the ester did not affect the structure of the selectivity filter or pore helices to any detectable level. The function of refolded KcsA with a native backbone has not been determined. This work is underway and will provide a crucial comparison between refolded KcsA with and without an ester-modified backbone. Based on our functional data at this point, we conclude that this small perturbation caused a drastic change in channel conductance, suggesting that the pore helix C-termini are involved in ion conduction.

More generally, these results are consistent with the ability for α-helix dipoles to participate in longer-range electrostatic interactions. It also demonstrates that the chemical modification of an amide to an ester is structurally tolerated at a helix C-terminus. This methodology can be a useful tool for the direct assessment of the helix dipole effect in proteins. With the growing body of literature on proteins made by peptide synthesis, EPL, or nonsense

suppression techniques, the incorporation of a backbone ester could be a general approach for studying a variety of proteins that have been proposed to utilize helix dipoles.

These studies also revealed a new conformation of KcsA. The conditions that affect the cavity structure will be discussed in detail in Chapter 3, and a physiological relevance for this conformation will be proposed in Chapter 4.

CHAPTER 3: FACTORS THAT AFFECT THE KcsA CAVITY STRUCTURE

As mentioned in Chapter 2, KcsA T74Aester and related control structures were crystallized in a new cavity conformation. The first part of this chapter presents the details of this conformation and the related control structures in more depth. Subsequently, we searched for conditions that would allow us to fold KcsA into its native cavity conformation. From these experiments, we successfully determined an approach for folding the cavity into its native conformation and we gained insight into factors that affect the cavity conformation of *in vitro* refolded or native recombinant KcsA.

3.1 Introduction

As introduced in Chapter 1, non-peptidic densities coming through lateral openings in the walls of the cavity have been observed in other cation channels (Payandeh et al., 2011; Brohawn et al., 2012; Miller and Long, 2012). An aromatic amino acid in the cavity of NavAb was proposed to interact with the non-peptidic density in that structure (Payandeh et al., 2011); however, the semisynthetic KcsA structures with D-Ala in the selectivity filter (Valiyaveetil et al., 2004b) or T74Aester in the pore helix (Chapter 2) are the first to suggest that a conformationally flexible amino acid sidechain (Phe103) guards access to the lateral openings (Figure 3.1). KcsA provided an opportunity to study the implications of this new density and conformational change in more detail.

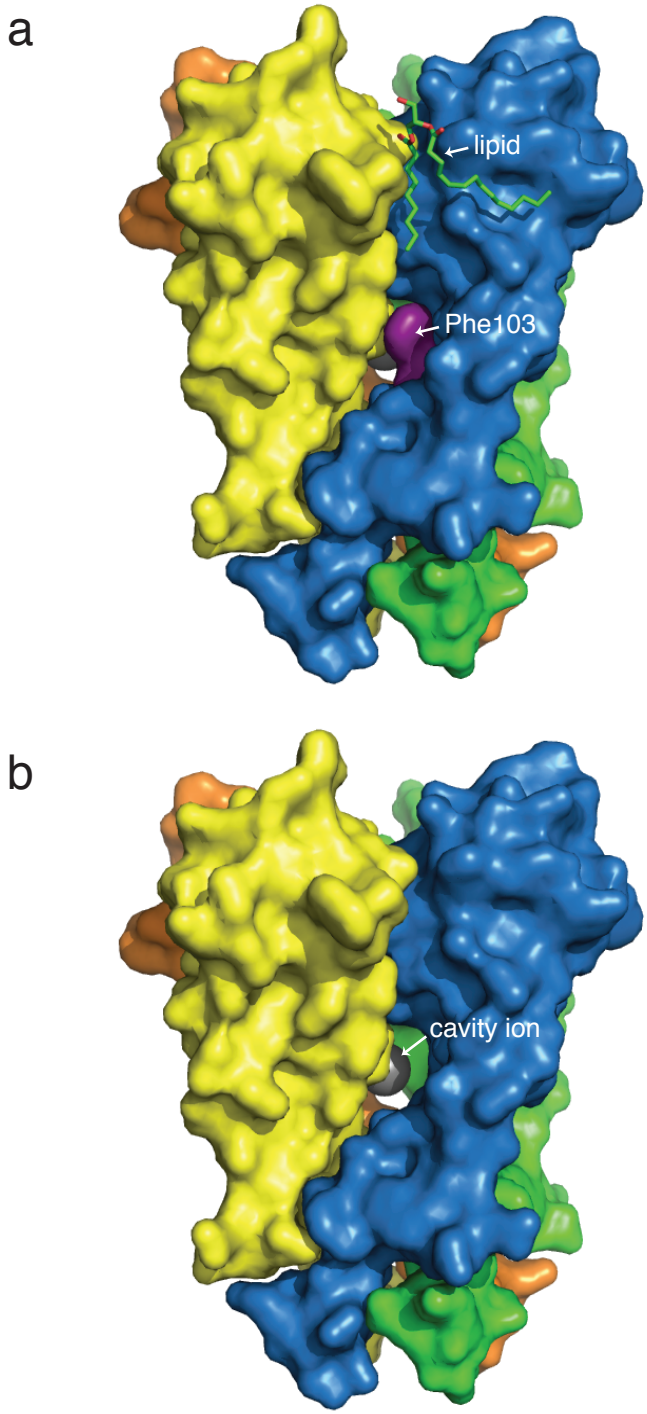

Figure 3.1: Surface renderings of KcsA with and without Phe103. Each subunit is colored a different color. (a) The model with Phe103 included, and shown in purple. The ordered part of the non-annular lipid is also shown in stick to display its proximity to Phe103 and the lateral opening. (b) The model with Phe103 as alanine. The cavity ion can now be seen in gray through the lateral opening.

3.2 Results

A new conformation of the KcsA cavity was observed for T74Aester, and experiments were performed to determine that this conformation was due to the *in vitro* folding step. In order to avoid this complication for future semisynthetic KcsA experiments, conditions were screened by crystallography in search of a strategy that would produce the native cavity conformation after *in vitro* folding. Several approaches were tested, including various *in vitro* folding conditions, lipid additives, mutations, and pore blocking small molecules. Through these experiments, we learned about factors that influence the cavity conformation of natively purified recombinant as well as *in vitro* refolded protein, including *in vitro* folding approaches that can produce a native cavity conformation.

3.2.1 Preface for the Interpretation of KcsA Structures

Several structures of KcsA will be presented throughout this chapter. For each of the structures, the overall protein backbone and the four potassium ions in the selectivity filter were very consistent. The features that varied were the presence or absence of a cavity ion, the conformation of Phe103, and the presence or absence of a non-peptidic density in the cavity. More specifically, Phe103 could either be observed in its native conformation, oriented vertically along the wall of the cavity, or in the flipped conformation, where the sidechain is oriented horizontally and directed in toward the center of the cavity. In most cases, these features are correlated to either produce the 'native' conformation (Phe103 pulled upward, blocking the lateral opening, and a cavity ion is present)

or the 'flipped' conformation (Phe103 flipped into the cavity, density coming through the lateral opening, and no cavity ion). All of the structural information presented is also summarized in Tables 2-10, as referenced throughout the text.

To convey this information in each figure, the selectivity filter is shown in stick, with the $2F_o$-F_c density map contoured at 2 σ (gray) and an ion-omit F_o-F_c map showing the ion density contoured at 5 σ (blue). Phe103 densities are shown with the same parameters as the selectivity filter. Cavity densities that are not from K^+ are also shown from the F_o-F_c map and colored in blue, but are contoured at 2 σ to show more detail. In short, $2F_o$-F_c maps show density based on the model presented; however, F_o-F_c maps highlight areas where the data deviate from the model. These are called omit maps, when the region of interest is removed from the model used to generate the map, and may show a less biased representation of that part of the structure.

3.2.2 Effects of the Method of Protein Preparation on KcsA Structure

The crystal structure of semisynthetic T74Aester revealed a new cavity conformation involving a conformational change in the KcsA protein in conjunction with the loss of a cavity ion and the presence of new non-peptidic densities that enter the cavity through lateral openings. The predominant conformational change in the protein occurs in the sidechain of Phe103. In natively purified recombinant protein, this sidechain is oriented mostly vertical with respect to the conduction axis, in the m-85° rotamer (χ_1=-68°); however, in the structures of the new cavity conformation, the Phe sidechain is close to

horizontal, in the t80° rotamer (χ_1=178°), and flipped into the center of the cavity. This phenylalanine conformation precludes cavity K^+ binding. The Phe103 conformational change also exposes lateral openings in the sides of the cavity, with non-peptidic densities observed coming through each of these openings. In this part of KcsA, Phe103 is the only residue separating the water-filled cavity from the lipid membrane environment (Figure 3.1).

To determine the factors responsible for the flipped conformation in the semisynthetic T74Aester structure, KcsA was prepared in a few different ways. Specifically, three different methods—native recombinant preparation, *in vitro* refolding, or protein semisynthesis—were compared while keeping the sequences of each protein the same. Semisynthetic KcsA was prepared as it was for T74Aester in Chapter 2, but with alanine at position 74 instead of lactic acid, so as to have no unnatural modifications in the protein. These proteins each included the S69C mutation for EPL and the T74A sidechain mutation for consistency with the helix dipole experiments. The cavity conformations were compared between these three conditions using protein structures. The statistics for these structures are summarized in Table 2.

The T74A natively purified recombinant protein revealed a native cavity structure, with a cavity ion and native Phe103 (Figure 3.2a). This suggested that the T74A sidechain mutation was not responsible for the flipped conformation. The structure of semisynthetic KcsA (T74Ass) was in the flipped conformation: no cavity ion, Phe103 flipped into the cavity, and a non-peptidic density through the lateral openings (Figure 3.2b). Because this structure was in the same

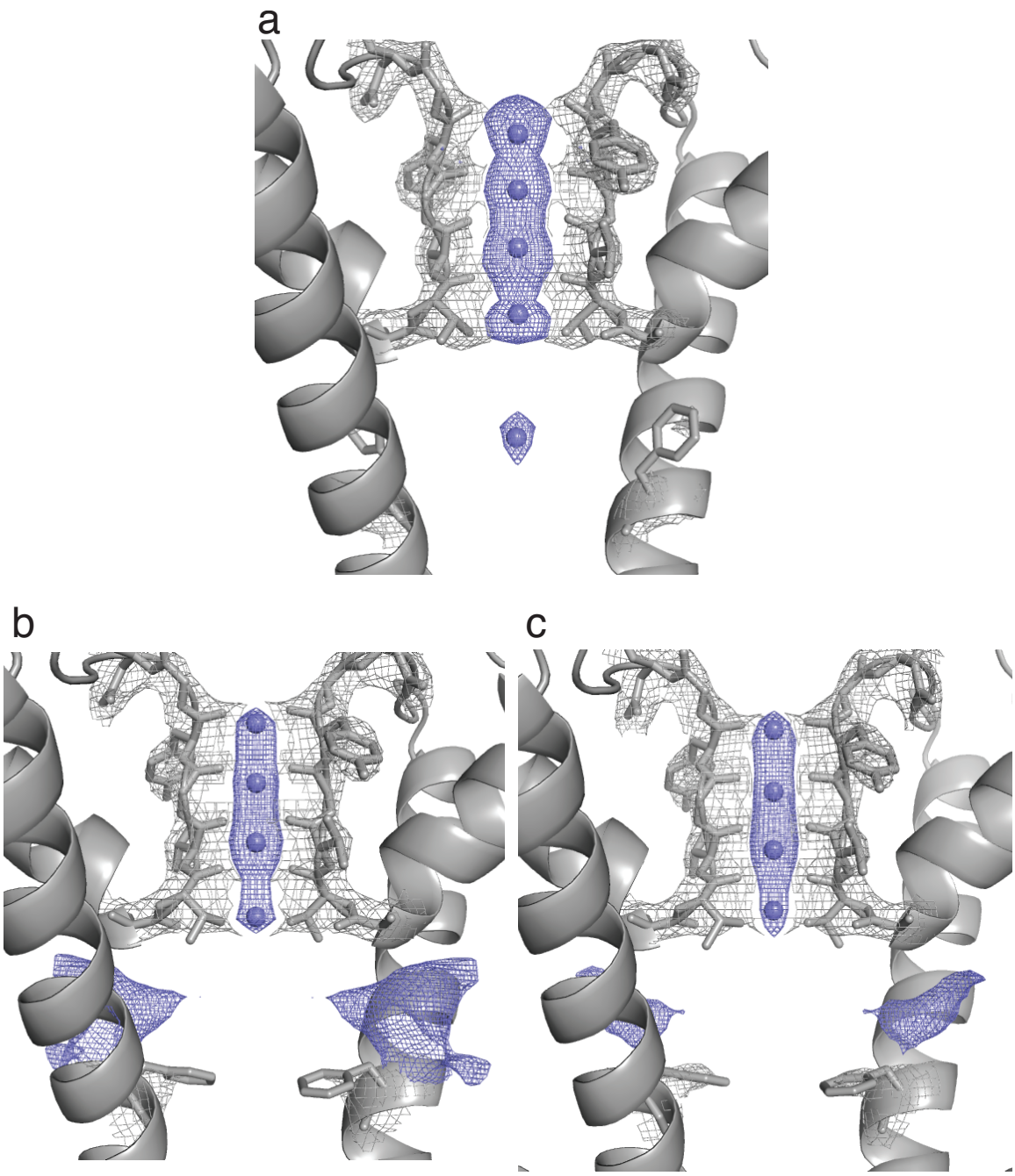

Figure 3.2: Structures of KcsA (S69C, T74A) prepared by various methods: (a) Natively prepared recombinant, (b) semisynthetic, and (c) recombinantly expressed, unfolded, and refolded *in vitro* preparations of KcsA S69C T74A. The structures were refined to 2.9 Å, 3.35 Å, and 3.05 Å resolution, respectively. The selectivity filter residues and Phe103 are shown in stick and the potassium ions are shown in blue. $2F_o$-F_c density maps for the protein are shown in gray at 2 σ. F_o-F_c omit maps for the ions are shown in blue at 5 σ and for the unmodeled density at 2 σ.

Table 2: Summary of structures of T74Aester and controls

	T74Aester	T74Aester	rT74A	T74Ass	T74Aref
crystal	43	044/20	211	98	215
date	8/17/10	11/21/10	1/23/11	11/21/10	1/23/11
mutations					
	S69C T74A ester	S69C T74A ester	S69C T74A	S69C T74A	S69C T74A
origin					
native rec.			rec		
native refolded					soy/MES
semisynthetic	soy/MES	soy/MES		soy/MES	
+ throughout					
+ folding only					
+ after purif.					
data					
resolution (Å)	2.7	2.3	2.9	3.35	3.05
spacegroup	I4	I4	I4	I4	I4
I/sigma	19.4(2.2)	24.6(0.7)	14.5(1.4)	14.9(2.4)	12.6(1.5)
redundancy	3.8(3.8)	3.4(3.1)	3.7(3.7)	7.4(7.5)	3.7(3.7)
completeness	99.8(100)	99.3(98.3)	100(100)	99.9(100)	100(100)
model					
R/Rfree	.254/.284	.250/.282	.223/.257	.220/.270	.244/.294
lengths/angles	.007/.981	.001/1.23	.011/1.42	.008/1.09	.010/1.32
RMSD		0.289			
structural features					
cavity ion	no	no	yes	no	no
flipped F103	yes	yes	no	yes	yes
filler density	yes	yes	outside	yes	some

Summary of structure data: *Mutations:* All mutations are listed, (-) denotes a WT sequence. *Method:* The method of preparation of the protein: natively purified recombinant (native rec.), recombinant unfolded and *in vitro* refolded (native refolded), or semisynthetic, with requisite *in vitro* folding. The (+) section lists additives, organized by when they were added during the protein preparation. *Data:* Statistics for the dataset, with data for the highest resolution shell in parentheses. *Model:* Statistics for the refined model are shown. *RMSD:* RMSDs calculated with all Cα atoms in the pore domain in comparison to WT KcsA (1k4c), when available. *Structure features:* Summarizes the cavity conformation for each structure, where density refers specifically to the non-peptidic density.

conformation as T74Aester, the flipped cavity conformation was not likely caused solely by the presence of the ester. Notably, *in vitro* refolded, recombinant KcsA (T74Aref) was also in the flipped conformation (Figure 3.2c). The cavity ion, Phe103, and extra density were consistent with T74Aester and T74Ass, suggesting that this conformational change arises generally from *in vitro* folding of the protein. From these structures, we were able to compare three different methods for preparing the same protein and determined that the folding conditions of KcsA can affect its three-dimensional structure.

3.2.3 Lipids in Membrane Protein Folding

This section will focus on the interactions between lipids and KcsA. Lipids are very important for membrane protein folding (Mitchell, 2012). Folding of KcsA *in vitro* requires the presence of lipids and anionic lipids are required for protein function (Valiyaveetil et al., 2002b), but little is known about whether different lipids affect KcsA structure in systematic ways. Recombinant KcsA was natively folded in the presence of phospholipids in *E. coli*. In order to study pure protein by electrophysiology or crystallography, a detergent extraction step was required in order to purify folded protein away from the lipid vesicles. All of our experiments with KcsA used n-decylmaltoside (DM) for extraction and solubilization. We studied native recombinant KcsA by extracting and purifying folded protein from *E. coli* membranes. We also studied *in vitro* refolded protein by unfolding recombinant KcsA and refolding it under particular conditions in the presence of lipid vesicles, followed by final extraction and purification.

In order to prepare KcsA by semisynthesis—with its ligation junction in the middle of the folded transmembrane domain—the protein must be subsequently folded *in vitro* in the presence of lipid vesicles (Valiyaveetil et al., 2002b). This methodology is currently limited by being able to only produce KcsA in the flipped cavity conformation, so we set out to find new conditions for the *in vitro* folding of KcsA that would achieve the native conformation in the cavity. To do this, we first explored several ways to alter the *in vitro* folding conditions or protein-lipid interactions of KcsA.

3.2.3.1 Comparing *In Vitro* Folding Conditions for KcsA

Three *in vitro* folding conditions have been reported for KcsA: a Tris buffered soybean lipid extract (Valiyaveetil et al., 2002b); a MES buffered soybean lipid extract (Muir lab protocol); and a recently optimized HEPES buffered 1-palmitoyl-2-oleoyl-sn-glycero-3-phosphocholine (POPC), with conditions graciously provided by Dr. Francis Valiyaveetil (personal communication). All of these conditions fold KcsA in the presence of phospholipids: either crude soybean polar lipid extract containing about 45% phosphatidylcholine (PC), or pure POPC lipids. Either of the soybean lipid conditions may have been used at the time of the published KcsA semisynthesis studies.

The Valiyaveetil lab has moved to using pure POPC lipids for protein folding as the reaction occurs with good yield and much more rapidly than in the presence of soybean lipid extract (personal communication). These results were

confirmed by my experiments comparing the rate and extent of KcsA folding in the different conditions (Figure 3.3a).

Folding conditions were next compared by solving X-ray crystal structures of KcsA prepared by each protocol. The statistics for these structures are summarized in Table 3. All three conditions still produced KcsA structures in the flipped conformation. The structures of KcsA T74A refolded in soy/MES and in POPC/HEPES are representative and shown in Figure 3.2 and Figure 3.3b respectively. These results suggested that a specific folding condition was not responsible for producing the flipped cavity conformation. It is possible, however, that other variables we have not tested could account for the conformational change of *in vitro* folded proteins, especially considering that the structure of semisynthetic KcsA containing G77ester in the selectivity filter had a native cavity conformation (Valiyaveetil et al., 2006b). For all subsequent folding studies, the POPC lipid conditions were used as they produced the folded product rapidly and in high yield.

3.2.3.2 KcsA Exposed to Lipid Vesicles

One possible explanation for observing this alternative conformation after *in vitro* folding is that some component of the folding cocktail or the subsequent detergent extraction biases the structure into the flipped state. To look more closely at the role of lipids or other small molecules on the conformations of KcsA, recombinant KcsA (T74A) was prepared and mixed 1:1 with soybean lipid vesicles either in standard buffer conditions for KcsA or in the soybean lipid

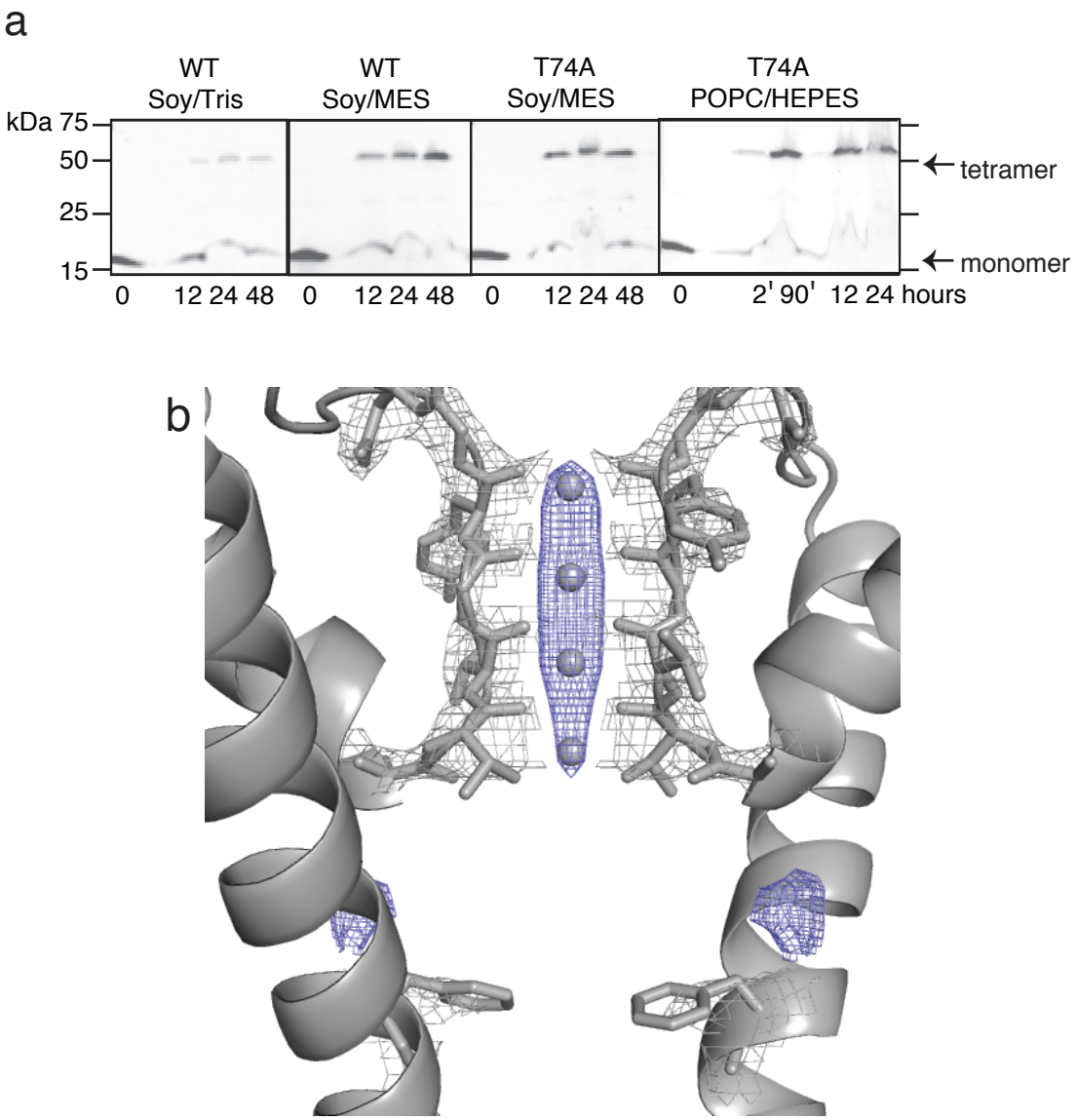

Figure 3.3: KcsA folded under varied conditions. (a) Timecourse of *in vitro* folding of KcsA WT or T74A, folded in the presence of different lipid folding conditions, listed as lipid/buffer, as monitored by SDS-PAGE. The timepoints shown are in hours, except where designated as minutes (2', 90') to show the faster kinetics of the POPC folding reaction. (b) The crystal structure of a representative folding condition is shown: T74A was folded in POPC lipids with HEPES buffer, with diffraction to 3.6 Å. The crystal structure of T74A in Soy/MES was shown previously in Figure 3.2. The selectivity filter residues and Phe103 are shown in stick and the potassium ions are shown in blue. $2F_o$-F_c density maps for the protein are shown in gray at 2 σ. F_o-F_c omit maps for the ions are shown in blue at 5 σ and for the unmodeled density at 2 σ.

Table 3: Summary of structures of refolded KcsA

	ssT74A	soyT74A	popcT74A	trisWT	mesWT	WT ref
crystal	98	215	373	293	239	1039
date	11/21/10	1/23/11	2/25/11	2/25/11	6/6/11	2/19/12
mutations						
	S69C T74A	S69C T74A	S69C T74A	-	-	-
origin						
native rec. native refolded semisynthetic	soy/MES	soy/MES	POPC	soy/Tris	soy/MES	POPC
+ throughout + folding only + after purif.						
data						
resolution (Å)	3.35	3.05	3.6	3.7	3	3.4
spacegroup	I4	I4	I4	I4	I4	I4
I/sigma	14.9(2.4)	12.6(1.5)	7.6(1.6)	7.2(1.7)	16.4(1.6)	7.65(1.3)
redundancy	7.4(7.5)	3.7(3.7)	3.3(2.9)	3.1(2.9)	3.7(3.7)	5.3(5.2)
completeness	99.9(100)	100(100)	99.8(99.5)	98.7(97.8)	99.7(99.3)	100(100)
model						
R/Rfree	.220/.270	.244/.294	.259/.329	.256/.324	.248/.292	.254/.284
lengths/angles RMSD	.008/1.09	.010/1.32	.007/1.05	.007/0.99	.009/1.18	.007/1.03
structural features						
cavity ion	no	no	no	no	no	no
flipped F103	yes	yes	yes	unclear	likely	likely
filler density	yes	some	hardly	unclear	likely	likely

Summary of structure data: *Mutations:* All mutations are listed, (-) denotes a WT sequence. *Method:* The method of preparation of the protein: natively purified recombinant (native rec.), recombinant unfolded and *in vitro* refolded (native refolded), or semisynthetic, with requisite *in vitro* folding. The (+) section lists additives, organized by when they were added during the protein preparation. *Data:* Statistics for the dataset, with data for the highest resolution shell in parentheses. *Model:* Statistics for the refined model are shown. *RMSD:* RMSDs calculated with all Cα atoms in the pore domain in comparison to WT KcsA (1k4c), when available. *Structure features:* Summarizes the cavity conformation for each structure, where density refers specifically to the non-peptidic density.

folding mixture. Though the protein in these conditions was never unfolded, the structures again reveal KcsA in the flipped conformation, further suggesting that there may be a specific molecular interaction taking place between the protein and lipids (Figure 3.4). The statistics for these structures are summarized in Table 4. Similar to the *in vitro* folding experiments, the proteins exposed to lipid vesicles required detergent extraction. It is also possible that the high concentration of detergent at this step could affect cavity conformation.

3.2.3.3 Exogenous Lipids Added to KcsA

KcsA must be purified away from the lipid membrane or lipid vesicles using DM detergent, in order to be studied structurally. However, we were able to explore whether small amounts of lipids, added to natively purified KcsA in detergent micelles, would affect its structure.

Low concentrations of phospholipids are sometimes added to purified proteins, such as some eukaryotic membrane proteins, to improve their stability in detergent (Long et al., 2007). A recent structure of an inward-rectifier (K_{ir}) potassium channel revealed a specific interaction between pyrophosphatidic acid (PPA) and the pore domain of the channel (Hansen et al., 2011). We performed similar experiments with KcsA by preparing purified recombinant KcsA and then introducing one of a variety of lipids just before crystallization. The statistics for these structures are summarized in Table 5.

KcsA was screened against several pure phospholipids: 1-palmitoyl-2-oleoyl-sn-glycero-3-phosphatidylcholine (POPC), 1-palmitoyl-2-oleoyl-sn-

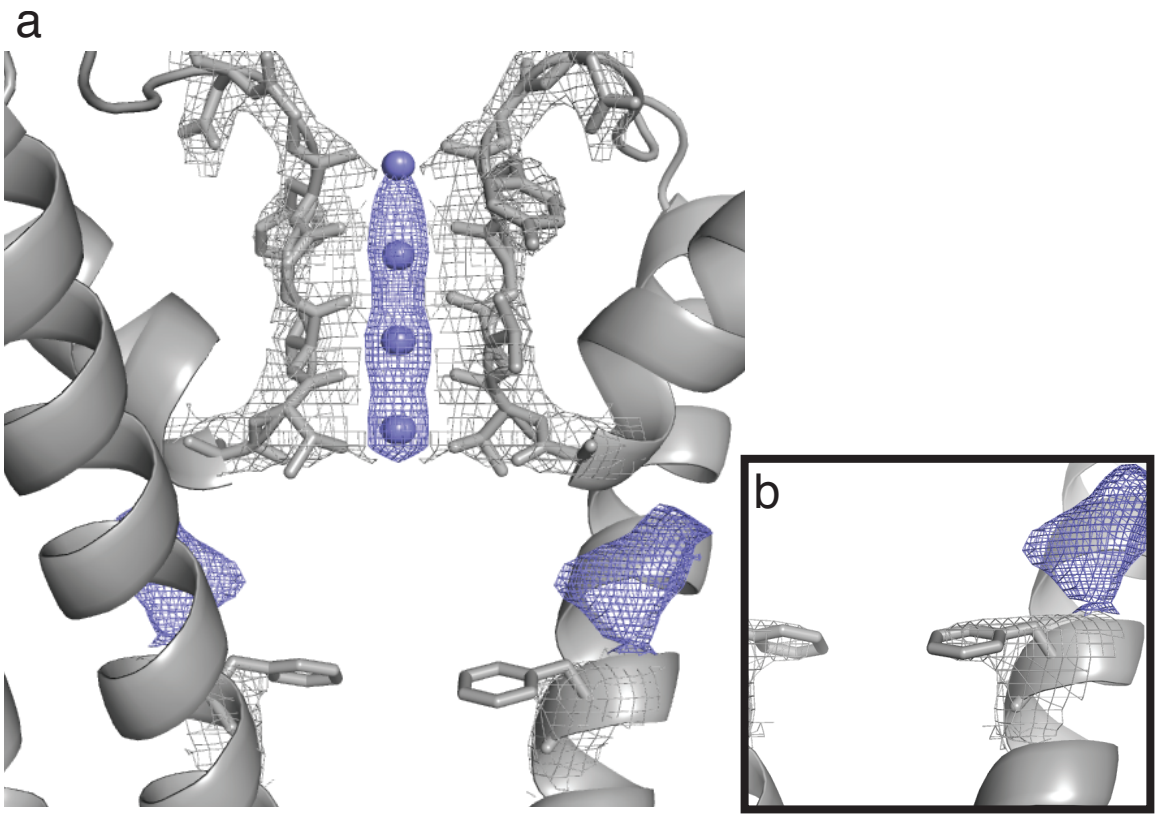

Figure 3.4: Structure of KcsA T74A exposed to soybean lipid vesicles. (a) Natively prepared recombinant KcsA was exposed to lipid vesicles, then extracted with detergent, and purified. This structure was refined to 3.2 Å resolution. The selectivity filter residues and Phe103 are shown in stick and the potassium ions are shown in blue. $2F_o$-F_c density maps for the protein are shown in gray at 2 σ. F_o-F_c omit maps for the ions are shown in blue at 5 σ and for the unmodeled density at 2 σ. (b) Inset shows the same view as panel (a) but with the Phe103 $2F_o$-F_c density map contoured at 1 σ to show density for the residue in this conformation.

Table 4: Summary of structures of KcsA exposed to lipid vesicles

	mixrT74A	soyrT74A
crystal	324	319
date	2/25/11	2/25/11
mutations		
	S69C T74A	S69C T74A
origin		
native rec.	rec	rec
native refolded		
semisynthetic		
+ throughout		
+ folding only		
+ after purif.		
+ exposed	soy/MES	soy only
data		
resolution (Å)	3.5	3.2
spacegroup	P4	P4
I/sigma	7.0(1.1)	12.6(1.2)
redundancy	3.4(2.3)	3.7(3.3)
completeness	96.7(89.4)	99.6(98.8)
model		
R/Rfree	.350/.408	.247/.286
lengths/angles	.008/1.12	.008/1.16
RMSD		
structural features		
cavity ion	no	no
flipped F103	yes	yes
filler density	unclear	yes

Summary of structure data: *Mutations:* All mutations are listed, (-) denotes a WT sequence. *Method:* The method of preparation of the protein: natively purified recombinant (native rec.), recombinant unfolded and *in vitro* refolded (native refolded), or semisynthetic, with requisite *in vitro* folding. The (+) section lists additives, organized by when they were added during the protein preparation. In this specific case 'exposed' refers to mixing native recombinant protein with lipid vesicles. *Data:* Statistics for the dataset, with data for the highest resolution shell in parentheses. *Model:* Statistics for the refined model are shown. *RMSD:* RMSDs calculated with all Cα atoms in the pore domain in comparison to WT KcsA (1k4c), when available. *Structure features:* Summarizes the cavity conformation for each structure, where density refers specifically to the non-peptidic density.

glycero-3-phosphatidylethanolamine (POPE), and 1-palmitoyl-2-oleoyl-sn-phosphatidylglycerol (POPG). Structures of KcsA were solved in the presence of POPE or POPC. In these structures, the cavity was consistently in a native-like conformation (Figure 3.5a). In most crystal structures of KcsA, the first 20 amino acid residues are unstructured; however, the POPE and POPC structures showed some added density that could be N-terminal residues in a more ordered conformation (Figure 3.5c). Attempts to build a model into this new density suggested that the newly-structured region is extending upward into what would be the lipid bilayer (or the detergent micelle) and is thus not likely physiologically relevant. An ordered lipid molecule was not observed in this part of the protein. A complete model was not determined for these conditions, in the interest of focusing on the structure of the cavity.

KcsA was also studied in the presence of 1-palmitoyl-2-oleoyl phosphatidic acid (POPA) and dioctanoyl glycerol pyrophosphatidic acid (PPA), in either their long-chain C18 (18-carbon) form or a truncated, detergent-like C8 (8-carbon) form. These conditions were studied by crystallography multiple times; however, depending on the batch, they would sometimes produce a native-like structure and other times a flipped structure. One representative structure of the flipped conformation is shown in Figure 3.5b. Interestingly, these structures consistently diffracted to high resolution; however, it is unclear whether the densities in the lateral openings could be composed of the specific phospholipid added.

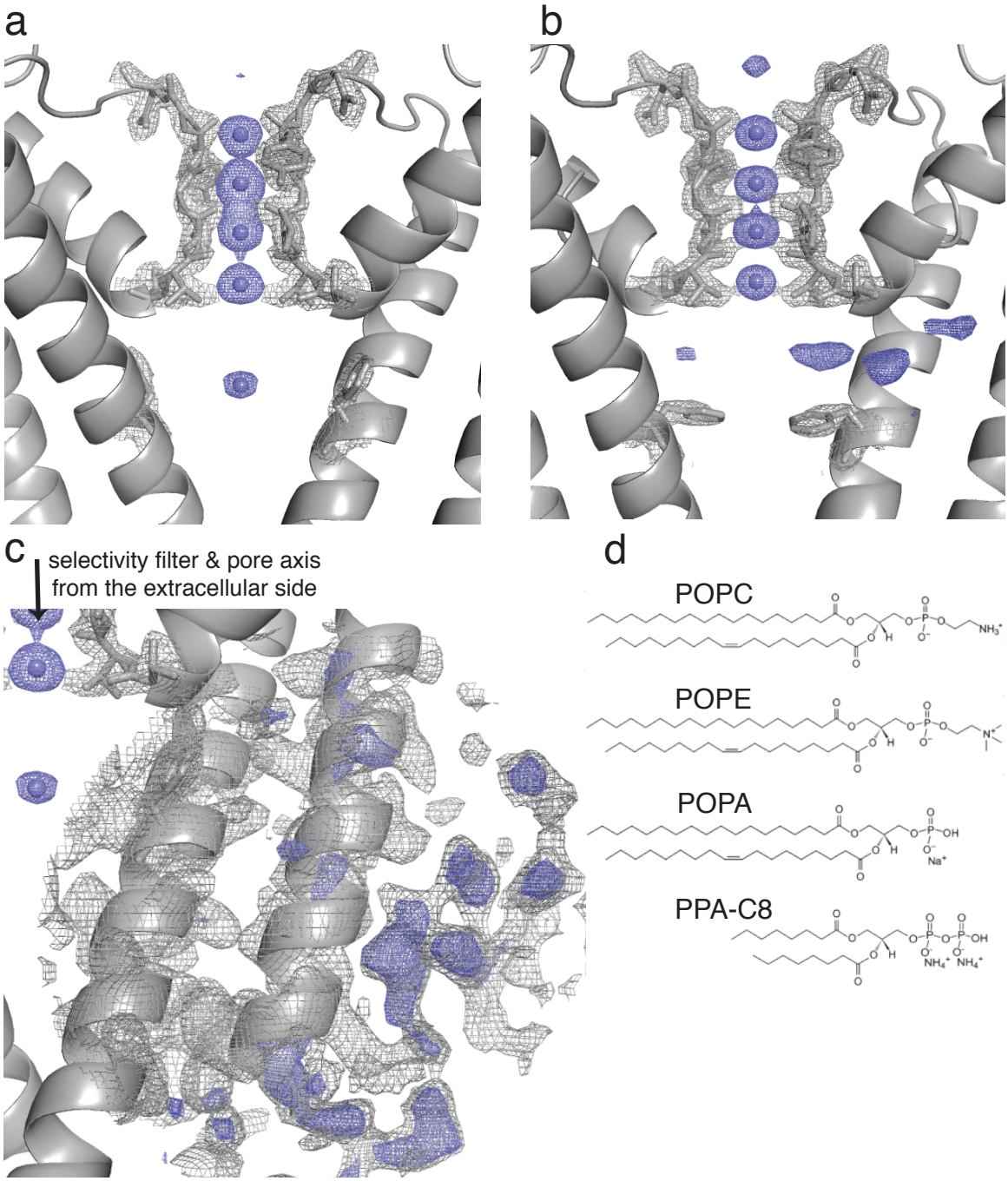

Figure 3.5: Structures of KcsA exposed to lipids. (a) KcsA exposed to POPE refined to 2.4 Å resolution. (b) A representative structure of KcsA exposed to PPA, refined to 2.07 Å resolution in the flipped conformation. Identical conditions also produced the native cavity conformation (not shown). $2F_o$-F_c density maps for the protein are shown in gray at 2 σ. F_o-F_c omit maps for the ions are shown in blue at 5 σ and for the unmodeled density at 2 σ. (c) KcsA from panel (a), looking at the lower part of the protein. The additional density is shown with both $2F_o$-F_c maps (gray) at 1 σ and F_o-F_c maps (blue) at 3 σ. (d) Structures of some of the lipids tested.

Table 5: Summary of structures of native KcsA with lipids added

		crystal	date	resolution (Å)	cavity ion	Phe103
PPA C8	1mM	669	9/6/11	2.06	yes	native
PPA C8	3 mM	673	9/6/11	2.15	yes	native
PPA C8	4 mM	713	10/7/11	2.4	yes	native
PPA C8	5 mM	529	7/27/11	2.07	no	flipped
PPA C8	10 mM	719	10/7/11	2.15	yes	native
PPA C8	10 mM	721	10/7/11	2.1	yes	native
PPA C18	1 mM	681	9/6/11	1.97	yes	native
PPA C18	3 mM	690	9/6/11	2.2	yes	native
POPA C8	1 mM	634	9/6/11	2.15	yes	native
POPA C8	4 mM	731	10/7/11	2.28	no	flipped
POPA C8	4 mM	936	12/11/11	2.4	yes	native
POPA C8	10 mM	736	10/7/11	3	no	flipped
POPA C8	10 mM	958	12/11/11	3.1	yes	native
POPA C18	1 mM	651	9/6/11	1.97	yes	native
POPA C18	4 mM	959	12/11/11	2.3	yes	native
POPA C18	0.5 mg/ml	501	7/27/11	2.5	yes	native
POPC (C18)	0.5 mg/ml	498	7/27/11	3	yes	native
POPE (C18)	0.5 mg/ml	489	7/27/11	2.4	yes	native

Summary of structure data: This table summarizes several conditions that were repeated several times, some of which gave inconsistent results. For all structures listed, lipids were added after purification at the concentration noted. The columns on the right summarize the cavity structure observed for each dataset. (abbreviations: PPA, pyrophosphatidic acid; POPA, phosphatidic acid; C8 or C18 refer to the alkly chain length)

In summary, exogenous lipids added to purified KcsA were able to affect the conformation of the cavity, though not in a reliable fashion, and we cannot conclude whether there are specific lipid interactions taking place in the lateral openings of the flipped conformation of KcsA. Hypotheses for the inconsistent role of the POPA and PPA lipids in KcsA will be presented in more detail in the discussion (Chapter 5).

3.2.3.4 Summary of Lipid Effects on KcsA

These experiments demonstrated several ways that lipids can alter the cavity conformation of native recombinant or *in vitro* refolded KcsA. The effect of exposing folded KcsA channels to lipid vesicles, or possibly to the subsequent detergent extraction step, is sufficient to convert the cavity into the flipped conformation. In contrast, the studies on the effects of exogenously added lipids showed that addition of small amounts of short chain lipids (C8) can produce the flipped conformation, although not consistently, while long-chain (C18) lipids had no effect. Variations in lipids did not reveal conditions that could produce the native cavity conformation for *in vitro* refolded KcsA, but these data suggest that lipids or detergents may still play an interesting role in the conformational change in the cavity of KcsA.

3.2.4 Mutagenesis of Residues That Affect KcsA Cavity Conformation

We were not able to determine *in vitro* folding conditions which produced structures with the native cavity conformation in KcsA. Therefore mutagenesis

was used to remove the Phe103 sidechain entirely or to try to stabilize the environment around Phe103 with nearby mutations. First, Phe103 was mutated to alanine to examine the effect of permanently exposed lateral openings. Then, amino acid residues near Phe103 were screened for higher tetramer stability. The most stabilizing mutations were studied by crystallography in both recombinant and *in vitro* refolded forms. The statistics for all of the structures presented in Section 3.2.4 are summarized in Table 6. Additionally, these mutants were characterized by electrophysiology. Through these experiments, conclusions were made about the role of selected amino acid residues in stabilizing the cavity conformation and mediating potassium conductance.

3.2.4.1 Mutation of Phe103

Most of the conformational change observed in the cavity between the recombinant and refolded structures involved Phe103. We were curious whether removal of this sidechain, through mutation to alanine, would perturb channel function. In a previous study, Phe103 was proposed to be important for the transition between the closed and inactivated states of KcsA through electrophysiology and crystallography experiments of the double mutant E71A/F103A (Cuello et al., 2010a). These data suggested that functionally the F103A mutation is conductive, and structurally it does not affect ion density in the cavity (Cuello et al., 2010b). Thus, the F103A mutation was explored as a new way to obtain *in vitro* folded KcsA with a native-like cavity, most importantly including a cavity ion.

Crystal structures of KcsA were obtained with the F103A mutation present (with and without T74A) (Figure 3.6a). The structure statistics are summarized in Table 6. Each of the structures contained a cavity ion and a non-peptidic density present behind the lateral opening, which was similar to the previously published structure (Cuello et al., 2010b). This density was situated over the lateral opening, but did not protrude into the cavity. The F103A mutant protein was also prepared through *in vitro* refolding and the structure looked identical to the native recombinant protein (Figure 3.6b).

Bilayer electrophysiology demonstrated that the F103A mutation only slightly reduced potassium conductance (Figure 3.6c). Consequently, this mutation presented a potential strategy for studying refolded proteins with a more native-like cavity structure. However, this protein showed lower stability by SDS-PAGE and had a lower folding efficiency than the WT protein.

The F103A mutation was incorporated into the semisynthetic strategy for the T74Aester protein. N-peptide and modified C-peptide (now with S69C, T74Aester, and F103A) were prepared and ligated; however, the combined destabilization of the ester and the F103A mutation prohibited the protein folding reaction, and no folded product was observed by ELISA. This mutation may be useful for preparing *in vitro* refolded KcsA under certain circumstances, so long as some reduction in protein stability is tolerable.

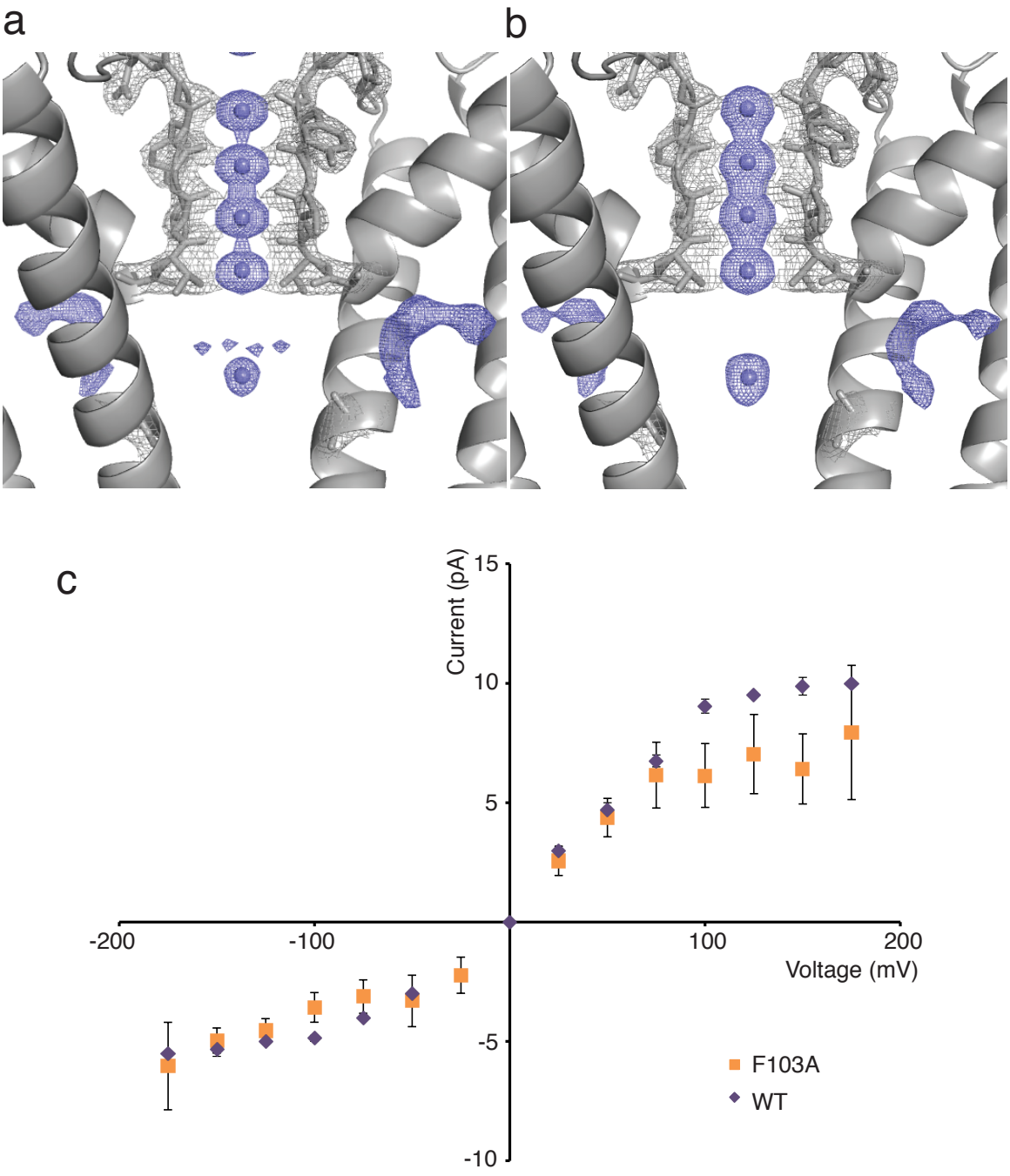

Figure 3.6: Structure and function of KcsA F103A. (a) Natively prepared recombinant and (b) *in vitro* folded F103A KcsA, refined to 2.6 Å and 2.7 Å resolution, respectively. The selectivity filter residues and F103A are shown in stick and the potassium ions are shown in blue. $2F_o$-F_c density maps for the protein are shown in gray at 2 σ. F_o-F_c omit maps for the ions are shown in blue at 5 σ and for the unmodeled density at 2 σ. (c) Current-voltage trace of F103A conductance (orange) compared to WT conductance (purple). Error bars are from an average of at least three independent bilayer recordings.

Table 6: Summary of structures with F103A mutations

	F103A	T74A F103A	POPC T74A F103A
crystal	235b	155	346
date	2/25/11	1/23/11	2/25/11
mutations			
	F103A	S69C T74A F103A	S69C T74A F103A
origin			
native rec. native refolded semisynthetic	rec	rec	POPC
+ throughout + folding only + after purif.			
data			
resolution (Å)	2.85	2.6	2.7
spacegroup	I4	I4	I4
I/sigma	11.6(1.6)	11.3(1.4)	12(2.2)
redundancy	3.7(3.7)	3.6(3.4)	3.7(3.8)
completeness	99.9(100)	99.5(98.7)	99.7(100)
model			
R/Rfree	.236/.285	.219/.266	.234/.273
lengths/angles RMSD	.011/1.42	.009/1.21	.007/1.03
structural features			
cavity ion	yes	yes	yes
flipped F103	-	-	-
filler density	outside	outside	outside

Summary of structure data: *Mutations:* All mutations are listed, (-) denotes a WT sequence. *Method:* The method of preparation of the protein: natively purified recombinant (native rec.), recombinant unfolded and *in vitro* refolded (native refolded), or semisynthetic, with requisite *in vitro* folding. The (+) section lists additives, organized by when they were added during the protein preparation. *Data:* Statistics for the dataset, with data for the highest resolution shell in parentheses. *Model:* Statistics for the refined model are shown. *RMSD:* RMSDs calculated with all Cα atoms in the pore domain in comparison to WT KcsA (1k4c), when available. *Structure features:* Summarizes the cavity conformation for each structure, where density refers specifically to the non-peptidic density.

3.2.4.2 Mutations That Affect Tetramer Stability

The complications due to the reduced stability of the F103A mutant channel led us to screen for other mutations that would produce a more stable protein. A simple assay was designed for screening mutants by analyzing tetramer stability in SDS-PAGE. Specifically, the samples were kept at 4 °C or room-temperature (RT) before and during SDS-PAGE or heated to 50 °C or 100 °C for various amounts of time before running SDS-PAGE at RT.

A series of proteins were designed with mutations in close proximity to F103A. A few tryptophan mutations were selected because previous work suggested that they conferred added stability in KcsA (Irizarry et al., 2002). The open and closed forms of the NaK channel (Shi et al., 2006; Alam and Jiang, 2009a) and the open MthK channel (Jiang et al., 2002a) were aligned with KcsA in order to suggest mutagenesis candidates. One phenylalanine residue in particular (Phe85 in NaK, corresponding to Val97 in KcsA) was in an optimal conformation for blocking the lateral opening of the closed channel. In total, seven of these mutations were screened in both the WT and the F103A backgrounds. An additional five proteins contained mutations of Phe103 to other amino acids (Figure 3.7a). Of the mutations at the Phe103 position, only F103V showed some tetramer stability. Of the mutations at other positions, the stability was consistently better for proteins containing Phe103 (Figure 3.7b). The trends were also consistent between the different temperatures tested.

V97F was selected as the most stable mutant (Figure 3.7c) and was studied by electrophysiology and crystallography, both independently and as an

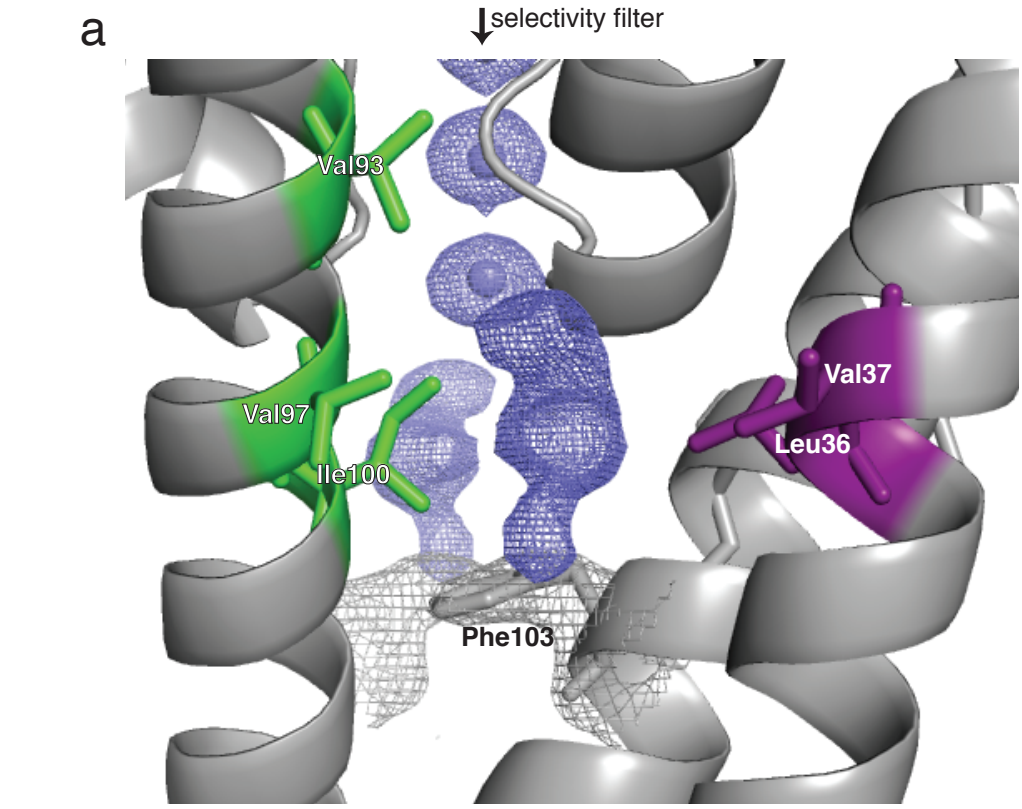

b

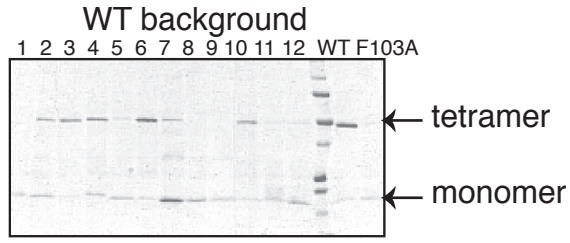

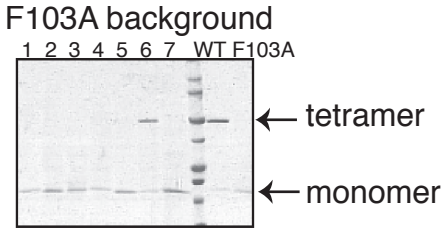

c

1	L36Y	D	+F103A	F
2	L36M	B	+F103A	F
3	V37F	A	+F103A	C
4	V37W	B	+F103A	F
5	V93W	D	+F103A	F
6	V97F	A+	+F103A	B
7	V97W	B	+F103A	F
8	I100F/F103I	F		
9	I100F/F103A	F		
10	F103V	B		
11	F103I	D		
12	F103T	D		

Figure 3.7: Mutants screened for stability near Phe103. (a) A zoomed in view of T74Aester (as shown in Figure 2.8) but looking from the side, through the lateral opening. Residues chosen for mutation are highlighted in green (inner helix of one subunit) and purple (outer helix of the next subunit). (b) Sample SDS-PAGE gels from stability assays, where tetramer bands suggest more stable protein. WT and F103A are shown on the right of each gel as controls. Numbers correspond to positions in the table in panel (c). (c) A table summarizing the relative stability of each mutation as observed by SDS-PAGE after incubating each mutant protein at various temperatures. Stability was graded, with A+ being the most stable.

F103A double mutant. Electrophysiology experiments for V97F (Figure 3.8b) demonstrated a slight reduction in channel conductance and the conductance for the double mutant, V97F/F103A (Figure 3.9b), behaves similarly to the WT channel, demonstrating that these mutations do not significantly perturb channel function.

For structural studies, each mutant was prepared both as the native recombinant protein and using the *in vitro* refolding method. The statistics for these structures are summarized in Table 7. Structures of the refolded proteins looked identical to the natively prepared recombinant versions, and thus only the refolded proteins are shown (Figure 3.8a, 3.9a). Each of these proteins showed a native cavity environment with a cavity ion. V97F was predicted to block the lateral opening from overlays of the KcsA and NaK channels, and the V97F KcsA structure is consistent with this hypothesis. V97F is oriented in an aromatic-aromatic T-shaped stacking orientation with Phe103 (Figure 3.8b) (Chourasia et al., 2011). Though the alignment of Phe103 and V97F is not quite optimal for this interaction, it may explain some of the added stability for the V97F mutant. The phenylalanine of V97F in the double mutant channels is in a different conformation than the single mutant channel, suggesting that V97F makes a specific interaction with Phe103. While it may be expected for the double mutant to have identical recombinant and *in vitro* folded structures, it is notable that the presence of V97F in the WT background is sufficient to hold Phe103 in its native, upright conformation through the folding process.

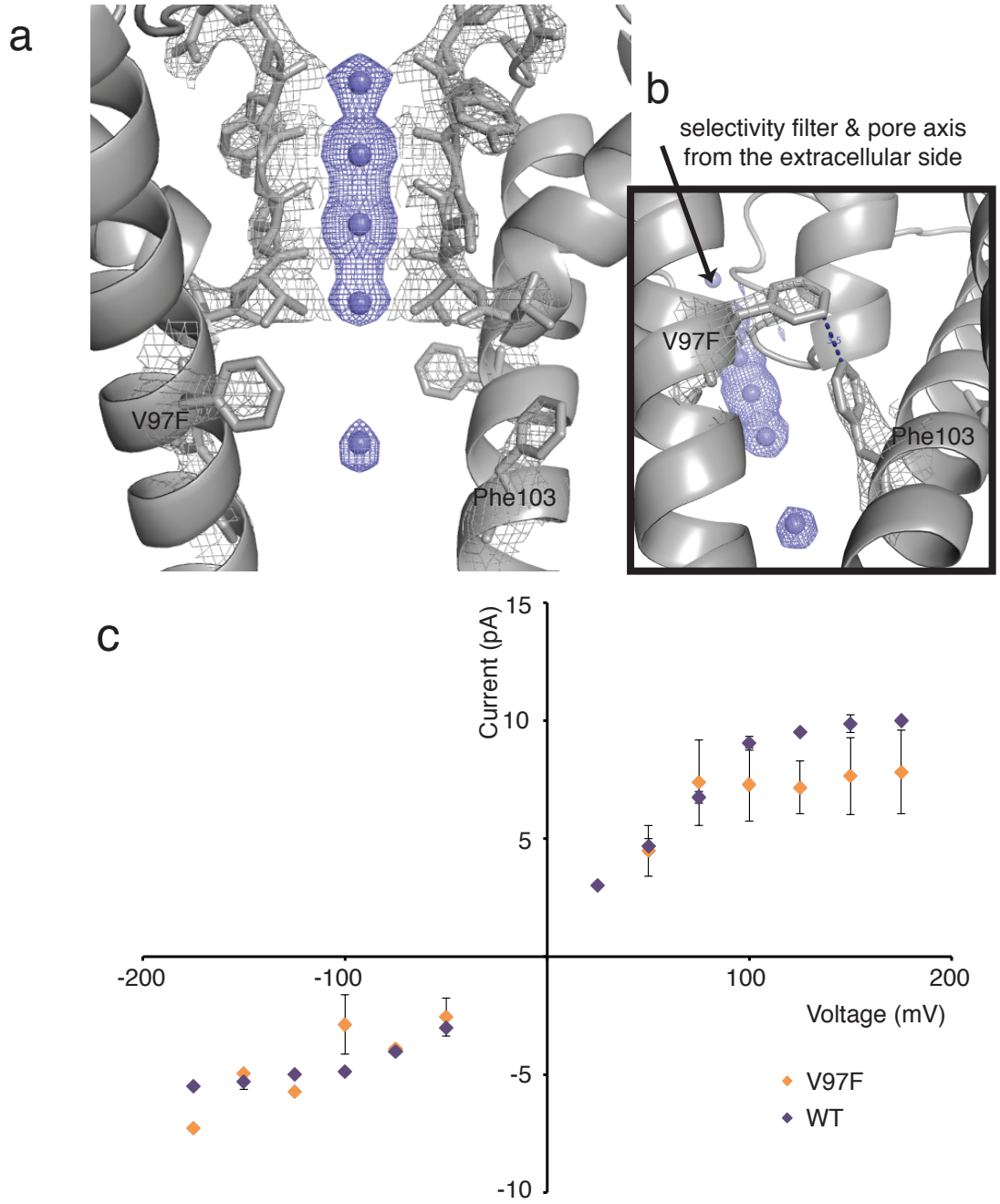

Figure 3.8: Structure and function of KcsA V97F. (a) The *in vitro* folded protein is shown, refined to 2.8 Å resolution, and looks identical to the recombinant protein, not shown. The selectivity filter residues, Phe103, and V97F are shown in stick and the potassium ions are shown in blue. $2F_o$-F_c density maps for the protein are shown in gray at 2 σ. F_o-F_c omit maps for the ions are shown in blue at 5 σ and for the unmodeled density at 2 σ. (b) An alternative view, looking from outside and below the lateral opening, highlights the interaction between Phe103 and V97F. The dashed line marks the 3.5 Å distance between the residues. (c) Current-voltage plot for V97F compared to WT. Error bars are from an average of at least three independent bilayer recordings.

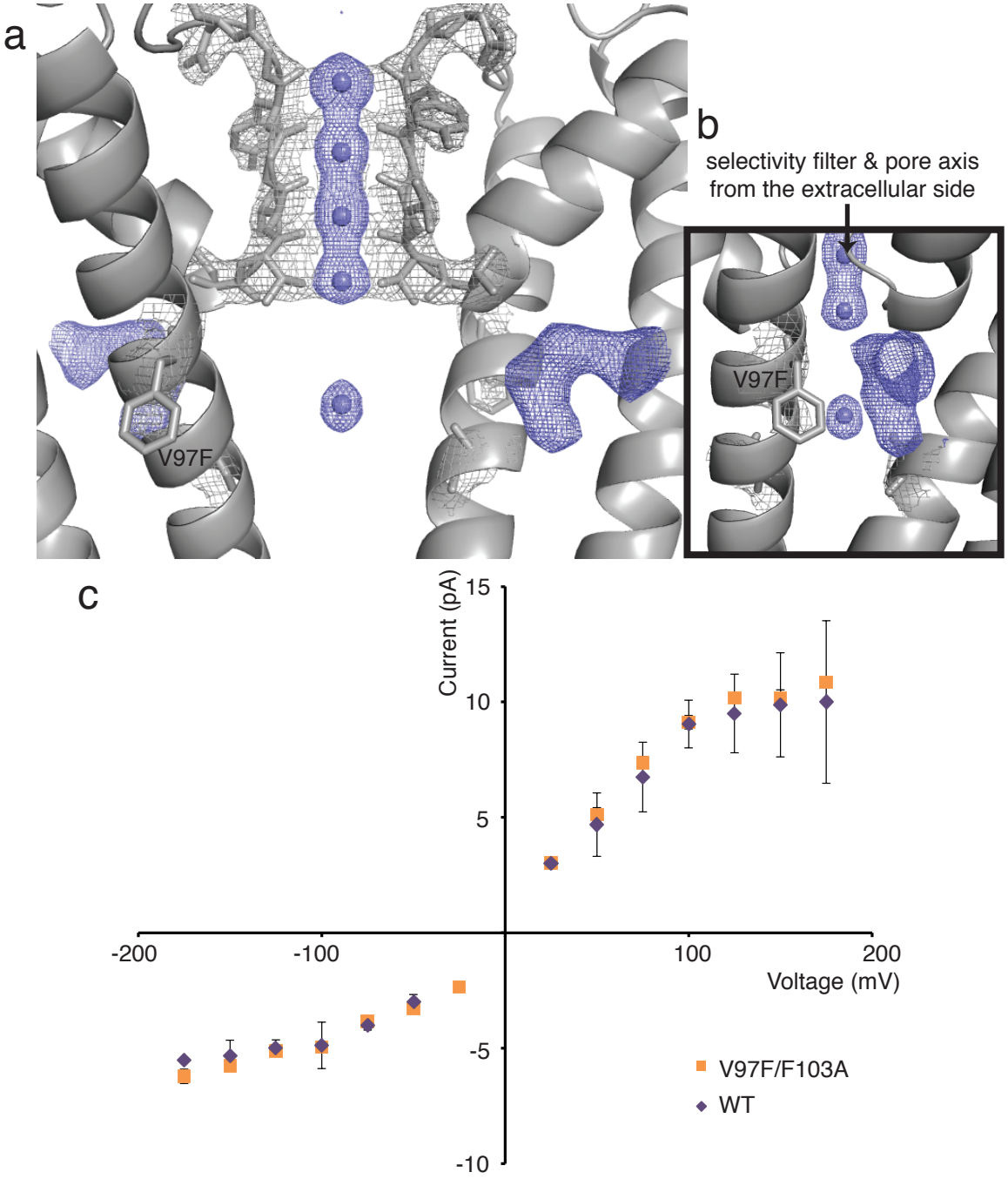

Figure 3.9: Structure and function of KcsA V97F/F103A. (a) The *in vitro* folded protein is shown, refined to 2.75 Å resolution, and looks identical to the recombinant protein, not shown. The selectivity filter residues, F103A, and V97F are shown in stick and the potassium ions are shown in blue. $2F_o$-F_c density maps for the protein are shown in gray at 2 σ. F_o-F_c omit maps for the ions are shown in blue at 5 σ and for the unmodeled density at 2 σ. (b) An alternative view, looking from outside the lateral opening, shows the relationship between the non-peptidic density and V97F. (c) Current-voltage plot for V97F/F103A compared to WT. Error bars are from an average of at least three independent bilayer recordings.

Table 7: Summary of structures with V97F, V97F/F103A mutations

	V97F	V97F folding	V97F F103A	V97F F103Aref
crystal	796	869	1087	1040
date	10/7/11	10/7/11	2/19/12	2/19/12
mutations				
	V97F	V97F	V97F F103A	V97F F103A
origin				
native native refolded semisynthetic	rec	POPC	rec	POPC
+ throughout + folding only + after purif.				
data				
resolution (Å)	3	2.8	2.75	2.75
spacegroup	I4	I4	I4	I4
I/sigma	11.2(2.0)	14.2(1.4)	11.6 (1.4)	12.0(1.36)
redundancy	3.2(3.0)	3.6(3.5)	4.7 (4.7)	99.8(100)
completeness	99.1(98.1)	99.8(99.8)	99.9(100)	5.1(5.1)
model				
R/Rfree	.317/.333	.281/.308	.297/.317	.298/.318
lengths/angles RMSD	.008/1.17	.006/1.00	.012/1.40	.012/1.35
structural features				
cavity ion	yes	yes	yes	yes
flipped F103	no	no	-	-
filler density				

Summary of structure data: *Mutations:* All mutations are listed, (-) denotes a WT sequence. *Method:* The method of preparation of the protein: natively purified recombinant (native rec.), recombinant unfolded and *in vitro* refolded (native refolded), or semisynthetic, with requisite *in vitro* folding. The (+) section lists additives, organized by when they were added during the protein preparation. *Data:* Statistics for the dataset, with data for the highest resolution shell in parentheses. *Model:* Statistics for the refined model are shown. *RMSD:* RMSDs calculated with all Cα atoms in the pore domain in comparison to WT KcsA (1k4c), when available. *Structure features:* Summarizes the cavity conformation for each structure, where density refers specifically to the non-peptidic density.

3.2.4.3 Summary of Mutagenesis Experiments

From these mutagenesis experiments, it was demonstrated that the F103A, V97F, and V97F/F103A mutations can each produce functional channels that maintain the native cavity conformation after *in vitro* refolding. These mutations could be very useful for future KcsA semisynthesis efforts.

3.2.5 Quaternary Ammonium Ions Affecting the Cavity Conformation

There is a delicate balance between the native and flipped conformations in the KcsA cavity. We were curious whether high-affinity cavity blockers, such as quaternary ammonium (QA) ions, would shift that equilibrium in favor of the native conformation. Previous studies demonstrated that tetrabutylammonium (TBA) has high affinity for blocking KcsA and a crystal structure of this complex is known (Faraldo-Gómez et al., 2007; Yohannan et al., 2007). Folding experiments were performed with TBA and then with tetramethylammonium (TMA) or tetraethylammonium (TEA) and the resulting structures were analyzed. Structure statistics for these proteins are summarized in Table 8.

3.2.5.1 Folding of KcsA in the Presence of TBA

Our objective was to introduce TBA in the *in vitro* folding reaction, and then to remove the TBA ion during the final steps of dialysis and size exclusion chromatography that the protein is always subjected to. The presence of TBA did not noticeably alter the folding reaction rate or yield. The resulting protein was crystallized and Phe103 was found in the native-like conformation; however, the

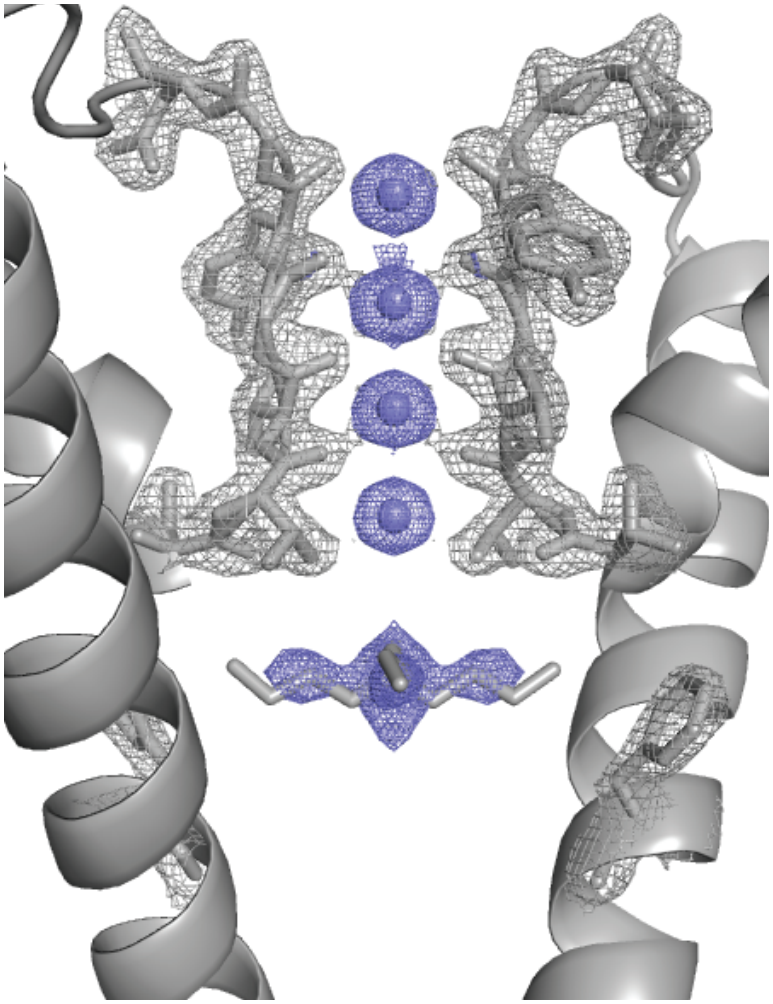

Figure 3.10: Structure of KcsA with TBA added during *in vitro* folding. The crystal structure was refined to 2.05 Å resolution. The selectivity filter residues, Phe103, and TBA are shown in stick and the potassium ions are shown in blue. $2F_o$-F_c density maps for the protein are shown in gray at 2 σ. F_o-F_c omit maps for the ions are shown in blue at 5 σ and for the TBA density at 2 σ.

TBA ion was still present in the cavity (Figure 3.10). It seems that the affinity for TBA was high enough that it could not be removed during the purification steps. Perhaps more stringent conditions could be used to remove it, but this has not been explored.

3.2.5.2 Folding of KcsA in the Presence of TMA or TEA

Folding reactions were performed in the presence of TMA or TEA during folding, along with control reactions where the QA ion was added just before crystallization. While one structure with TEA was previously published, it was unclear whether a TEA ion was bound in the cavity (Lenaeus et al., 2005). A control structure with TEA added just before crystallization was refined to 1.94 Å resolution (Figure 3.11a). Interestingly, the density in the cavity resembled the density of a hydrated potassium ion, rather than a continuous density as expected for TEA. Similar results were observed for KcsA with added TMA, that was refined to 2.25 Å resolution (Figure 3.11b). The affinity for these QA ions may be too low to bind for a substantial amount of time in the KcsA cavity.

KcsA was also prepared with TMA present during the refolding steps, but not the final purification (similar to TBA above), and two structures were obtained. The first structure showed a native-like cavity conformation (refined to 3.0 Å resolution, Figure 3.11c), which was not high enough resolution to confirm that the density in the cavity was a potassium ion, and the second structure (refined to 2.4 Å resolution, FIgure 3.11d) revealed that the Phe103 residues were flipped into the cavity. These two structures were inconsistent with each other, and

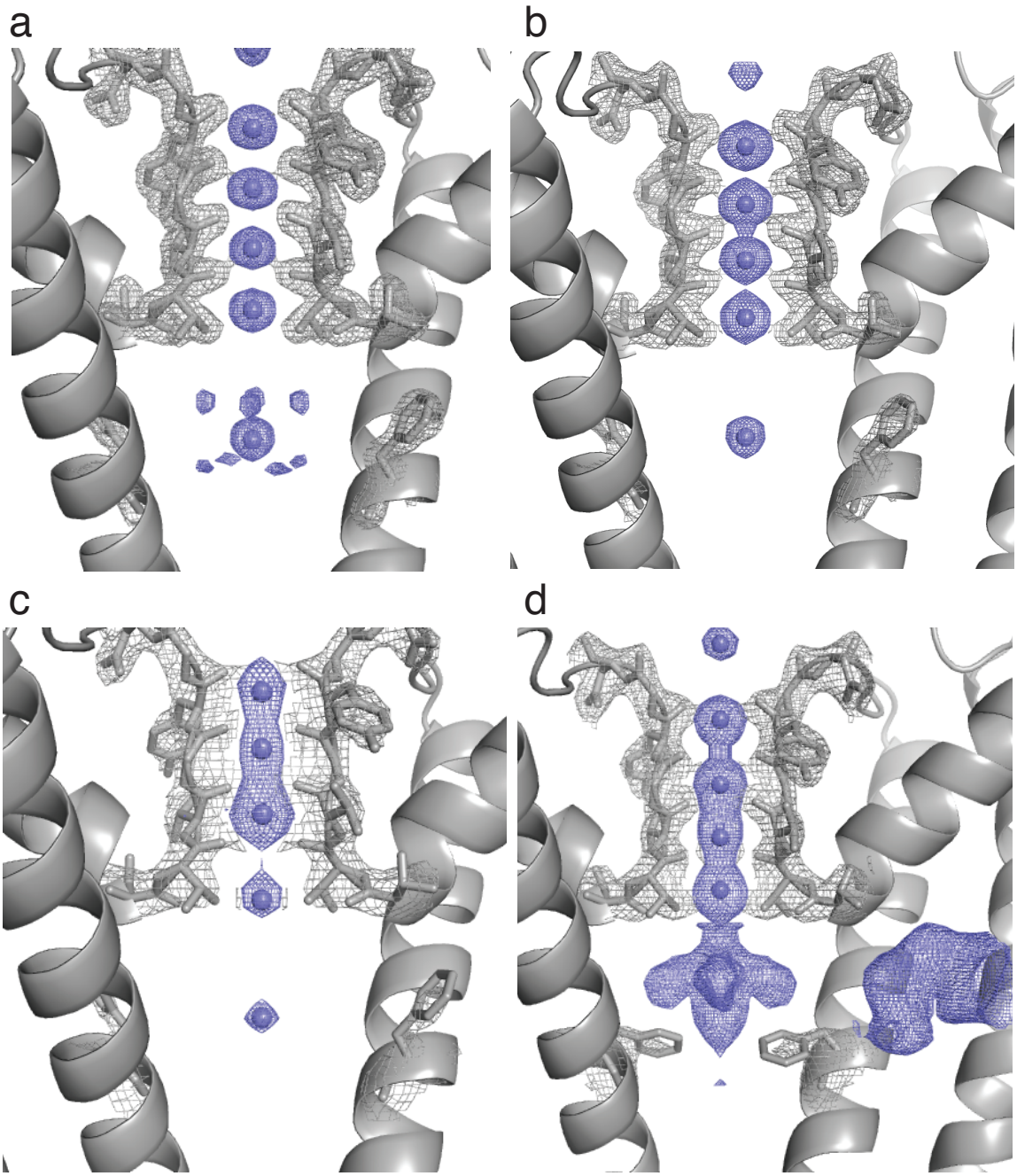

Figure 3.11: Structures of KcsA with small QA ion blockers. (a,b) *In vitro* folding in the presence of QA ion throughout the *in vitro* folding preparation, for (a) TEA and (b) TMA, refined to 1.9 Å and 2.25 Å resolution, respectively. (c,d) Two different preparations of in vitro folded KcsA in the presence of TMA only during the folding steps, with two conformations observed. The structures in (c) and (d) were refined to 3 Å and 2.4 Å resolution, respectively. The selectivity filter residues and Phe103 are shown in stick and the potassium ions are shown in blue. $2F_o$-F_c density maps for the protein are shown in gray at 2 σ. F_o-F_c omit maps for the ions are shown in blue at 5 σ and for the unmodeled cavity and lateral opening densities in panel (d) at 2 σ.

Table 8: Summary of structures with small QA ions

	10mM TBA	TBA folding	10mM TEA	10mM TMA	TMA folding	TMA folding
crystal	609	696	915	780	840	1074
date	9/6/11	9/6/11	12/11/11	12/11/11	10/7/11	2/19/12
mutations						
	-	-	-	-	-	-
method						
native rec. native refolded semisynthetic	POPC	POPC	rec	rec	POPC	POPC
+ throughout + folding only + after purif.	TBA	TBA	TEA	TMA	TMA	TMA
data						
resolution (Å)	2.45	2.05	1.94	2.25	3	2.4
spacegroup	I4	I4	I4	I4	I4	I4
I/sigma	12.8(1.5)	13.3(1.6)	19.9(3.6)	16.4(2.2)	8.14(1.7)	19.0(1.6)
redundancy	3.7(3.6)	3.3(2.9)	4.9(4.8)	3.7(3.7)	4.0(3.7)	4.5(4.4)
completeness	99.9(99.8)	99.6(97.6)	98.9(99.1)	99.9(100)	99.2(99.4)	98.8(95.3)
model						
R/Rfree	.310/.313	.299/.316	.250.272	.239/.260	.291/.308	.250/.271
lengths/angles RMSD	-	.006/.997	.006/1.06	.006/1.03	.011/1.31	.01/1.31
structural features						
cavity ion	TBA	TBA	yes	yes	yes	TMA?
flipped F103	no	no	no	no	no	yes
density	no	no	no	no	no	outside

Summary of structure data: *Mutations:* All mutations are listed, (-) denotes a WT sequence. *Method:* The method of preparation of the protein: natively purified recombinant (native rec.), recombinant unfolded and *in vitro* refolded (native refolded), or semisynthetic, with requisite *in vitro* folding. The (+) section lists additives, organized by when they were added during the protein preparation. *Data:* Statistics for the dataset, with data for the highest resolution shell in parentheses. *Model:* Statistics for the refined model are shown. *RMSD:* RMSDs calculated with all Cα atoms in the pore domain in comparison to WT KcsA (1k4c), when available. *Structure features:* Summarizes the cavity conformation for each structure, where density refers specifically to the non-peptidic density.

without more repetitions and higher resolution data it is difficult to say whether QA ions could aid in producing a native KcsA conformation after *in vitro* folding.

3.2.5.3 Summary of Folding Experiments in the Presence of QA Ions

QA ions were introduced during *in vitro* folding of KcsA; however, there were inconsistencies between crystal structures. This may be due to the lower affinity of smaller QA ions, thus potentially repeating these experiments at a higher ion concentration or with tetrapropylammonium (TPrA) would be more successful. These studies did, however, lead to more interesting work looking at QA blockers in KcsA that will be the subject of Chapter 4.

3.3 Conclusions

From these studies, we determined that KcsA can access an alternative cavity conformation through *in vitro* folding, or exposure to the lipids used for refolding. However, the incorporation of QA ions during protein folding or the addition of lipids to folded protein created inconsistent structural results and further experiments are needed to be able to use QA ions to achieve the native cavity conformation. Successfully, the KcsA mutations F103A, V97F, or the double mutant V97F/F103A produce protein that will remain in a native-like conformation after *in vitro* folding.

CHAPTER 4: QUATERNARY AMMONIUM IONS IN THE KcsA CENTRAL CAVITY

Quaternary ammonium (QA) ions with methyl- to hexyl-length alkyl chains have been shown to block potassium channels by electrophysiology. After analyzing the structures of KcsA with small QA ions bound, we were curious to see how large QA ions would bind in the cavity, and whether the flipped cavity conformation may be required for the cavity to accommodate longer alkyl chains. We solved a set of KcsA structures in complex with larger QA ions: tetrapentylammonium (TPA) and tetraoctylammonium (TOA). These structures indeed demonstrated that larger QA ions bind to the cavity in its flipped conformation, and TPA block of KcsA was confirmed in the bilayer. This work led us to hypothesize that a subset of human potassium channels may employ a similar mechanism of block, and will be discussed in Chapter 5.

4.1 Introduction

Well before the availability of high resolution structures of potassium channels, it was proposed that the central cavity of these proteins must be at least 11 Å wide in order to accommodate the size of known QA blockers (Bezanilla and Armstrong, 1972; Swenson, 1981). These molecules included asymmetric derivatives of TEA that included one longer alkyl chain or symmetric QA ions up to tetrahexylammonium (THA) (Armstrong, 1971; French and Shoukimas, 1981; Swenson, 1981). More recently, a structure with the quaternary ammonium ion TBA bound in the central cavity revealed that its alkyl

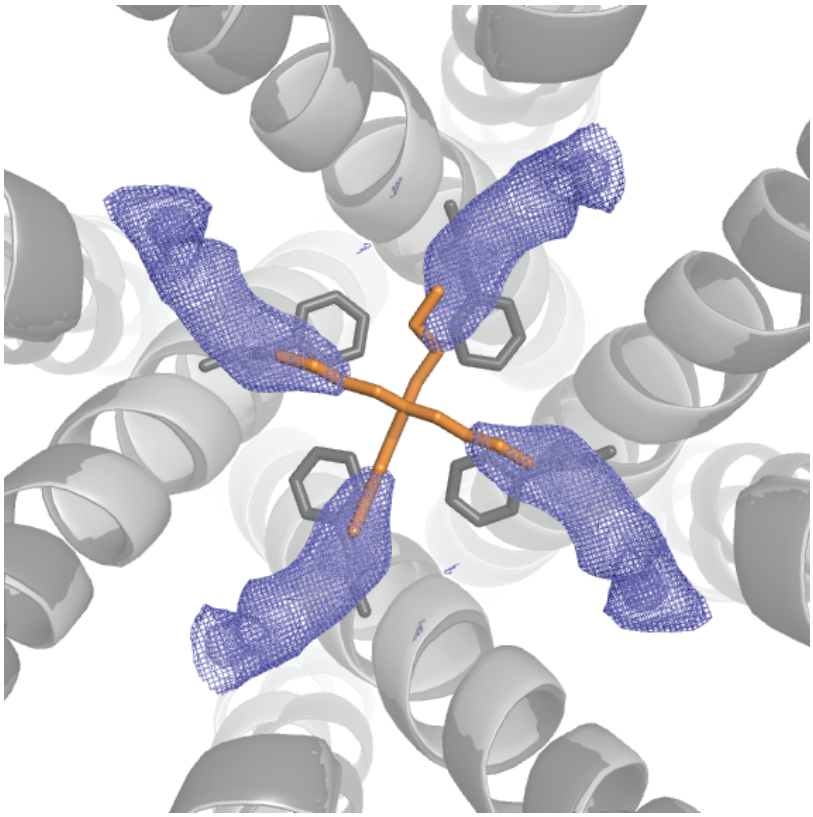

Figure 4.1: Overlay of TBA structure and non-peptidic density. T74Aester structure is shown in dark gray, and overlaid with TBA structure (2hvk) in light gray. The view is rotated to look from the top down. The TBA molecule is shown as orange sticks. The phenylalanine residues below TBA are Phe103 from T74Aester, shown in stick. Phe103 residues from the structure with TBA are not shown. F_o-F_c omit maps for the cavity density in T74Aester are shown at 2 σ.

chains stretch out laterally toward each of the four subunits (Zhou et al., 2001a; Faraldo-Gómez et al., 2007; Yohannan et al., 2007). Interestingly, when KcsA is in the flipped conformation, the non-peptidic density present above each of the Phe103 residues extends laterally in an orientation well aligned with TBA, as if the unmodeled densities could be extensions of the alkyl chains of TBA (Figure 4.1).

4.2 Results

Inspired by the alternative cavity conformation of KcsA and the inhibition of potassium channels by a wide variety of QA ions, we crystallized KcsA in the presence of the large QA ion cavity blockers TPA and TOA, and demonstrated block by TPA in a reconstituted system in the lipid bilayer. The structure statistics for these proteins are summarized in Table 9. These results demonstrate a new conformation for cavity block in KcsA and this may have implications for the inhibition of human potassium channels.

4.2.1 Structures of KcsA with Large Quaternary Ammonium Ions

We solved crystal structures of KcsA with two different large QA ions bound in the cavity: TPA (Figure 4.2) and TOA (Figure 4.3). These QA ions were added to recombinantly-prepared KcsA just before crystallization, as was done for the published TBA structures (Zhou et al., 2001a; Faraldo-Gómez et al., 2007; Yohannan et al., 2007). Even though TPA is only one methyl group longer than TBA on each alkyl chain, TPA and TOA were each sufficient to flip the Phe103

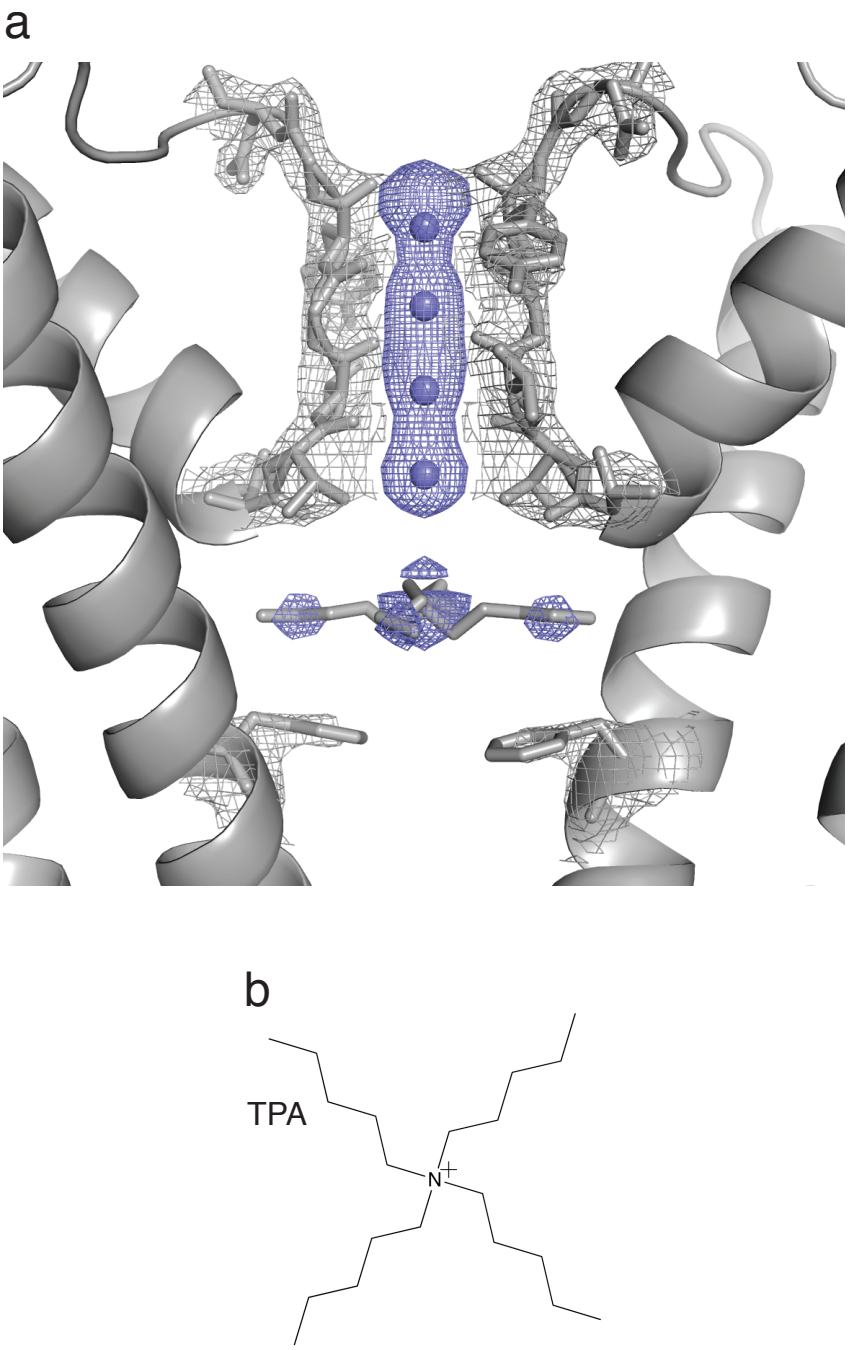

Figure 4.2: Structure of KcsA with TPA bound. (a) Recombinant KcsA with tetrapentylammonium (TPA) bound in the cavity, refined to 2.85 Å resolution. The selectivity filter residues, Phe103, and TPA are shown in stick and the potassium ions are shown in blue. $2F_o$-F_c density maps for the protein are shown in gray at 2 σ. F_o-F_c omit maps for the ions are shown in blue at 5 σ and for the unmodeled density at 2 σ. (b) Chemical structure of TPA.

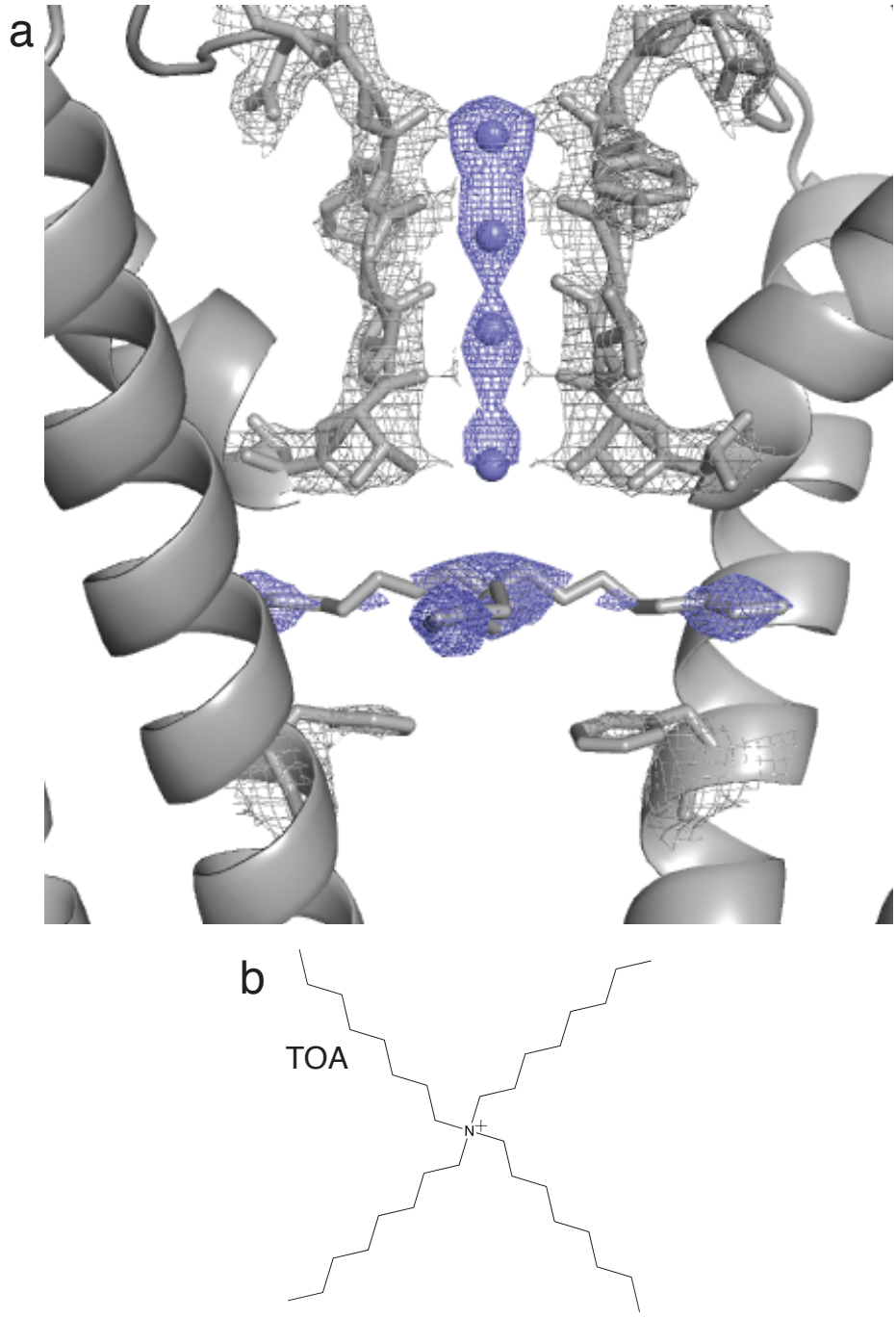

Figure 4.3: Structure of KcsA with TOA bound. (a) Recombinant KcsA with tetraoctylammonium (TOA) bound in the central cavity, refined to 2.8 Å resolution. The selectivity filter residues, Phe103, and TOA are shown in stick and the potassium ions are shown in blue. $2F_o$-F_c density maps for the protein are shown in gray at 2 σ. F_o-F_c omit maps for the ions are shown in blue at 5 σ and for the unmodeled density at 2 σ. (b) Chemical structure of TOA.

sidechains into the cavity, producing a flipped cavity conformation consistent with structures presented in Chapters 2 and 3. The non-peptidic densities of the T74Aester structure have been replaced by the long alkyl chains of the QA ion chains, and no other ordered density is observed within the cavity. The orientations of TBA, TPA, and TOA are all well aligned in the cavity.

TOA was also crystallized in complex with the V97F mutant channel to see whether these added phenylalanine residues would inhibit binding. Interestingly, TOA was bound to V97F KcsA in the same flipped conformation as the WT channel (Figure 4.4). This argues that the affinity for TOA in this conformation out-competes the interaction between V97F and F103 in its native conformation. The position of the phenylalanine sidechain of V97F is in the same conformation as compared to the unblocked structure. These crystal structures suggest that the flipped conformation of KcsA may be relevant for channel inhibition by larger pore blocking molecules.

4.2.2 Inhibition of KcsA by Tetrapentylammonium (TPA)

To correlate these structures of a new conformation of cavity block in KcsA with function, we confirmed that TPA blocks KcsA in the membrane bilayer (Figure 4.5). Macroscopic currents for KcsA were recorded in order to look at the properties of inhibition in aggregate. The kinetics of TPA block were slow, and it was difficult to perform quantitative measurements from single channel or macroscopic recordings because of the low open probability of KcsA (LeMasurier et al., 2001). Nonetheless, our data demonstrate that TPA inhibits KcsA in the

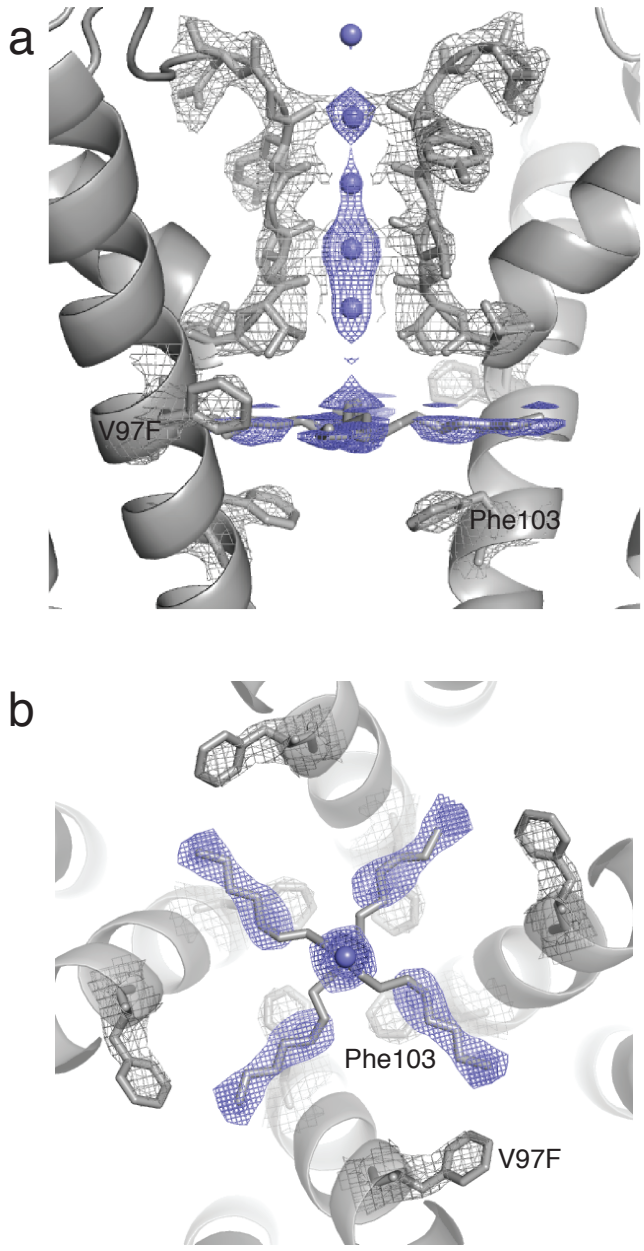

Figure 4.4: Structure of KcsA V97F with TOA bound. (a) Crystal structure refined to 3.0 Å resolution. (b) The same structure but rotated to look from the top down. The phenylalanine residues lining the walls of the cavity are V97F and the faint phenylalanine residues below TOA are Phe103. The selectivity filter residues, Phe103, V97F, and TOA are shown in stick and the potassium ions are shown in blue. $2F_o$-F_c density maps for the protein are shown in gray at 2 σ. F_o-F_c omit maps for the ions are shown in blue at 5 σ and for the TOA density at 2 σ.

Table 9: Summary of structures with large QA ions

	10mM TPA	1mM TPA	1mM TOA	V97F TOA	1mM clofilium
crystal	901	1022	832	801	924
date	12/11/11	2/19/12	10/7/11	10/7/11	12/11/11
mutations					
	-	-	-	V97F	-
origin					
native rec. native refolded semisynthetic	rec	rec	rec	rec	rec
+ throughout + folding only + after purif.	TPA	TPA	TOA	TOA	clofilium
data					
resolution (Å)	3.05	2.85	2.8	3	2.3
spacegroup	I4	P4	P4	P4	I4
I/sigma	8.5(1.5)	8.68(1.41)	10.6(1.8)	6.4(1.4)	11.6 (1.5)
redundancy	3.7(3.7)	4.8(4.6)	4.3(4.2)	3.4(3.2)	4.1(3.8)
completeness	99.7(99.7)	100(100)	100(100)	99.1(99.0)	99.9(99.2)
model					
R/Rfree	.249/.274	.236/.266	.249/.275	.368/.399	.242/.256
lengths/angles RMSD	.007/1.02	.005/0.923	.007/1.06	.005/0.82	.009/1.28
structural features					
cavity ion	TPA	TPA	TOA	TOA	yes
flipped F103	yes	yes	yes	yes	no
filler density	outside	no	no	no	no

Summary of structure data: *Mutations:* All mutations are listed, (-) denotes a WT sequence. *Method:* The method of preparation of the protein: natively purified recombinant (native rec.), recombinant unfolded and *in vitro* refolded (native refolded), or semisynthetic, with requisite *in vitro* folding. The (+) section lists additives, organized by when they were added during the protein preparation. *Data:* Statistics for the dataset, with data for the highest resolution shell in parentheses. *Model:* Statistics for the refined model are shown. *RMSD:* RMSDs calculated with all Cα atoms in the pore domain in comparison to WT KcsA (1k4c), when available. *Structure features:* Summarizes the cavity conformation for each structure, where density refers specifically to the non-peptidic density.

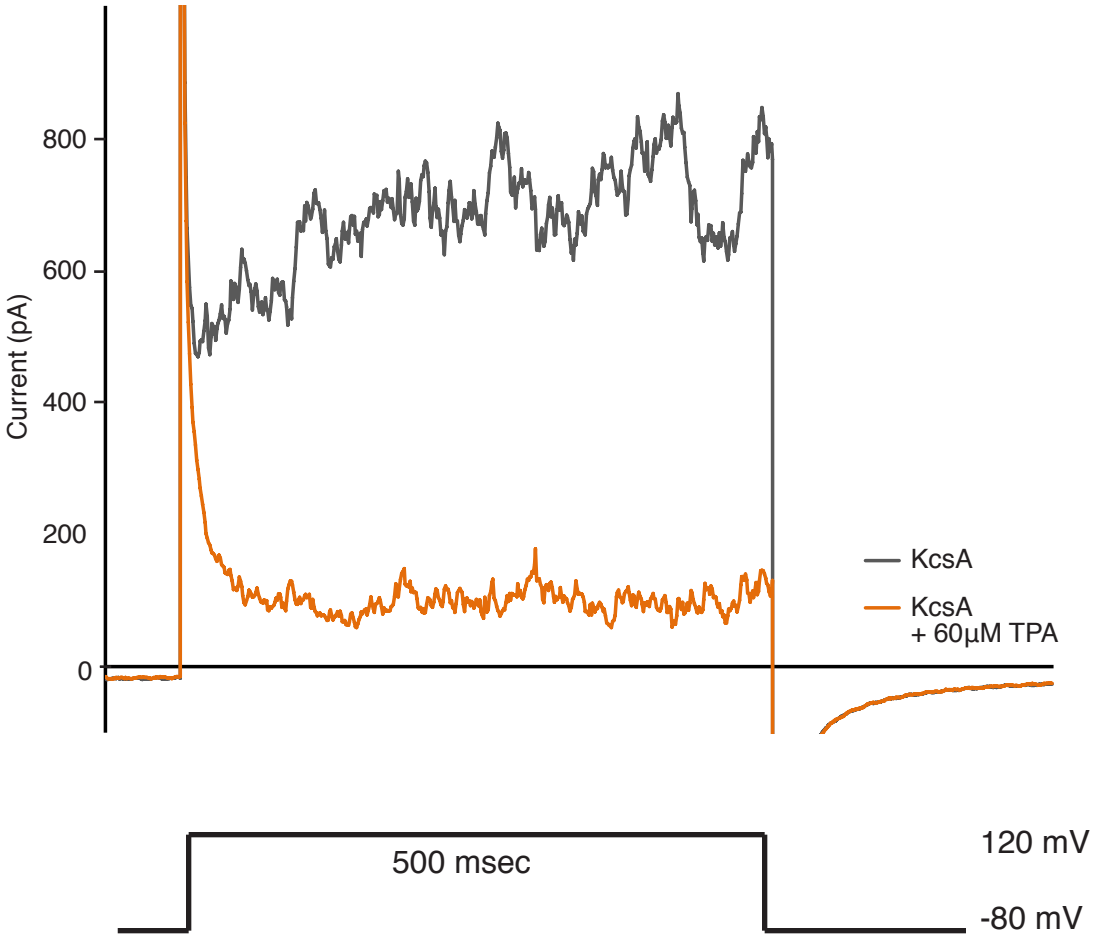

Figure 4.5: KcsA inhibition by TPA. Macroscopic currents were recorded to look at aggregate channel inhibition upon addition of TPA. The gray trace shows current for KcsA at a step to 120 mV. The orange trace is for the same voltage step, but recorded 5 minutes after addition of 60 µM TPA. These recordings were performed in the presence of 150 mM internal KCl and 150 mM external NaCl. The pulse sequence is shown below the trace.

micromolar range. We did not study inhibition by TOA in the bilayer because it has been previously reported that molecules with long alkyl chains are destabilizing to the membrane (Armstrong and Hille, 1972).

4.3 Conclusions

Crystal structures of KcsA in the presence of large pore blocking molecules—TPA and TOA—show that these blockers cause the Phe103 residues to flip into the cavity. This conformational change expands the width of the cavity, by creating access to the lateral openings, allowing molecules longer than the diameter of the native cavity to block the channel. The interactions of TPA or TOA with the cavity are sufficient to cause Phe103 to flip, including in the context of the Phe-stabilizing V97F mutation, and may provide more information about the interactions of Phe103 with the surrounding protein and cavity environments. The inhibition of KcsA by TPA has been confirmed by bilayer electrophysiology experiments. Finally, we will explore the possibility that this conformation of cavity block could be relevant to human potassium channels. The implications of this work will be discussed in detail in the next chapter.

CHAPTER 5: CONCLUSIONS AND DISCUSSION

In our initial work with KcsA, we sought to understand the effects of helix dipoles on electrostatic stabilization in proteins. Although unexpected complications arose, they opened up a series of new experiments. We described a new conformation of the central cavity of KcsA and sought to understand the factors that induce this conformational change, including *in vitro* protein folding, the addition of lipids and QA ions, and mutagenesis. Finally, crystal structures revealed that block by large QA ions also induced the alternative cavity conformation. Conclusions and potential future directions regarding each of these aspects of this work will be presented.

5.1 The Helix Dipole Effect in KcsA

Structural and functional studies of KcsA T74Aester (containing an amide-to-ester modification at the end of the pore helix) were performed in order to study the role of the helix dipole effect in KcsA. In the bilayer, potassium conductance of T74Aester was reduced by almost an order of magnitude compared to WT protein, suggesting that the helix dipole effect may play an important role in potassium channel function. X-ray crystallography of T74Aester confirmed that the pore helices and potassium ions in the selectivity filter were not structurally perturbed; however, the conformation of Phe103 in the cavity—the flipped conformation—precluded analysis of the effects of this modification on cavity ion occupancy.

The reduced conductance of T74Aester may be due to the reduced helix dipole, the conformational change in the cavity, or both. Control electrophysiology recordings of refolded recombinant KcsA are still needed to independently characterize any functional implications of the flipped conformation. Several factors suggest that channel function will not be greatly perturbed by protein folding. The first semisynthesis of KcsA verified the methodology by demonstrating potassium conductance indistinguishable from recombinant KcsA (Valiyaveetil et al., 2004a). The structure for semisynthetic D-Ala-modified KcsA had a flipped cavity conformation, and electrophysiology experiments demonstrated conductance similar to WT protein (Valiyaveetil et al., 2004b; 2006a). It is also important to note that truncated KcsA used for electrophysiology studies contains the A98G mutation in order to be functional in the bilayer. It is unknown whether this mutation may affect comparisons between the structure of the cavity and functional studies. Based on these previous experiments with semisynthetic KcsA, we don't expect that the flipped cavity conformation will alter conductance; however, final conclusions are pending further data.

If there are subsequent studies on KcsA using the semisynthetic methodology, they should be performed in the presence of the V97F or V97F/ F103A mutations in order to be able to compare the cavity environment with and without changes to the helix dipole. In such cases, further electrophysiology and crystallography experiments could aid in our understanding of the role of helix dipoles in KcsA. Electrophysiology experiments could be performed to better understand the mechanism by which the helix dipole affects conductance. For

example, electrophysiology recordings could be performed over a range of potassium concentrations in order to see whether the helix dipoles affect potassium affinity in the cavity (which would demonstrate sensitivity to potassium concentration) versus a change in the rate of potassium dehydration (which would be be less sensitive to potassium concentration). Crystal structures of modified KcsA with a cavity ion present could allow for further study of ion occupancy or variations in binding between different cations. In particular, the anomalous signal of thallium could be used to quantify cavity ion occupancy and selectivity in comparison to previous studies (Zhou and MacKinnon, 2004).

The breadth of computational studies of KcsA also makes this an interesting system for studying helix dipoles. Experimental measurements from a helix dipole modification in KcsA could be compared directly to a change in electrostatics calculated *in silico*. Whether or not these results agree, such data could improve our theoretical understanding of helix dipole effects by supporting or refining the current models for calculating helix dipoles.

KcsA has proven to be challenging to work with by semisynthesis, both due to the structural complications in the cavity as well as the previously documented difficulties in synthesizing and working with the unstructured, hydrophobic polypeptides required to prepare KcsA by EPL (Valiyaveetil et al., 2002a; Komarov et al., 2009a). Some initial steps were taken toward establishing a three-piece ligation for KcsA that would be suitable for more thorough studies of the helix dipole effect, but this work is currently unfinished (Figure 5.1). Ligation sites have been selected, and protein has been expressed and

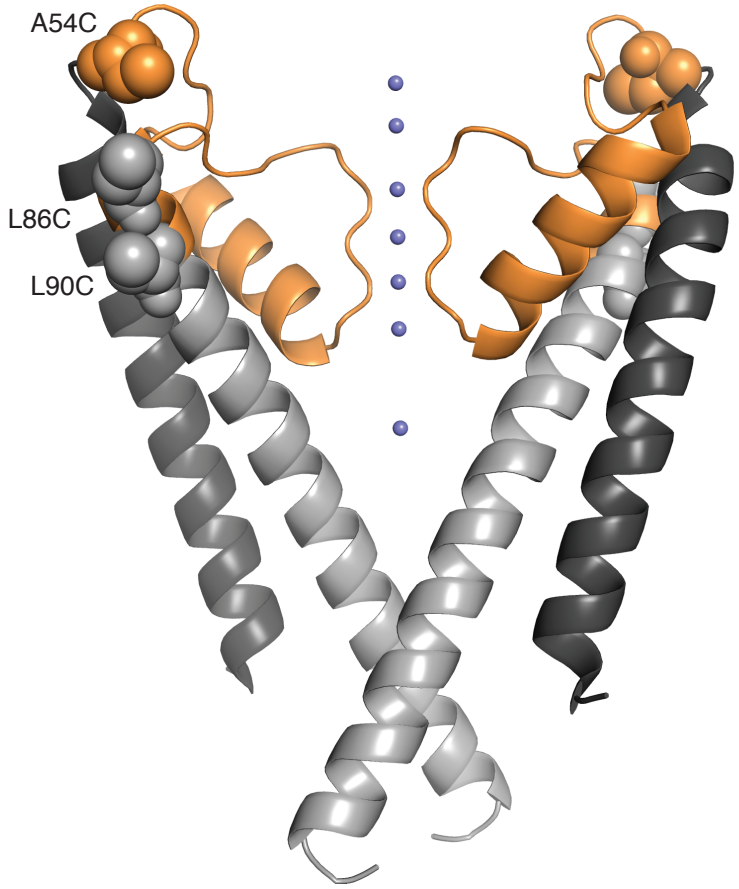

Figure 5.1: Three-piece ligation strategy for KcsA. KcsA is shown marking the three ligation fragments, with one possible N-terminal ligation site in orange (A54C) and two possible C-terminal ligation sites in light gray (L86C or L90C). The N-terminal residues (1-53) are in dark gray, the middle residues (54-86 or 90) are in orange, and the C-terminal residues (86 or 90-122) are in light gray. With this strategy, the C-peptide could be extended to the full-length protein as well (residues 86 or 90-160). The middle orange fragment would be made synthetically, providing access to the pore helices and selectivity filter for further modifications. The A54C/A86C and A54C/A90C double mutants must still be tested for functional activity in the lipid bilayer before proceeding with this strategy.

reconstituted containing cysteines at these ligation junctions in order to determine whether the possible sites will affect channel function. Further work on this semisynthetic strategy, or adapting a similar published strategy (Komarov et al., 2009a), could improve the throughput of experiments on modified KcsA.

Through the use of EPL as a general protein modification strategy, an amide-to-ester modification could be used to study helix dipoles in a variety of proteins. As we have described, the ester modification can be incorporated into any polypeptide by Boc-SPPS. However, the ester coupling protocol could be optimized to improve the efficiency at that step. NCL and EPL strategies can be used to introduce the ester-containing peptide into a variety of proteins, provided that the protein of interest can be folded *in vitro*. Esters have also been incorporated into proteins using the nonsense suppression strategy, which could be adapted for studying helix dipole effects in various ways, though this methodology is less amenable for producing the high quantities of protein needed for structural studies.

Using EPL, other modifications could also be introduced into the protein backbone to alter helix dipoles in other ways. N-methylated amino acids are potentially useful modifications for blocking a hydrogen-bonding interaction specifically, without greatly affecting the amide bond dipole. However, the added bulk on the backbone often disrupts α-helix formation (Chang and Zehfus, 1996). Alternatively, thioamides have been shown to be tolerated in α-helices and are predicted to have a slightly weaker dipole than an amide, while maintaining the ability to form a backbone hydrogen bond (Batjargal et al., 2012). A triazole may

be interesting to consider for modification of a dipeptide in order to introduce a stronger dipole moment (>5 D) that would oppose the dipole of the α-helix (Horne et al., 2004).

At this stage, the magnitude of the helix dipole in proteins, as well as its effects on function, are still debated. The work presented here will hopefully contribute to future studies of helix dipole effects in KcsA and other proteins in order to develop a more comprehensive understanding of their role in protein function. For example, the intrinsic unfolding and refolding properties of the von Willebrand factor (VWF) A2 domain have been proposed to rely on helix dipole-capping interactions (Zhang et al., 2009). As this domain is small and easily folded *in vitro*, EPL could be used to modify the helix backbone in order to study the role for helix dipoles in protein stability more directly. Helix dipoles have also been suggested to be important for the stability of lysozyme, a protein for which a synthetic strategy and crystal structure have already been determined (Durek et al., 2007). A better understanding of protein electrostatics is useful for a variety of current research areas including drug design and optimization, the study of protein-protein interactions, and the enigma of protein folding.

In summary, we plan to complete the current study of helix dipoles in KcsA by recording the activity of recombinant, refolded KcsA. This will provide important information for drawing conclusions on the functional effects of the modified helix dipole. Subsequent experiments could be conducted, based on our optimized *in vitro* folding strategies, to gain additional insight into the role of

helix dipoles in KcsA. Finally, we have proposed that backbone modification strategies could be extended to study the role of helix dipoles in other systems.

5.2 The Cavity Conformations of KcsA

Several interesting observations emerge from analyzing the flipped cavity conformation and comparing this conformation with the native state. Phe103 and the non-peptidic density will each be discussed briefly.

5.2.1 The Conformations of Phe103

The new cavity conformation observed in KcsA is largely due to the conformational change of one amino acid sidechain: Phe103. By comparing the native and flipped states through a backbone alignment, such as that shown in Figure 2.8, a distortion of the backbone near Phe103 is observed for the WT protein. It looks as though the flipped or F103A states allow the helix to have a normal helical alignment. When Phe103 is present, the sidechain seems to be pulled upward to make sufficient contact with nearby residues and close off the lateral opening. A calculation of the contact between Phe103 and the surrounding protein (ignoring the nonpeptidic density) suggests that the flipped conformation has an additional 54 $Å^2$ of buried surface area compared to the native conformation.

The role of Phe103 can be further analyzed based on its interactions with V97F. The interaction formed between these two aromatic sidechains is sufficient to allow KcsA to fold with a native cavity conformation. Possibly V97F provides

some additional hydrophobic stabilization that holds Phe103 in the native conformation. The buried surface area specifically between Phe103 and V97F is calculated to be 37.7 $Å^2$. In the presence of TOA, the Phe103 sidechains flip into the cavity, suggesting that TOA binding outcompetes this interaction between V97F and Phe103. The surface area between Phe103 and TOA is smaller (27 $Å^2$), but it is likely offset by additional energy from the binding of such a large, hydrophobic molecule in the hydrophobic cavity environment.

In all of the structures presented of KcsA in this thesis, KcsA is the truncated pore domain of the channel, and its inner gate is in the closed conformation. The position of this phenylalanine in the open channel, relative to this closed structure, is not fully understood. X-ray crystallography has suggested several states along the open or inactivation trajectory of KcsA (Cuello et al., 2010a). While it is unknown whether these open-inactivated structures are relevant to KcsA in its open, conductive form, it is interesting to consider that the Phe103 residues in the inner helices are observed in a similar rotamer to our flipped KcsA structures (Cuello et al., 2010b).

Considering these factors, it is interesting to speculate on the folding process of KcsA (Figure 5.2). For example, the flipped conformation could arise from a low affinity for K^+ in the cavity during folding that draws the phenylalanine residues into the cavity. Alternatively, it could occur due to Phe103 relaxing into the flipped conformation, pushing out the potassium ion and pulling in the non-peptidic density. Finally, it could be initiated by the presence of some molecule that pushes itself through the lateral opening, possibly due to a high

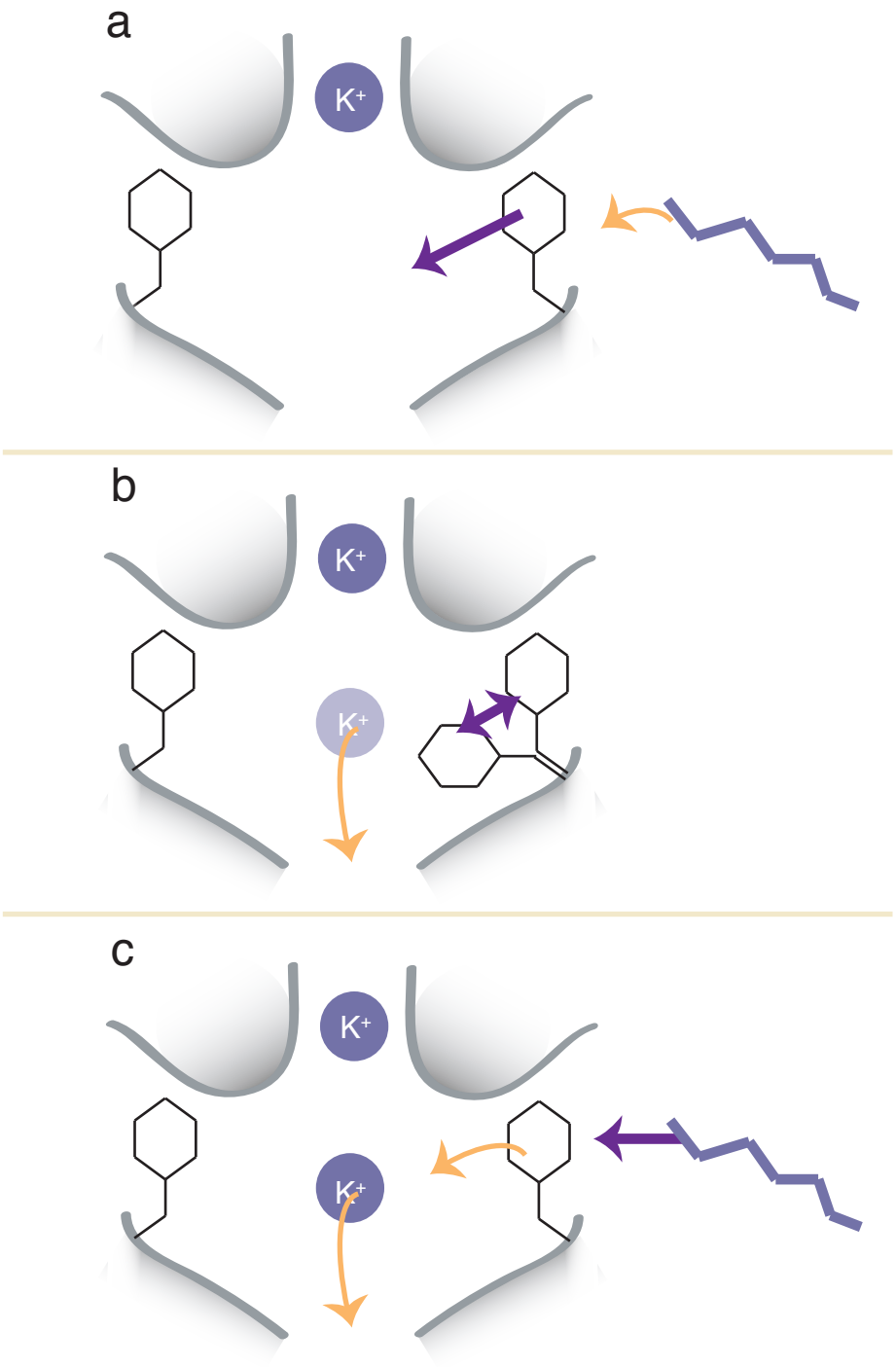

Figure 5.2: Proposed mechanisms of cavity conformational change. These three panels depict different forces driving the conformational change in the cavity. The protein is in gray, the K^+ ions are blue spheres, Phe103 is in black, and the non-peptidic density is a blue line. Purple arrows suggest the cause, and orange arrows the resulting action(s). (a) A void of K^+ in the cavity drives Phe103 to flip into the cavity; (b) conformational flexibility in Phe103 initiates the conformational change; or (c) the presence of a non-peptidic density pushes its way into the cavity, moving Phe103 and displacing the cavity ion.

concentration of lipids or detergents. While it is impossible to distinguish between these cases with the current data, understanding this process could aid in determining how various conditions will affect cavity conformation.

In order to further explore the interaction between Phe103 and V97F, crystallization of the V97F mutant protein with a shorter QA ion, such as TPA, could test whether the interactions between the alkyl chains and Phe103 sidechains are sufficient to induce the flipped conformation. If KcsA can be folded in various concentrations of potassium, structures could be compared to provide insight into whether the flipped conformation is dependent on K^+ affinity during folding. Better understanding the specific roles of lipids and detergents in the *in vitro* folding process is very compelling, but from the experiments presented, this may be a more difficult hypothesis to test.

5.2.2 The Nature of the Non-Peptidic Density in the Cavity

Crystal structures of the flipped conformation of KcsA and the F103A mutant, as well as the published NavAb, TWIK-1, and TRAAK structures, all show a non-peptidic density in the cavity. The long, thin shapes of these densities are consistent with the density for alkyl chains, such as from a detergent or lipid molecule.

The structures of the F103A mutant suggest that it is unfavorable for the non-peptidic density to enter the aqueous cavity in the absence of the Phe103 sidechain. Additionally, while TPA may be small enough to fit into the cavity in the native cavity conformation, its alkyl chains are long enough to make hydrophobic

interactions with the phenyl groups in the flipped conformation. These structures are consistent with there being a hydrophobic interaction between the phenyl ring of Phe103 and the non-peptidic density. Additionally, the shape and character of the densities for the alkyl chains of TPA and TOA are similar to those observed for the non-peptidic densities. Both vary in intensity along the alkyl chain, suggesting that these molecules have some conformational flexibility inside the cavity. Considering these factors, alkyl chains are a likely candidate for occupying the densities in the lateral openings.

To date, no one has attempted to rigorously characterize the non-peptidic species observed in KcsA, NavAb, or the two K2P channels, but its identification could contribute greatly to our understanding of the functional states that these structures represent. Previously, lipids that interact strongly with membrane proteins have been identified by mass spectrometry (Zhou et al., 2011a), and potentially similar experiments could be performed on *in vitro* folded KcsA, NavAb, or the K2P channels. KcsA could be an especially useful system for these experiments as the recombinant and refolded structures could be compared, where the refolded structure may contain a new small molecular weight species.

5.3 Variability in Cavity Conformation

Several crystal structures of KcsA have been obtained in varied folding conditions, with different lipid additives or QA ions, or in the presence of selected mutations (Tables 2-9). The results of these experiments have produced two

classes of structures for KcsA—either natively folded KcsA, or the flipped conformation with Phe103 rotated into the central cavity. However, some of the conditions tried were variable, producing structures in both conformations. In this section, the inconsistent results will be summarized, followed by a discussion of the implications and future directions for studying this alternative cavity conformation in KcsA.

5.3.1 Conditions that May Affect Cavity Conformation

We have not been able to identify many conditions that definitively affect the conformation of the central cavity in KcsA, so other factors must be important for inducing one conformation or the other. A few of the variables that potentially could be important are summarized below.

While there are several possibilities for the variabilities observed, the role of detergents and lipids may be particularly important, in part because the least consistent results were produced in conditions when small amounts of lipids were added to prepared and concentrated protein. All of the proteins for these studies were concentrated using spin columns with low molecular weight cutoffs due to the small size of the truncated KcsA protein. This method has the drawback that in addition to concentrating the protein, empty detergent micelles will also be concentrated, leading to final protein solutions with high and variable detergent concentrations. High detergent concentrations could alter the concentration dependence of lipid or small molecule interactions with KcsA, or could even affect the structure of KcsA directly.

Structures in both native and flipped conformations were also observed for the *in vitro* folding experiments in the presence of small QA ions. These molecules are functionalized with short alkyl chains (methyl or ethyl groups) that could be sensitive to changing detergent concentrations as mentioned above; however, it is more likely that these low-affinity cavity blockers have not been introduced at a high enough concentration to produce consistent effects on potassium channel structure. Electrophysiology studies have demonstrated that the apparent dissociation constant ($K_{1/2}$) of TEA in KcsA is highly dependent on voltage and permeant ion concentration, but at 0 mV and 150 mM KCl, the apparent $K_{1/2}$ could be as high as 78 mM (Kutluay et al., 2005). These values are lower affinity than those reported for other channels (Yellen et al., 1991), which could reflect differences in experimental parameters or fundamental differences in the mechanism of inhibition in the cavity of KcsA compared to other channels. KcsA block by TMA or TPrA have not been well studied, but trends of inhibition in other potassium channels would suggest that TPrA may be a higher affinity blocker than TEA (French and Shoukimas, 1981), and thus either TEA or TPrA would be better candidates for the refolding experiments than TMA.

We should also consider possible variability in the crystallography process itself. All crystal trials are set up as 1 µL drops of protein mixed with an equal volume of well solution; however, these drops are set up manually and subject to some amount of variability in volume and amount of mixing. Crystals then grow in these conditions in a highly variable time window. Often some crystals of KcsA will grow fully within three days, while others will not start to appear until weeks

later. For some of the conditions tested, crystals could be harvested at different timepoints and compared. For example, one batch of T74Aester protein was prepared and structures from crystals harvested after a few weeks and 2 months both showed the same flipped structure. It is not possible to compare crystals at different timepoints from the same drop using the current protocol because the whole well is subjected to cryoprotection at the same time. The current data suggest that variability in crystallization parameters are likely not responsible for the change in cavity conformation in KcsA.

It is also worth considering that one crystal structure of semisynthetic KcsA (with the G79-ester modification in the selectivity filter) had a native cavity environment. I was not yet in the lab for these experiments and have not been able to identify any specific changes in the process between that structure and all subsequent work. It is possible that the formulation of lipids or detergents has changed. While I did not try other detergents besides n-decylmaltoside (DM), I tried various lipids that came as crude extract, pure lipids in chloroform, or pure lyophilized lipids, but no consistent effects on cavity conformation were observed. We are confident that small molecules from the ligation are not responsible because recombinant unfolded and refolded protein has the same structure as semisynthetic protein (Chapter 3.2.2).

5.3.2 Lipid-Protein Interactions

The structural variability in the cavity of KcsA is curious and begs the question of whether many other proteins are as affected by the nature of their

environments, especially considering the rise in experimentation on reconstituted membrane proteins. There are few proteins that have been studied by crystallography under so many conditions, and I have not found another membrane protein to be crystallized from both native and *in vitro* refolded conditions, so the implications of this discovery are still unknown. It will be interesting to see if other proteins will reveal new conformations under some conditions, especially as structural studies are becoming more accessible. It will be interesting to see whether the detergent and lipid constraints of membrane proteins make them particularly susceptible to these types of changes.

We have suggested that the non-peptidic density in KcsA may be a lipid alkyl chain, and similar suggestions were made from the NavAb and TWIK-1 structures (Payandeh et al., 2011; Miller and Long, 2012). Increasingly, specific protein-lipid interactions are being identified that can affect protein function and structure in various eukaryotic proteins (Schmidt et al., 2006; Hansen et al., 2011; Zhou et al., 2011a). The lipid composition of various *Streptomyces* species have been studied (Batrakov and Bergelson, 1978); however, nothing is known about the specific lipid composition of *S. lividans*. While it may not be worthwhile to study the lipid composition of *S. lividans* solely for this purpose, other potassium channels come from organisms with better characterized lipid membranes and it has been proposed that lipid binding can be conserved within a protein family (Hunte and Richers, 2008).

5.3.3 Future Directions for Studying Structural Variability in the Cavity

KcsA is a popular model system for studying potassium channel structure and function, and understanding the conformational change in the cavity is relevant to experiments involving semisynthesis, *in vitro* folding, or addition of small molecule additives such as lipids or QA ions. Several experiments will be proposed to further explore the conformational change in the cavity of KcsA.

The addition of QA ions has had inconsistent effects on KcsA folding; however, further experiments should be able to establish a reliable protocol. Because these small QA ions may have very weak affinity for the central cavity, TEA or TPrA should be used at higher concentrations in order to establish a condition where the ion will allow the cavity to assemble in its native conformation, but then be easily removed prior to structural or functional studies. Though no one has studied the block of KcsA by TPrA, it is suggested to have an intermediate affinity between TBA and TEA in other potassium channels, which could be useful for these experiments (French and Shoukimas, 1981).

While crystallography proved to be a powerful tool for observing this subtle cavity conformational change, it reports the structure of the protein in aggregate and at a highly-controlled end point. Since some of these crystallography experiments have been inconsistent, other structural tools may be useful for studying this system. Several NMR experiments have provided useful information about KcsA (Patching, 2011), and the changing environment in the central cavity due to *in vitro* folding or protein-lipid interactions would potentially be well suited for these types of analysis.

Biophysical experiments could also provide more information about the conformational change. We tried to perform circular dichroism (CD) experiments to look at the thermal denaturation of KcsA and whether that was correlated to the F103A mutation or the presence of blockers that would bind in the native versus flipped conformations. Unfortunately, we could not find conditions that produced robust unfolding. Future efforts would be better spent trying to look at similar questions using isothermal titration calorimetry (ITC). KcsA has been studied previously by ITC (Lockless et al., 2007), and the heat of binding of various cavity blockers could provide a very precise way of studying the thermodynamics of this process. In addition, hydrophobic or dielectric sensitive probes introduced in the cavity may be sensitive to changes in the ion occupancy or aqueous volumes of the two cavity conformations. These could give more dynamic information about the conformation in the cavity, and possibly even in a lipid bilayer system. In fact, para-fluoro-phenylalanine has been incorporated at Phe103, but experiments using this modified protein have not yet been published (Komarov et al., 2009b).

We have proposed several directions for continuing to study the nature of the conformational change in KcsA; however, it may be most interesting to focus on the application of this conformation to inhibition of potassium channels more generally.

5.4 Inhibition of KcsA in the Flipped Conformation

The structures of KcsA blocked by TPA and TOA suggest a new mechanism for inhibition in the potassium channel cavity. Our observations suggest that QA blockers can be bound to KcsA in the closed state, unlike what is reported for most potassium channels. Careful kinetics of block in KcsA have not been reported, so it would be interesting to follow up on whether QA ions can bind to KcsA in the closed state in the membrane. It is also interesting to consider whether the conformational change in the cavity is responsible for closed channel block. The Phe103 residues are suggested to be in their 'flipped' rotamer in the open conformation, but much farther from the conduction axis. It is possible to imagine that large QA ions are able to block and form interactions with these residues to induce closure of the channel, thus explaining the long dwell times reported for QA ions in some potassium channels.

We attempted to crystallize KcsA with one physiologically relevant molecule, clofilium. Clofilium is an antiarhythmic drug that is structurally similar but asymmetric in comparison to the QA ions we have previously tested (Figure 5.3). It has been shown to block some eukaryotic potassium channels (Suessbrich et al., 1997; Perry et al., 2004; 2006). This molecule was added to KcsA for similar crystallography trials; however, the channel was in the native conformation and only K^+ was observed in the cavity. This suggests that KcsA may not be able to sufficiently mimic the inhibition of eukaryotic proteins. One possibility is that KcsA is a more stable protein, which makes it easy to work with, but also enhances the interactions between the four subunits and alters the

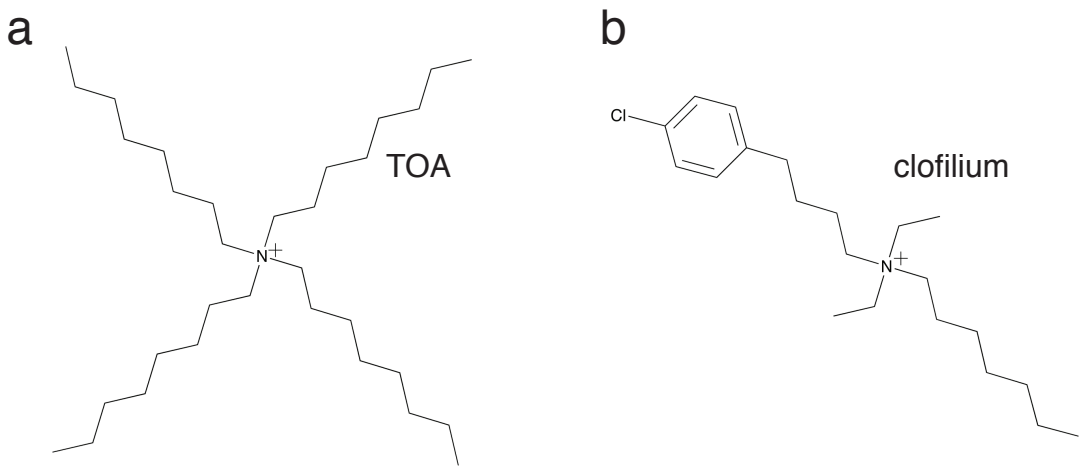

Figure 5.3: Chemical structure of clofilium compared to TOA. The chemical structures of (a) TOA and (b) clofilium. The latter was used used for cavity block crystallography experiments, but no density for this molecule was observed (data not shown).

dynamics of conformational changes in the cavity in comparison to eukaryotic proteins. If this is the case, mutations could possibly be introduced that would decrease the interactions between subunits. Similarly, blocking studies in the bilayer could be improved by incorporating mutations known to increase the open probability of KcsA (Faraldo-Gómez et al., 2007). It is worth studying a few known eukaryotic cavity blockers in KcsA; however, ultimately it may be more appropriate to study these interactions in a eukaryotic protein that can more faithfully reflect physiologically relevant cavity block.

5.5 Implications for Inhibition of Human Potassium Channels

The structures of TPA or TOA block in KcsA suggest that Phe103 plays an important role in inhibition—both by providing a hydrophobic interaction surface and by allowing access to the lateral openings that increase the accessible space in the cavity. We were curious whether this residue is conserved between this bacterial potassium channel and the human potassium channel family.

A sequence alignment was prepared to compare KcsA with 78 human potassium channel subtypes (Figure 5.4 and Appendix 1). Phe103 in KcsA is conserved as phenylalanine in Kca1.1 (BK), Kca5.1 (Slo3), K2p2.1 (TREK-1), K2p4.1 (TRAAK), K2p10.1 (TREK-2) (in both subunits of all K2p's listed), and all Kv7 (KvLQT1-type) channels. It is a tyrosine in all Kv10 (EAG2-type) and Kv11 (HERG-type) channels, and never a tryptophan. This alignment revealed that only a subset of proteins contain an aromatic residue at the position of Phe103.

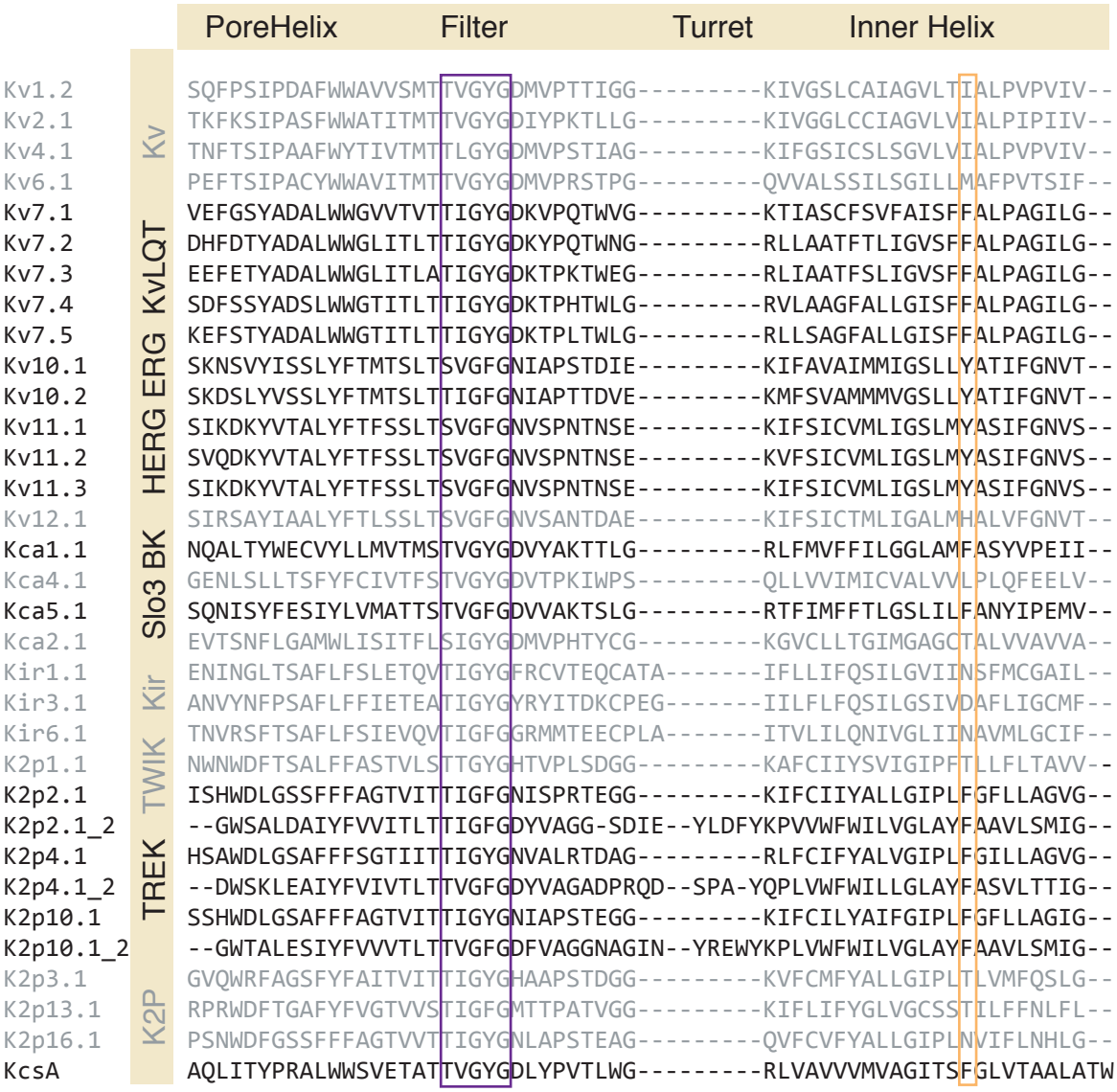

Figure 5.4: Sequence alignment of selected human potassium channels compared to KcsA. The selectivity filter is highlighted with a purple box and Phe103 is highlighted in an orange box. Only sequences containing an aromatic residue at this position are shown in black; others are present as a representative comparison. A full sequence alignment is included in Appendix 1.

Most of these proteins have also been suggested to have interesting cavity properties through structural or biochemical experiments.

Notably, TRAAK is one of the potassium channels with a hydrophobic residue aligned with Phe103 (Phe157 and Phe270 in the two concatenated subunits, respectively). The recent crystal structure of TRAAK is in the open conformation (Brohawn et al., 2012). Phe270 sits along the edge of the larger lateral openings and close to the density observed in the cavity. This suggests that the role of Phe103 to regulate the cavity environment in KcsA may be relevant to eukaryotic potassium channel structures as well.

As a brief side note, the NavAb channel that was crystallized also contains an important phenylalanine residue (Phe203) that interacts with the cavity density (Payandeh et al., 2011). Interestingly, Phe203 in NavAb is aligned with Phe85 in NaK as well as with the V97F mutation introduced into KcsA, suggesting that these different families of cation channels can use the same mechanism to line their lateral openings. In the sequence alignment with human potassium channels, only two K2P channels have an aromatic residue the V97F position. Consistent with their evolutionary relationship, human potassium channels are more likely to have an aromatic residue aligned with Phe103 of KcsA.

Some interesting human potassium channels without crystal structures are also proposed to have an aromatic residue aligned with Phe103. The BK channel contains a phenylalanine at this position (Phe315). It has been proposed that the central cavity of BK may be larger than potassium channels of known structure because of the large molecules known to bind to the cavity of BK, including in its

closed conformation (Li and Aldrich, 2004; Brelidze and Magleby, 2005; Chen and Aldrich, 2011; Geng et al., 2011; Zhou et al., 2011b). Considering the structures of KcsA with TPA or TOA, BK could have a normal cavity shape while also accommodating large molecules through lateral openings in the cavity walls.

Finally, and of particular interest, the HERG channel contains a tyrosine (Tyr652) aligned with Phe103. Off-target interactions between a variety of small molecules and HERG channels have been particularly deleterious to the development of new pharmaceutical agents. Specifically, many of the molecules that block HERG channels do so through interactions with aromatic residues including Tyr652 in the central cavity. Some molecules seem to make contact specifically at this position, while others are affected by mutations more broadly distributed through the cavity (Chen et al., 2002; Perry et al., 2004; Witchel et al., 2004; Kamiya et al., 2006; Perry et al., 2006; Imai et al., 2009). It has been suggested the highly sensitive block of HERG channels is due specifically to a tyrosine at this residue, where mutation to phenylalanine reduces voltage-dependent block (Sánchez-Chapula et al., 2002). Future studies of KcsA F103Y may provide additional insight into this observation.

These examples demonstrate the importance of one particular aromatic amino acid in the cavity of various eukaryotic proteins. Our structures of KcsA inhibition—through a conformational change at this same aromatic position—have the potential to shed new light on the function and inhibition of eukaryotic potassium channels.

5.6 In Conclusion

In this work, several experiments have been presented that provide new insight into the central cavity of KcsA, with implications for potassium channels and membrane proteins more broadly. We observed a 10-fold reduction in K^+ conduction in the presence of a reduced peptide bond dipole at the helix C-termini, suggesting that helix dipoles may make an important contribution to the electrostatic environment in the central cavity. Through these experiments, we also studied a new cavity conformation: Phe103 residues are flipped into the cavity, displacing the cavity K^+, and producing lateral openings between the cavity and the surrounding membrane. This conformation was produced through *in vitro* protein folding or avoided using F103A or V97F mutations. Large QA ions bound in the cavity by making specific interactions with Phe103 in the flipped conformation and extending their alkyl chains into the lateral openings. Sequence alignments with human potassium channels have identified a few candidate proteins with an aromatic amino acid at this position that may have similar importance for channel structure and function.

Experiments have been proposed to improve our understanding of this novel conformational change in the potassium channel cavity. HERG and BK channels share important similarities with the cavity of KcsA, and are of particular interest for the development of pharmaceutical agents. This work inspires new questions about protein electrostatics as well as the inhibition of human potassium channels.

MATERIALS AND METHODS

General methods and materials

Ready-gel 4-20% Tris HCl gels were purchased from Bio-Rad, and used for all gels throughout this work. PCR purification and gel extraction kits were purchased from Qiagen. Restriction enzymes, ligases, and chitin resin were purchased from New England Biolabs. Co^{2+} TALON Metal Affinity resin was from Clontech. Centricon spin concentrators were from Millipore and Microcon concentrators were from Amicon. Amino acids and coupling agents, unless otherwise noted, were purchased from Novabiochem. Pre-loaded Boc-Arg(Tos)-PAM resin was purchased from Advanced Chemtech. Detergents were from Affimetrix and all lipids were from Avanti Polar Lipids. All QA ions were used as bromine salts. All other chemical reagents, unless otherwise noted, were purchased from Sigma-Aldrich or Fisher Scientific. Analytical scale reverse-phase high performance liquid chromatography (RP-HPLC) were performed on a Hewlett-Packard 1100 series instrument using Vydac C18 columns (4 x 150 mm) at 1 ml/min. Preparative and process scale RP-HPLC were performed on a Waters prep LC system comprised of a Waters 2545 Binary Gradient Module and a Waters 2489 UV detector, using Vydac C4 preparative and process scale columns (22 x 250 mm; 50 x 250 mm) at 15-20 and 30-50 ml/min respectively. Size exclusion chromatography was performed on an AKTA FPLC system from GE Healthcare with a P-920 pump and a UPC-900 monitor. ESI-MS was performed on a SciexAPI-100 single quadrupole mass spectrometer. Ultra thin-layer MALDI mass spectra were recorded with a PerSeptive Voyager-DE STR

MALDI time-of-flight mass spectrometer operated in the reflectron mode. ELISA fluorescence measurements were performed on a SpectraMax 190 from Molecular Devices. Electrophysiology was performed with an Axopatch 200 amplifier and Digidata 1322A digitizer, with data collection and processing using Clampex and Clampfit 10.2 software, all from Axon Technologies. Primer synthesis was performed by Integrated DNA Technologies and DNA sequencing was performed by Genewiz.

Preparation of Recombinant full-length KcsA

The full-length KcsA protein (1-160) was prepared similar to previously reported (Doyle et al., 1998). Full-length KcsA with a C-terminal His_6 tag, in the pQE-60 vector was expressed in XL1-Blue *E. coli* cells at 37 °C in LB media with 100 mg/L ampicillin. Protein expression was induced at OD=1 by addition of 1 mM 0.4 mM isopropyl-β-D-thiogalactopyranoside (IPTG). Cells were grown for 3.5 hours and then centrifuged, and the cell pellets were stored at 4 °C overnight. Cells were lysed by ultrasonic probe sonication in lysis buffer (50 mM Tris, 10 mM $MgCl_2$, 150 mM KCl, 250 mM sucrose, 1 mM phenylmethanesulfonyl fluoride (PMSF), and 50 ug/ml DNAse, adjusted to pH 7.5 with HCl). 40 mM n-Decyl-β-D-maltopyranoside was added and incubated at room temperature (RT) for 3 hours to extract the membrane proteins, and then centrifuged at 16,000 rpm for 20 minutes to remove the insoluble fraction. The supernatant was purified over a Co2+ affinity column equilibrated in DM buffer (50 mM Tris, 300 mM KCl, 5 mM DM, adjusted to pH 7.5 with HCl), using a 1 ml bed volume for each 1 L of expression media. Tetrameric KcsA was eluted in 300-500 mM imidazole, was

concentrated in a 10K MWCO spin column (Centricon), and immediately dialyzed in DM buffer at 4 °C to remove the imidazole. Protein was digested with chymotrypsin (Worthington) to remove the C-terminal cytoplasmic domain of the channel using 1:15 (w/w) chymotripsin:KcsA at RT 3 hours. The protein was purified by size-exclusion chromatography (SEC) using a Superdex S200 on an AKTA FPLC, in the presence of DM buffer. Pure protein fractions were combined and again concentrated with a 10K MWCO spin column.

Purification of Antibody fragment antigen-binding (FAB) domain

KcsA-specific antibody (KcsA-1) was purified from mouse hybridoma serum similar to previously reported (Zhou et al., 2001b). Serum was dialyzed overnight in buffer A (10 mM NaCl, 10 mM Tris, adjusted to pH 8.0 with HCl at 4 °C). A MonoQ sepharose column was prepared, with 1.5 ml bed volume per 15-20 mg protein present, and incubated in buffer A. Dialyzed serum was added and IgG antibodies were purified over a gradient from buffer A to 40% buffer B (1 M NaCl, 10 mM Tris, adjusted to pH 8.0 with HCl at 4 °C) in buffer A. Antibody fractions were combined and dialyzed overnight against phosphate buffered saline (PBS). Antibody was concentrated in a 4 ml 10K MWCO spin column (Centricon) to 2mg/ml and then diluted 1:1 with cutting buffer (20 mM cysteine-HCl, 20 mM EDTA, 20 mM β-mercaptoethanol, in PBS at pH 7) and incubated with 1:100 papain:KcsA-1 at 37 °C for 3.5 hours. Papain (Worthington) was inactivated with iodoacetamide. Cleaved product was dialyzed into buffer A at 4 °C overnight. A second MonoQ column was prepared in buffer A. Cleaved FAB eluted in the

flowthrough and was concentrated again by spin column and stored in aliquots at -20 °C.

Preparation of pure KcsA-FAB complex

Pure tetramer from SEC was immediately mixed with purified FAB in a 1:1.5 KcsA:FAB stoichiometry, and incubated at 4 °C for 15 minutes. The sample was then purified again by SEC in DM buffer. Pure complex was isolated and concentrated to an OD~7-9, corresponding to a complex concentration of ~6-8 mg/ml.

KcsA crystallization

Crystal trials of KcsA were prepared under refined conditions (Zhou et al., 2001b): 20-26% PEG400, 50 mM magnesium acetate, pH 5.5-7.5. Most often, 1 µL drops (1 µL each KcsA-FAB complex and screening solution) were set up by hand as hanging drops on siliconized glass coverslips (Hampton) with one or two drops per coverslip. Samples were incubated in 26-well plates (VDX or Hampton), containing 0.5 ml screening solution in the well, and incubated at 20 °C. Occasionally, the crystal screen was prepared in 96-well plate format with 0.1-0.3 µL hanging drops prepared by a Mosquito liquid-handling robot (TTP Labtech). Drops with crystals were cryoprotected by increasing the well to 35% PEG 400 in 3 steps over 24 hours. Crystals were harvested and frozen in liquid nitrogen.

X-ray data collection and processing

Crystals were screened and data was collected at beamlines X25 or X29 at the National Synchrotron Light Source (NSLS, Brookhaven National Lab). Data was

processed using HKL2000 and refined using the CCP4 suite of software. All structures were solved by molecular replacement (MolRep) using the 1k4c structure for KcsA but lacking water molecules, K^+ ions, and sidechains at S69, T74, and F103. Refmac and Coot were used for structure refinement and FFT was used to generate maps for figures. Phenix was used for final refinement of the structure containing the backbone ester modification. Structure figures were made in Pymol.

Reconstitution of pure KcsA for electrophysiology

3:1 POPE:POPG lipids were dried down from chloroform and washed with pentane, then rehydrated in reconstitution buffer (10 mM HEPES, 450 mM KCl, 4 mM NMG, adjusted to pH 7.0 with HCl) at 10 mg/ml by shaking. 33 mM 3-[(3-cholamidopropyl)dimethylammonio]-1-propanesulfonate (CHAPS) was added and rotated for 1 hour, followed by sonication until the solution became clear. Pure KcsA tetramer from SEC was concentrated and mixed with prepared lipid vesicles by diluting the lipids no more than 10%. For high protein:lipid ratios, vesicles were prepared at 20 mg/ml with 50-80 mM CHAPS, and protein was added to prepared vesicles in a 1:1 ratio protein:vesicle ratio. Vesicles were incubated 1-2 hours at RT and then dialyzed in reconstitution buffer with 2-3 buffer changes daily for 2-3 days. For less stable protein, vesicles were incubated and dialyzed at 4 °C, with dialysis steps over 4-5 days. Reconstituted vesicles were aliquoted and flash frozen at -80 °C.

Bilayer electrophysiology

KcsA activity was recorded in a horizontal bilayer electrophysiology setup as previously described (Chen and Miller, 1996; LeMasurier et al., 2001). The setup consisted of a polystyrene partition, made from an overhead transparency with a ~50-100 μm hole in the center, that divides two chambers. The inner chamber was filled with 50 mM succinic acid, 150 mM KCl, pH 4.0, and the outer chamber with 50 mM HEPES, 150 mM KCl, pH 7.0. The solutions were connected to electrodes by 1% agarose salt bridges in 150 mM KCl solution. The membrane was prepared by painting a layer of lipids over the hole and letting it dry before adding well solutions. Then a membrane was painted over the hole with a glass wand. Channels were fused into the membrane by breaking the current membrane, and then adding 0.2-0.5 μL lipid vesicles with a pipette and reforming the membrane in the process. Single channels were recorded in gap-free mode, with at least three consistent channel openings at each recorded voltage. Recordings were sampled at 20 kHz and low-pass filtered to 2 kHz. In some cases, digital filtering to 0.75-1 kHz was used to resolved low conductance channel openings. Error bars represent one standard deviation and were determined by averaging the mean current between at least three different channels in different membranes. Macroscopic currents were recorded with Na^+ in the outer chamber (50 mM HEPES, 150 mM NaCl, pH 7.0) to reduce leak. Pulse families were recorded by holding at -80 mV for 2 seconds between pulses and stepping from -10 to 120 mV in 10 mV increments for 500 ms each. Recordings were sampled at 10 kHz and low-pass filtered to 1 kHz. For block

experiments, inhibitors were added from a concentrated stock solution and diluted 10- to 100-fold into the desired well solution.

Preparation of Recombinant KcsA N-terminal fragment α-thioester

The GST-His6-KcsA(1-68)-GyrA Intein construct (Valiyaveetil et al., 2002a) was expressed in BL21(DE3) *E. coli* cells at 37 °C in LB media with 100 mg/L ampicillin. Protein expression was induced at OD=1 by addition of 1 mM 0.4 mM isopropyl-β-D-thiogalactopyranoside (IPTG) and protein went to the inclusion bodies. Cells were grown for 3.5 hours and then centrifuged, and the cell pellets were stored at -80 °C overnight. This procedure was usually performed on a 12 L scale, as will be reported here. Cell pellets were thawed and resuspended in buffer (50 mM Tris, 200 mM NaCl, 1 mM EDTA, adjusted to pH 7.5 at 4 °C). The sample was put through an 18.5 gauge needle and then PMSF and $MgCl_2$ were added to 1 mM final concentration and DNaseI was added at 5 µg/ml. Cells were lysed with four passes through a French Press (pressure 5,000-10,000 psi). Triton X-100 was added to 1% and stirred to mix thoroughly. Lysate was centrifuged at 10,000 rpm for 20-30 min and the supernatant was discarded. The pellets were washed with 2 M urea buffer (2 M urea, 50 mM Tris, 1 mM EDTA, 1% Triton X-100, pH 7.5, 4 °C), centrifuged, and repeated to wash the pellet a second time. The protein was extracted with 6 M urea buffer (6 M urea, 50 mM Tris, 1 mM EDTA, 2 mM DTT, 1% N-lauryl sarcosine, 1% Triton X-100, pH 7.5, 4 °C) in two rounds of resuspending the pellet and centrifuging, with a final supernatant volume of 200 ml. Fractions were combined and dialyzed in 10K MWCO dialysis tubing in N-peptide buffer (50 mM Tris, 200 mM NaCl, 0.5%

Triton X-100, pH 7.5, 4 °C) with three 4 L dialysis steps. Sample was warmed to RT and 100 mM 2-mercaptoethanesulfonic acid (MESNA) was added to form the thioester. Sample shook in the dark for 48 hours. Thrombin was added at 5 units/ 45 ml in the presence of 5 mM $CaCl_2$ and cleavage occurred over 24 hours to remove GST. A Co^{2+} column was prepared with a 15 ml bed volume and sample was loaded and incubated overnight. Sample was washed in 5 mM and 50 mM imidazole steps and eluted in 300 mM imidazole. The eluted peptide was precipitated with TCA at 15% (w/v) and centrifuged at 4,000 rpm. Pellets were washed twice with -20 °C acetone to remove residual Triton X-100 and lyophilized. The crude peptide was purified by RP-HPLC. The purified peptide was characterized as the desired product by ES-MS (KcsA 1-68 MESNA α-thioester: 8,763.57, expected; 8763.7±1.0 observed).

Chemical Synthesis of KcsA(69-122, T74A) by SPPS

The peptide, NH2-CVETAA$_{74}$TVGYGDLYPVTLWGRLVAVVVMVGGITSFGLVTA ALATWFVGREQERR-COOH, was synthesized by manual SPPS using a slightly modified version of the in situ neutralization/HBTU activation protocol for Boc chemistry (Schnölzer et al., 2007). Synthesis was initiated on the preloaded Boc-Arg(Tos)-PAM resin on a 0.5 mmol scale (926 mg, 0.54 mmol/g). Amino acids were prepared in at least 4.4 mmol excess to the resin, with quantity increasing as the peptide became very long. At around half way through the synthesis, the resin was split into two vessels to improve mixing. Most β-branched amino acids (Val, Ile, Thr) were double-coupled, with dimethyl sulfoxide (DMSO) used as the solvent for the second coupling. Most couplings were monitored by Kaiser test

(Sarin et al., 1981). Upon completion of the synthesis, the peptide resin was dried under vacuum and cleaved in 500-600 mg batches by anhydrous hydrofluoric acid (HF) (15 ml HF, 400 µl ρ-cresol) at 0 °C for 1 hour. Cleaved peptide was isolated by precipitation with cold anhydrous ether containing 2% β-mercaptoethanol (β-ME), and then dissolved in 50% TFE:H_2O containing 0.1% TFA. The crude peptide was purified by RP-HPLC. The purified peptide was characterized as the desired product by ES-MS (KcsA 69-122, S69C, T74A: 5,801.7 Da, expected; 5,803.2±1.4 Da, observed).

Chemical Synthesis of KcsA(69-122, T74Aester) by SPPS

SPPS was performed as described above, for residues 75-122. To couple position 74 (T74A derivative L-lactic acid), L-lactic acid was coupled by carbodiimide formation (4.4 eq DIC, 4.8 eq. HOBt) in the presence of N-ethyl-morpholine (1.6 eq). Formyl protecting groups were deprotected by treatment with ethanolamine prior to the ester coupling step. Ala73 (Boc-Ala-OH) was coupled first by carbodiimide formation (4.4 eq. DIC, 4.8 eq. HOBt) in the presence of 4-Dimethylaminopyridine (DMAP, 0.03 eq.), at 4 °C for 30 minutes, and then a second coupling was performed with 4.4 eq. PyAOP and 17.6 eq. DIEA at 4 °C for 30 minutes. More recent syntheses used symmetric anhydride formation (4.4 eq. DIC, 2.4 eq. HOBt, 0.1 eq DMAP) at 4 °C for 30 min, repeated two or three times. Amino acids 69-72 were the coupled by standard Boc-SPPS. The peptide was cleaved and purified as for the unmodified protein, with the exception of excluding β-ME from the cleaved peptide precipitation. The purified

peptide was characterized as the desired product by ES-MS (KcsA 69-122, S69C, T74Aester: 5,802.7 Da, expected; 5804.7±1.8 Da, observed).

Chemical Synthesis of KcsA(69-122, T74Aester, F103A) by SPPS

The protocol for synthesis of KcsA(69-122, T74Aester) was repeated for the synthesis of the T74Aester-F103A peptide, with incorporation of the F103A substitution. The purified peptide was characterized as the desired product by ES-MS (KcsA 69-122, S69C, T74A, F103A: 5,725.6 Da, expected; 5725.9±1.5 Da, observed).

Purification of peptides

Peptides (N-terminal fragment α-thioester and synthetic C-peptide) were dissolved in 50:50 TFE:H_2O with 0.1% TFA. Peptides were purified by RP-HPLC in gradients of 55-90% B (90% acetonitrile, 0.1%TFA, in H_2O) or shallower.

KcsA protein ligation

Pure N-terminal fragment α-thioester and C-peptide were quantified by A_{280} absorbance and aliquoted into eppendorph tubes for 41 nmol scale ligations (360 µg N-peptide, 470 µg C-peptide) along with 2.48 µl 10% SDS solution (final SDS concentration in the ligation reaction will be 0.3%), and lyophilized. Samples were redissolved in ligation buffer (100 mM phosphate, pH 7.8) and 2.25% thiophenol was added to initiate the reaction. Reactions were performed under argon and proceeded at 37 °C with shaking for 18-24 hours. Immediately following the ligation, 10 mM TCEP was added at 37 °C for 30 min. The crude ligation mixture was used directly in the folding reaction.

Enzyme Linked Immunosorbent Assay (ELISA) to detect folded KcsA

An ELISA assay was developed to detect folded KcsA tetramer that could not be observed by SDS-PAGE, by using serum from the KcsA-1 antibody (also the source of FAB for structural studies). ELISAs were performed in NUNC Maxisorb 96-well plates blocked with 5% (w/v) bovine serum albumin (BSA) solution in DM buffer (50 mM Tris, 150 mM KCl, 5 mM DM, pH 7.5, 4 °C). Control folded KcsA was prepared by serial dilution (1 ng/well - 3,333 ng/well), along with the test samples (usually 10%, and 1% of starting concentration), and each sample was assayed in duplicate or triplicate wells. 50 µl samples were added in DM buffer for detergent extracted KcsA, or in lipid buffer (50 mM HEPES, 150 mM KCl, 20 mg/ml POPC, pH 7.5, 4 °C) for crude folding reactions, and the respective buffer system was maintained throughout the ELISA. Sample was incubated at least one hour at RT. KcsA-1 primary antibody was added at 1:5,000, with 2% (w/v) BSA in the appropriate buffer, for one hour at RT, and finally α-mouse HRP was incubated at 1:10,000 with 2% (w/v) BSA at RT for 30 min. 1-Step Ultra TMB ELISA solution (Pierce) was used for the colorimetric readout.

KcsA unfolding

Recombinant KcsA was prepared for unfolding by 15% TCA precipitation and lyophilization. Protein was redissolved in 50:50 TFE:H_2O with 0.5% TFA and boiled for at least 15 minutes. Protein unfolding was confirmed by SDS-PAGE. Protein was then aliquoted and supplemented with SDS to produce a final concentration of 0.1% in the folding reaction. Samples were lyophilized and

resuspended in 50 mM phosphate buffer, pH 7.8 at 0.3-0.5 mM protein concentration.

KcsA *in vitro* folding

Protein folding (MES/Soy conditions)

Crude soybean lipids in pellet form were dissolved in cyclohexane and lyophilized. Lipids were suspended in 'MES' folding buffer (50 mM MES, 300 mM KCl, 10 mM DTT, pH 6.4) at 27 mg/ml in a glass vial and sonicated until fully resuspended. Protein in phosphate buffer and 1% SDS (from ligations or unfolding preparation) was diluted 1:5 with H_2O, followed by a 1:2 dilution with the lipid mixture. This resulted in a 10-fold dilution of protein and a 2-fold dilution of the folding lipids, to a final concentration of 13.5 mg/ml. The folding mixture was sonicated again and let sit at RT for 36-60 hours. Folding progress was analyzed by SDS-PAGE or ELISA, depending on the stability of the protein.

Protein folding (Tris/Soy conditions)

This protocol was perfomed as previously published (Valiyaveetil et al., 2002a). Crude soybean lipids in pellet form were dissolved in cyclohexane and lyophilized. Lipids were suspended in 'Tris' folding buffer (100 mM Tris, 200 mM NaCl, 15 mM KCl, 10% glycerol, 10 mM DTT, pH 7.5) at 30 mg/ml in a glass vial and sonicated until resuspended. Protein in phosphate buffer and 1% SDS (from ligations or unfolding preparation) was diluted 1:5 with Tris folding buffer, followed by a 1:2 dilution with the lipid mixture. This resulted in a 10-fold dilution of protein and a 2-fold dilution of the folding lipids, to a final concentration of 13.5 mg/ml.

The folding mixture was sonicated again and incubated at RT for 36-60 hours. Folding progress was analyzed by SDS-PAGE.

Protein folding (HEPES/POPC conditions)

This protocol was obtained from Dr. Valiyaveetil (personal communication). Pure POPC lipids in chloroform were aliquoted into a glass vial and dried down with argon. Lipids were washed twice with pentane, dried with argon, and lyophilized to ensure that the lipids were dry. Lipids were suspended in 'HEPES' folding buffer (50 mM HEPES, 150 mM KCl, 10 mM DTT) at 20 mg/ml and sonicated until translucent. Protein in phosphate buffer and 1% SDS (from ligations or unfolding preparation) was diluted 1:10 with folding mixture to give a final lipid concentration of 18 mg/ml. The folding mixture was sonicated again and let sit at RT for 90 min - 3 hours. Folding progress was analyzed by SDS-PAGE.

Purification of folded protein

Folded product was dialyzed overnight in buffer without DM (50 mM Tris, 300 mM KCl, pH 7.5) to remove DTT and TCEP. Folded channels were extracted with 50 mM DM for 3 hours at RT. The sample was centrifuged and purified by Co^{2+} column, with a 5 mM imidazole wash and 300 mM imidazole elution in DM buffer. Fractions containing folded tetramer were pooled, concentrated, and dialyzed in buffer with DM overnight to remove imidazole. Semisynthetic protein was digested with trypsin at a 1:100 (molar) ratio at RT overnight. Recombinant, refolded protein was digested with chymotrypsin as described for recombinant KcsA, above. Cleaved protein was purified by SEC in DM buffer. Protein was concentrated and prepared for electrophysiology or crystallography.

Ultra Thin-Layer Mass spectrometry

Ultra Thin-Layer MS was performed exactly as described (http://www.jove.com/video/192/maldi-sample-preparation-the-ultra-thin-layer-method) (Cadene and Chait, 2000). Cytochrome C was used for mass calibration.

Appendix 1: Sequence alignment of human K^+ channels and KcsA.

	PoreHelix	Filter	Turret	Inner Helix
Kv1.1	SHFSSIPDAFWWAVVSMTTVGYGDMYPVTIGG	---------	KIVGSLCAIAGVLTIALPVPVIV--	
Kv1.2	SQFPSIPDAFWWAVVSMTTVGYGDMVPTTIGG	---------	KIVGSLCAIAGVLTIALPVPVIV--	
Kv1.3	SGFSSIPDAFWWAVVTMTTVGYGDMHPVTIGG	---------	KIVGSLCAIAGVLTIALPVPVIV--	
Kv1.4	THFQSIPDAFWWAVVTMTTVGYGDMKPITVGG	---------	KIVGSLCAIAGVLTIALPVPVIV--	
Kv1.5	THFSSIPDAFWWAVVTMTTVGYGDMRPITVGG	---------	KIVGSLCAIAGVLTIALPVPVIV--	
Kv1.6	SLFPSIPDAFWWAVVTMTTVGYGDMYPMTVGG	---------	KIVGSLCAIAGVLTIALPVPVIV--	
Kv1.7	SHFTSIPESFWWAVVTMTTVGYGDMAPVTVGG	---------	KIVGSLCAIAGVLTISLPVPVIV--	
Kv1.8	SHFSSIPDGFWWAVVTMTTVGYGDMCPTTPGG	---------	KIVGTLCAIAGVLTIALPVPVIV--	
Kv2.1	TKFKSIPASFWWATITMTTVGYGDIYPKTLLG	---------	KIVGGLCCIAGVLVIALPIPIIV--	
Kv2.2	TKFTSIPASFWWATITMTTVGYGDIYPKTLLG	---------	KIVGGLCCIAGVLVIALPIPIIV--	
Kv3.1	THFKNIPIGFWWAVVTMTTLGYGDMYPQTWSG	---------	MLVGALCALAGVLTIAMPVPVIV--	
Kv3.2	TQFKNIPIGFWWAVVTMTTLGYGDMYPQTWSG	---------	MLVGALCALAGVLTIAMPVPVIV--	
Kv3.3	TYFKNIPIGFWWAVVTMTTLGYGDMYPKTWSG	---------	MLVGALCALAGVLTIAMPVPVIV--	
Kv3.4	TDFKNIPIGFWWAVVTMTTLGYGDMYPKTWSG	---------	MLVGALCALAGVLTIAMPVPVIV--	
Kv4.1	TNFTSIPAAFWYTIVTMTTLGYGDMVPSTIAG	---------	KIFGSICSLSGVLVIALPVPVIV--	
Kv4.2	SKFTSIPAAFWYTIVTMTTLGYGDMVPKTIAG	---------	KIFGSICSLSGVLVIALPVPVIV--	
Kv4.3	SKFTSIPASFWYTIVTMTTLGYGDMVPKTIAG	---------	KIFGSICSLSGVLVIALPVPVIV--	
Kv5.1	TLFKSIPQSFWWAIITMTTVGYGDIYPKTTLG	---------	KLNAAISFLCGVIAIALPIHPII--	
Kv6.1	PEFTSIPACYWWAVITMTTVGYGDMVPRSTPG	---------	QVVALSSILSGILLMAFPVTSIF--	
Kv6.2	RDFSSVPASYWWAVISMTTVGYGDMVPRSLPG	---------	QVVALSSILSGILLMAFPVTSIF--	
Kv6.3	KDFTSIPAACWWVIISMTTVGYGDMYPITVPG	---------	RILGGVCVVSGIVLLALPITFIY--	
Kv6.4	LEFTSIPASYWWAIISMTTVGYGDMVPRSVPG	---------	QMVALSSILSGILIMAFPATSIF--	
Kv7.1	VEFGSYADALWWGVVTVTTIGYGDKVPQTWVG	---------	KTIASCFSVFAISFFALPAGILG--	
Kv7.2	DHFDTYADALWWGLITLTTIGYGDKYPQTWNG	---------	RLLAATFTLIGVSFFALPAGILG--	
Kv7.3	EEFETYADALWWGLITLATIGYGDKTPKTWEG	---------	RLIAATFSLIGVSFFALPAGILG--	
Kv7.4	SDFSSYADSLWWGTITLTTIGYGDKTPHTWLG	---------	RVLAAGFALLGISFFALPAGILG--	
Kv7.5	KEFSTYADALWWGTITLTTIGYGDKTPLTWLG	---------	RLLSAGFALLGISFFALPAGILG--	
Kv8.1	TTFTSVPCAWWWATTSMTTVGYGDIRPDTTTG	---------	KIVAFMCILSGILVLALPIAIIN--	
Kv8.2	TNFTTIPHSWWWAAVSISTVGYGDMYPETHLG	---------	RFFAFLCIAFGIILNGMPISILY--	
Kv9.1	VGFNTIPACWWWGTVSMTTVGYGDVVPVTVAG	---------	KLAASGCILGGILVVALPITIIF--	
Kv9.2	EGLATIPACWWWATVSMTTVGYGDVVPGTTAG	---------	KLTASACILAGILVVVLPITLIF--	
Kv9.3	SSLTSIPICWWWATISMTTVGYGDTHPVTLAG	---------	KLIASTCIICGILVVALPITIIF--	
Kv10.1	SKNSVYISSLYFTMTSLTSVGFGNIAPSTDIE	---------	KIFAVAIMMIGSLLYATIFGNVT--	
Kv10.2	SKDSLYVSSLYFTMTSLTTIGFGNIAPTTDVE	---------	KMFSVAMMMVGSLLYATIFGNVT--	
Kv11.1	SIKDKYVTALYFTFSSLTSVGFGNVSPNTNSE	---------	KIFSICVMLIGSLMYASIFGNVS--	
Kv11.2	SVQDKYVTALYFTFSSLTSVGFGNVSPNTNSE	---------	KVFSICVMLIGSLMYASIFGNVS--	
Kv11.3	SIKDKYVTALYFTFSSLTSVGFGNVSPNTNSE	---------	KIFSICVMLIGSLMYASIFGNVS--	
Kv12.1	SIRSAYIAALYFTLSSLTSVGFGNVSANTDAE	---------	KIFSICTMLIGALMHALVFGNVT--	
Kv12.2	SLRSAYITSLYFALSSLTSVGFGNVSANTDTE	---------	KIFSICTMLIGALMHAVVFGNVT--	
Kv12.3	SRRSAYIAALYFTLSSLTSVGFGNVCANTDAE	---------	KIFSICTMLIGALMHAVVFGNVT--	
Kca1.1	NQALTYWECVYLLMVTMSTVGYGDVYAKTTLG	---------	RLFMVFFILGGLAMFASYVPEII--	
Kca2.1	EVTSNFLGAMWLISITFLSIGYGDMVPHTYCG	---------	KGVCLLTGIMGAGCTALVVAVVA--	
Kca2.2	DVTSNFLGAMWLISITFLSIGYGDMVPNTYCG	---------	KGVCLLTGIMGAGCTALVVAVVA--	
Kca2.3	DVTSNFLGAMWLISITFLSIGYGDMVPHTYCG	---------	KGVCLLTGIMGAGCTALVVAVVA--	
Kca3.1	NATGHLSDTLWLIPITFLTIGYGDVVPGTMWG	---------	KIVCLCTGVMGVCCTALLVAVVA--	
Kca4.1	GENLSLLTSFYFCIVTFSTVGYGDVTPKIWPS	---------	QLLVVIMICVALVVLPLQFEELV--	
Kca4.2	GKKLNLFDSLYFCIVTFSTVGFGDVTPETWSS	---------	KLFVVAMICVALVVLPIQFEQLA--	
Kca5.1	SQNISYFESIYLVMATTSTVGFGDVVAKTSLG	---------	RTFIMFFTLGSLILFANYIPEMV--	

(continued on the subsequent page)

Appendix 1 (cont): Sequence alignment of human K^+ channels and KcsA.

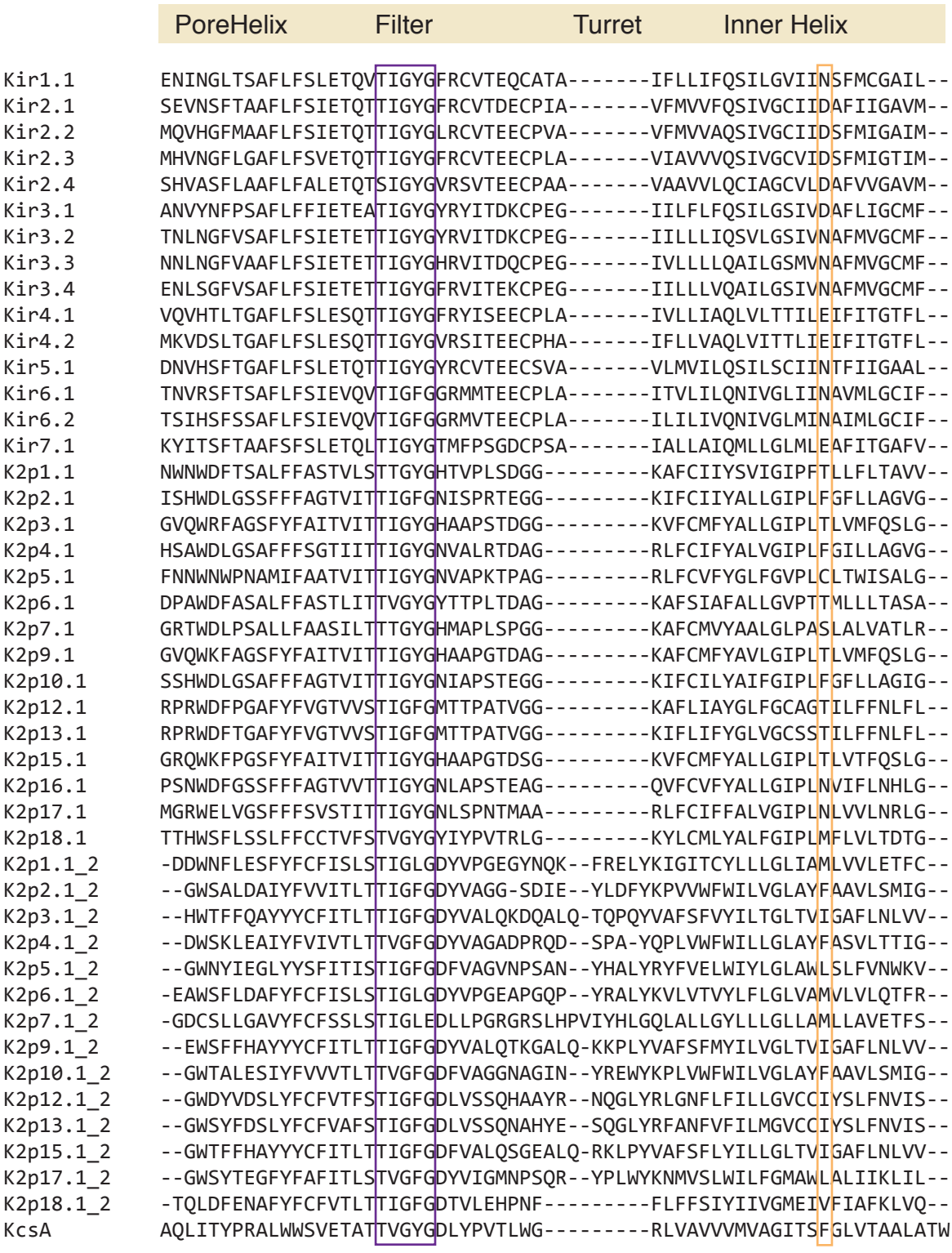

BIBLIOGRAPHY

Ahern, C.A., and Kobertz, W.R. (2009). Chemical tools for K^+ channel biology. Biochemistry *48*, 517–526.

Ahern, C.A., Eastwood, A.L., Lester, H.A., Dougherty, D.A., and Horn, R. (2006). A Cation-π Interaction between Extracellular TEA and an Aromatic Residue in Potassium Channels. The Journal of General Physiology *128*, 649–657.

Alam, A., and Jiang, Y. (2009a). High-resolution structure of the open NaK channel. Nat Struct Mol Biol *16*, 30–34.

Alam, A., and Jiang, Y. (2009b). Structural analysis of ion selectivity in the NaK channel. Nat Struct Mol Biol *16*, 35–41.

Allen, T.W., Kuyucak, S., and Chung, S.H. (1999). Molecular dynamics study of the KcsA potassium channel. Biophysical Journal *77*, 2502–2516.

Allison, J.R., Müller, M., and van Gunsteren, W.F. (2010). A comparison of the different helices adopted by α- and β-peptides suggests different reasons for their stability. Protein Science *19*, 2186–2195.

Applequist, J., and Mahr, T.G. (1966). The conformation of poly-L-tyrosine in quinoline from dielectric dispersion studies. J. Am. Chem. Soc. *88*, 5419–5429.

Aqvist, J., and Luzhkov, V. (2000). Ion permeation mechanism of the potassium channel. Nature *404*, 881–884.

Aqvist, J., Luecke, H., Quiocho, F.A., and Warshel, A. (1991). Dipoles localized at helix termini of proteins stabilize charges. Proceedings of the National Academy of Sciences *88*, 2026–2030.

Armstrong, C.M. (1966). Time course of TEA^+-induced anomalous rectification in squid giant axons. The Journal of General Physiology *50*, 491.

Armstrong, C.M. (1969). Inactivation of the Potassium Conductance and Related Phenomena Caused by Quaternary Ammonium Ion Injection in Squid Axons. J Gen Physiol *54*, 553–553575.

Armstrong, C.M. (1971). Interaction of Tetraethylammonium Ion Derivatives with Potassium Channels of Giant Axons. The Journal of General Physiology *58*, 413–437.

Armstrong, C.M. (1975). Ionic pores, gates, and gating currents. Q. Rev. Biophys. *7*, 179–210.

Armstrong, C.M., and Binstock, L. (1965). Anomalous Rectification in the Squid Giant Axon Injected with Tetraethylammonium Chloride. J Gen Phys *48*, 859–872.

Armstrong, C.M., and Hille, B. (1972). The inner quaternary ammonium ion receptor in potassium channels of the node of Ranvier. The Journal of General Physiology *59*, 388.

Armstrong, C.M., and Taylor, S.R. (1980). Interaction of barium ions with potassium channels in squid giant axons. Biophysical Journal *30*, 473–488.

Armstrong, K., and Baldwin, R.L. (1993). Charged Histidine Affects Alpha-Helix Stability at All Positions in the Helix by Interacting with the Backbone Charges. Proceedings of the National Academy of Sciences of the United States of America *90*, 11337–11340.

Baker, E.N., and Hubbard, R.E. (1984). Hydrogen bonding in globular proteins. Progress in Biophysics and Molecular Biology *44*, 97–179.

Bang, D., and Kent, S.B.H. (2004). A One-Pot Total Synthesis of Crambin. Angewandte Chemie International Edition *43*, 2534–2538.

Batjargal, S., Wang, Y.J., Goldberg, J.M., Wissner, R.F., and Petersson, E.J. (2012). Native Chemical Ligation of Thioamide-Containing Peptides: Development and Application to the Synthesis of Labeled α-Synuclein for Misfolding Studies. J. Am. Chem. Soc. *Article ASAP*.

Batrakov, S.G., and Bergelson, L.D. (1978). Lipids of the Streptomycetes. Structural investigation and biological interrelation a review. Chem. Phys. Lipids *21*, 1–29.

Beligere, G.S., and Dawson, P.E. (2000). Design, Synthesis, and Characterization of 4-Ester CI2, a Model for Backbone Hydrogen Bonding in Protein α-Helices. J Am Chem Soc *122*, 12079–12082.

Bernèche, S., and Roux, B. (2001). Energetics of ion conduction through the K^+ channel. Nature *414*, 73–77.

Bezanilla, F., and Armstrong, C.M. (1972). Negative conductance caused by entry of sodium and cesium ions into the potassium channels of squid axons. The Journal of General Physiology *60*, 588–608.

Bezanilla, F., and Armstrong, C.M. (1974). Gating Currents of Sodium Channels - 3 Ways to Block Them. Science *183*, 753–754.

Bichet, D., Haass, F.A., and Jan, L.Y. (2003). Merging functional studies with structures of inward-rectifier K(+) channels. Nat. Rev. Neurosci. *4*, 957–967.

Bjornholm, B., Jorgensen, F., and Schwartz, T.W. (1993). Conservation of a Helix-Stabilizing Dipole-Moment in the Pp-Fold Family of Regulatory Peptides. Biochemistry *32*, 2954–2959.

Blagdon, D.E., and Goodman, M. (1975). Letter: Mechanisms of protein and polypeptide helix initiation. Biopolymers *14*, 241–245.

Blankenship, J.W., Balambika, R., and Dawson, P.E. (2002). Probing Backbone Hydrogen Bonds in the Hydrophobic Core of GCN4. Biochemistry *41*, 15676–15684.

Blom, C., and Gunthard, H. (1981). Rotational-Isomerism in Methyl Formate and Methyl Acetate; A Low-Temperature Matrix Infrared Study Using Thermal Molecular-Beams. Chem Phys Lett *84*, 267–271.

Boheim, G., Hanke, W., and Jung, G. (1983). Alamethicin Pore Formation - Voltage-Dependent Flip-Flop of Alpha-Helix Dipoles. Biophys Struct Mech *9*, 181–191.

Brant, D., Tonelli, A., and Flory, P. (1969). Configurational Statistics of Random Poly(Lactic Acid) Chains 2. Theory. Macromolecules *2*, 228–&.

Brelidze, T.I., and Magleby, K.L. (2005). Probing the Geometry of the Inner Vestibule of BK Channels with Sugars. The Journal of General Physiology *126*, 105–121.

Brohawn, S.G., del Mármol, J., and MacKinnon, R. (2012). Crystal structure of the human K2P TRAAK, a lipid- and mechano-sensitive K^+ ion channel. Science *335*, 436–441.

Cadene, M., and Chait, B.T. (2000). A Robust, Detergent-Friendly Method for Mass Spectrometric Analysis of Integral Membrane Proteins. Anal Chem *72*, 5655–5658.

Chang, C.F., and Zehfus, M.H. (1996). The effect of N-methylation on helical peptides. Biopolymers *40*, 609–616.

Chatelain, F.C., Alagem, N., Xu, Q., Pancaroglu, R., Reuveny, E., and Minor, D.L.J. (2005). The pore helix dipole has a minor role in inward rectifier channel function. Neuron *47*, 833–843.

Chen, J., Seebohm, G., and Sanguinetti, M.C. (2002). Position of aromatic residues in the S6 domain, not inactivation, dictates cisapride sensitivity of HERG and eag potassium channels. Proceedings of the National Academy of Sciences *99*, 12461–12466.

Chen, T.Y., and Miller, C. (1996). Nonequilibrium gating and voltage dependence of the ClC-0 Cl^- channel. The Journal of General Physiology *108*, 237–250.

Chen, X., and Aldrich, R.W. (2011). Charge substitution for a deep-pore residue reveals structural dynamics during BK channel gating. The Journal of General Physiology *138*, 137–154.

Choe, S., and Roosild, T. (2002). Regulation of the K Channels by Cytoplasmic Domains . Biopolymers *66*, 294–299.

Choi, H., and Heginbotham, L. (2004). Functional influence of the pore helix glutamate in the KcsA K^+ channel. Biophysical Journal *86*, 2137–2144.

Choi, K.L., Mossman, C., Aubé, J., and Yellen, G. (1993). The internal quaternary ammonium receptor site of Shaker potassium channels. Neuron *10*, 533–541.

Chourasia, M., Sastry, G.M., and Sastry, G.N. (2011). Aromatic-Aromatic Interactions Database, A(2)ID: an analysis of aromatic π-networks in proteins. Int. J. Biol. Macromol. *48*, 540–552.

Chung, S.-H., Allen, T.W., Hoyles, M., and Kuyucak, S. (1999). Permeation of Ions Across the Potassium Channel: Brownian Dynamics Studies. Biophysical Journal *77*, 2517–2533.

Clayton, D., Shapovalov, G., Maurer, J.A., Dougherty, D.A., Lester, H.A., and Kochendoerfer, G.G. (2004). Total chemical synthesis and electrophysiological characterization of mechanosensitive channels from Escherichia coli and Mycobacterium tuberculosis. Proceedings of the National Academy of Sciences *101*, 4764–4769.

Cortes, D.M., and Perozo, E. (1997). Structural Dynamics of the Streptomyces lividans K^+ Channel (SKC1): Oligomeric Stoichiometry and Stability. Biochemistry *36*, 10343–10352.

Cortes, D.M., Cuello, L.G., and Perozo, E. (2001). Molecular Architecture of Full-Length KcsA. The Journal of General Physiology *117*, 165–180.

Cuello, L.G., Jogini, V., Cortes, D.M., and Perozo, E. (2010a). Structural mechanism of C-type inactivation in K^+ channels. Nature *466*, 203–208.

Cuello, L.G., Jogini, V., Cortes, D.M., Pan, A.C., Gagnon, D.G., Dalmas, O., Cordero-Morales, J.F., Chakrapani, S., Roux, B., and Perozo, E. (2010b). Structural basis for the coupling between activation and inactivation gates in K^+ channels. Nature *466*, 272–275.

Cuello, L.G., Jogini, V., Cortes, D.M., Sompornpisut, A., Purdy, M.D., Wiener, M.C., and Perozo, E. (2010c). Design and characterization of a constitutively open KcsA. FEBS Lett *584*, 1133–1138.

Cuello, L.G., Romero, J.G., Cortes, D.M., and Perozo, E. (1998). pH-dependent gating in the Streptomyces lividans K^+ channel. Biochemistry *37*, 3229–3236.

Dart, C. (2010). Lipid microdomains and the regulation of ion channel function. J. Physiol. (Lond.) *588*, 3169–3178.

Dawson, P.E., and Kent, S.B. (2000). Synthesis of native proteins by chemical ligation. Annual Review of Biochemistry *69*, 923–960.

Deechongkit, S., Nguyen, H., Powers, E.T., Dawson, P.E., Gruebele, M., and Kelly, J.W. (2004). Context-dependent contributions of backbone hydrogen bonding to beta-sheet folding energetics. Nature *430*, 101–105.

del Camino, D., Holmgren, M., Liu, Y., and Yellen, G. (2000). Blocker protection in the pore of a voltage-gated K+ channel and its structural implications. Nature *403*, 321–325.

Dirksen, A., and Dawson, P.E. (2008). Expanding the scope of chemoselective peptide ligations in chemical biology. Current Opinion in Chemical Biology *12*, 760–766.

Doran, J.D., and Carey, P.R. (1996). Alpha-helix dipoles and catalysis: absorption and Raman spectroscopic studies of acyl cysteine proteases. Biochemistry *35*, 12495–12502.

Dougherty, D.A. (2008). Physical organic chemistry on the brain. J. Org. Chem. *73*, 3667–3673.

Dougherty, D.A., and Stauffer, D.A. (1990). Acetylcholine binding by a synthetic receptor: implications for biological recognition. Science *250*, 1558–1560.

Doyle, D.A., Morais Cabral, J., Pfuetzner, R.A., Kuo, A., Gulbis, J.M., Cohen, S.L., Chait, B.T., and MacKinnon, R. (1998). The structure of the potassium channel: molecular basis of K+ conduction and selectivity. Science *280*, 69–77.

Durek, T., Torbeev, V.Y., and Kent, S.B.H. (2007). Convergent chemical synthesis and high-resolution X-ray structure of human lysozyme. Proceedings of the National Academy of Sciences *104*, 4846–4851.

Dutzler, R., Campbell, E.B., Cadene, M., Chait, B.T., and MacKinnon, R. (2002). X-ray structure of a ClC chloride channel at 3.0 Å reveals the molecular basis of anion selectivity. Nature *415*, 287–294.

Edmonds, D.T. (1985). The alpha-helix dipole in membranes: a new gating mechanism for ion channels. Eur. Biophys. J. *13*, 31–35.

Eisenman, G., and Dani, J.A. (1987). An introduction to molecular architecture and permeability of ion channels. Annu Rev Biophys Bio *16*, 205–226.

England, P.M., Zhang, Y., Dougherty, D.A., and Lester, H.A. (1999). Backbone mutations in transmembrane domains of a ligand-gated ion channel: implications for the mechanism of gating. Cell *96*, 89–98.

Enyedi, P., and Czirják, G. (2010). Molecular background of leak K^+ currents: two-pore domain potassium channels. Physiological Reviews *90*, 559–605.

Erlanson, D.A., Chytil, M., and Verdine, G.L. (1996). The leucine zipper domain controls the orientation of AP-1 in the NFAT.AP-1.DNA complex. Chemistry and Biology *3*, 981–991.

Evans, T.C., Benner, J., and Xu, M.Q. (1998). Semisynthesis of cytotoxic proteins using a modified protein splicing element. Protein Sci *7*, 2256–2264.

Evans, T.C., Benner, J., and Xu, M.Q. (1999). The *in vitro* ligation of bacterially expressed proteins using an intein from *Methanobacterium thermoautotrophicum*. The Journal of Biological Chemistry *274*, 3923–3926.

Faraldo-Gómez, J.D., Kutluay, E., Jogini, V., Zhao, Y., Heginbotham, L., and Roux, B. (2007). Mechanism of Intracellular Block of the KcsA K^+ Channel by Tetrabutylammonium: Insights from X-ray Crystallography, Electrophysiology and Replica-exchange Molecular Dynamics Simulations. Journal of Molecular Biology *365*, 649–662.

Fehrentz, T., Schönberger, M., and Trauner, D. (2011). Optochemical genetics. Angew Chem Int Ed Engl *50*, 12156–12182.

Focke, P.J., and Valiyaveetil, F.I. (2010). Studies of ion channels using expressed protein ligation. Curr Opin Chem Biol *14*, 797–802.

French, R., and Shoukimas, J. (1981). Blockage of squid axon potassium conductance by internal tetra-N-alkylammonium ions of various sizes. Biophysical Journal *34*, 271–291.

French, R.J., and Adelman, W.J., Jr. (1976). Competition, Saturation, and Inhibition-Ionic Interactions Shown by Membrane Ionic Currents in Nerve, Muscle, and Bilayer Systems. In Current Topics in Membranes and Transport, F.B.A.A. Kleinzeller, ed. (Academic Press), pp. 161–207.

French, R.J., and Wells, J.B. (1977). Sodium ions as blocking agents and charge carriers in the potassium channel of the squid giant axon. The Journal of General Physiology *70*, 707–724.

Geng, Y., Niu, X., and Magleby, K.L. (2011). Low resistance, large dimension entrance to the inner cavity of BK channels determined by changing side-chain volume. The Journal of General Physiology *137*, 533–548.

Grosse, W., Essen, L.-O., and Koert, U. (2011). Strategies and Perspectives in Ion-Channel Engineering. Chembiochem *12*, 830–839.

Guidoni, L., Torre, V., and Carloni, P. (2000). Water and potassium dynamics inside the KcsA K^+ channel. FEBS Lett *477*, 37–42.

Guo, M., Xu, F., Yamada, J., Egelhofer, T., Gao, Y., Hartzog, G.A., Teng, M., and Niu, L. (2008). Core Structure of the Yeast Spt4-Spt5 Complex: A Conserved Module for Regulation of Transcription Elongation. Structure/Folding and Design *16*, 1649–1658.

Guy, H.R., and Seetharamulu, P. (1986). Molecular model of the action potential sodium channel. Proceedings of the National Academy of Sciences *83*, 508–512.

Hagiwara, S., Miyazaki, S., Krasne, S., and al, E. (1977). Anomalous Permeabilities of Egg Cell-Membrane of a Starfish in K+-Tl+ Mixtures. The Journal of General Physiology *70*, 269–281.

Hall, J.E. (1981). Voltage-dependent lipid flip-flop induced by alamethicin. Biophysical Journal *33*, 373–381.

Hansen, S.B., Tao, X., and MacKinnon, R. (2011). Structural basis of PIP2 activation of the classical inward rectifier K^+ channel Kir2.2. Nature *477*, 495–498.

Harada, A., Yagi, H., Saito, A., Azakami, H., and Kato, A. (2007). Relationship between the stability of hen egg-white lysozymes mutated at sites designed to interact with alpha-helix dipoles and their secretion amounts in yeast. Biosci. Biotechnol. Biochem. *71*, 2952–2961.

Harp, J.M., Hanson, B.L., Timm, D.E., and Bunick, G.J. (2000). Asymmetries in the nucleosome core particle at 2.5 A resolution. Acta Crystallogr. D Biol. Crystallogr. *56*, 1513–1534.

Heginbotham, L., Abramson, T., and MacKinnon, R. (1992). Functional Connection Between the Pores of Distantly Related Ion Channels as Revealed by Mutant K^+ Channels. Science *258*, 1152–1155.

Heginbotham, L., and MacKinnon, R. (1993). Conduction properties of the cloned Shaker K+ channel. Biophysical Journal *65*, 2089–2096.

Heginbotham, L., LeMasurier, M., Kolmakova-Partensky, L., and Miller, C. (1999). Single Streptomyces lividans k+ channels. The Journal of General Physiology *114*, 551.

Heginbotham, L., Lu, Z., Abramson, T., and MacKinnon, R. (1994). Mutations in the K^+ channel signature sequence. Biophysical Journal *66*, 1061–1067.

Heginbotham, L., Odessey, E., and Miller, C. (1997). Tetrameric stoichiometry of a prokaryotic K^+ channel. Biochemistry *36*, 10335–10342.

Hille, B. (1973). Potassium channels in myelinated nerve. Selective permeability to small cations. The Journal of General Physiology *61*, 669–686.

Hille, B. (2001). Ionic channels of excitable membranes (Sinauer Associates).

Hodgkin, A.L., and Huxley, A.F. (1952a). Currents carried by sodium and potassium ions through the membrane of the giant axon of Loligo. J. Physiol. (Lond.) *116*, 449–472.

Hodgkin, A.L., and Huxley, A.F. (1952b). The components of membrane conductance in the giant axon of Loligo. J. Physiol. (Lond.) *116*, 473–496.

Hodgkin, A.L., and Huxley, A.F. (1952c). The dual effect of membrane potential on sodium conductance in the giant axon of Loligo. J. Physiol. (Lond.) *116*, 497–506.

Hodgkin, A.L., and Keynes, R. (1955). The Potassium Permeability of a Giant Nerve Fibre. J. Physiol. (Lond.) *128*, 61–88.

Hodgkin, A.L., Huxley, A.F., and Katz, B. (1952). Measurement of current-voltage relations in the membrane of the giant axon of Loligo. J. Physiol. (Lond.) *116*, 424–448.

Hol, W.G. (1985). The role of the alpha-helix dipole in protein function and structure. Prog Biophys Mol Biol *45*, 149–195.

Hol, W.G., Halie, L., and Sander, C. (1981). Dipoles of the Alpha-Helix and Beta-Sheet - Their Role in Protein Folding. Nature *294*, 532–536.

Hol, W.G., van Duijnen, P.T., and Berendsen, H.J. (1978). The alpha-helix dipole and the properties of proteins. Nature *273*, 443–446.

Horne, W.S., Yadav, M.K., Stout, C.D., and Ghadiri, M.R. (2004). Heterocyclic peptide backbone modifications in an alpha-helical coiled coil. J. Am. Chem. Soc. *126*, 15366–15367.

Huang, K.S., Bayley, H., Liao, M.J., London, E., and Khorana, H.G. (1981). Refolding of an integral membrane protein. Denaturation, renaturation, and reconstitution of intact bacteriorhodopsin and two proteolytic fragments. The Journal of Biological Chemistry *256*, 3802–3809.

Hunte, C., and Richers, S. (2008). Lipids and membrane protein structures. Curr Opin Struc Biol *18*, 406–411.

Huyghues-Despointes, B., Scholtz, J., and Baldwin, R.L. (1993). Effect of a Single Aspartate on Helix Stability at Different Positions in a Neutral Alanine-Based Peptide. Protein Sci *2*, 1604–1611.

Imai, Y.N., Ryu, S., and Oiki, S. (2009). Docking Model of Drug Binding to the Human Ether-a-go-go Potassium Channel Guided by Tandem Dimer Mutant Patch-Clamp Data: A Synergic Approach. J Med Chem *52*, 1630–1638.

Ingwall, R.T., and Goodman, M. (1974). Polydepsipeptides. III. Theoretical conformational analysis of randomly coiling and ordered depsipeptide chains. Macromolecules *7*, 598–605.

Irizarry, S.N., Kutluay, E., Drews, G., Hart, S.J., and Heginbotham, L. (2002). Opening the KcsA K^+ channel: tryptophan scanning and complementation analysis lead to mutants with altered gating. Biochemistry *41*, 13653–13662.

Iwamoto, T., Grove, A., Montal, M.O., Montal, M., and Tomich, J.M. (1994). Chemical synthesis and characterization of peptides and oligomeric proteins designed to form transmembrane ion channels. International Journal of Peptide and Protein Research *43*, 597–607.

Jensen, M.O., Borhani, D.W., Lindorff-Larsen, K., Maragakis, P., Jogini, V., Eastwood, M.P., Dror, R.O., and Shaw, D.E. (2010). Principles of conduction and hydrophobic gating in K^+ channels. Proceedings of the National Academy of Sciences of the United States of America *107*, 5833–5838.

Jiang, Y., and MacKinnon, R. (2000). The barium site in a potassium channel by X-ray crystallography. The Journal of General Physiology *115*, 269–272.

Jiang, Y., Lee, A., Chen, J., Cadene, M., Chait, B.T., and MacKinnon, R. (2002a). Crystal structure and mechanism of a calcium-gated potassium channel. Nature *417*, 515–522.

Jiang, Y., Lee, A., Chen, J., Cadene, M., Chait, B.T., and MacKinnon, R. (2002b). The open pore conformation of potassium channels. Nature *417*, 523–526.

Jiang, Y., Lee, A., Chen, J., Ruta, V., Cadene, M., Chait, B.T., and MacKinnon, R. (2003a). X-ray structure of a voltage-dependent K^+ channel. Nature *423*, 33–41.

Jiang, Y., Ruta, V., Chen, J., Lee, A., and MacKinnon, R. (2003b). The principle of gating charge movement in a voltage-dependent K^+ channel. Nature *423*, 42–48.

Kamiya, K., Niwa, R., Mitcheson, J., and Sanguinetti, M. (2006). Molecular determinants of hERG channel block. Mol. Pharmacol. *69*, 1709–1716.

Kawakami, T., and Aimoto, S. (2003). A photoremovable ligation auxiliary for use in polypeptide synthesis. Tetrahedron Lett *44*, 6059–6061.

Kent, S. (1988). Chemical synthesis of peptides and proteins. Annual Review of Biochemistry *57*, 957–989.

Kent, S.B.H. (2009). Total chemical synthesis of proteins. Chem Soc Rev *38*, 338–351.

Knopfel, T., Diez-Garcia, J., and Akemann, W. (2006). Optical probing of neuronal circuit dynamics: genetically encoded versus classical fluorescent sensors. Trends Neurosci *29*, 160–166.

Kochendoerfer, G.G., Salom, D., Lear, J.D., Wilk-Orescan, R., Kent, S.B., and DeGrado, W.F. (1999). Total chemical synthesis of the integral membrane protein influenza A virus M2: role of its C-terminal domain in tetramer assembly. Biochemistry *38*, 11905–11913.

Koh, J.T., Cornish, V.W., and Schultz, P.G. (1997). An experimental approach to evaluating the role of backbone interactions in proteins using unnatural amino acid mutagenesis. Biochemistry *36*, 11314–11322.

Komarov, A.G., Linn, K.M., Devereaux, J.J., and Valiyaveetil, F.I. (2009a). Modular Strategy for the Semisynthesis of a K^+ Channel: Investigating Interactions of the Pore Helix. ACS Chemical Biology *4*, 1029–1038.

Komarov, A.G., Linn, K.M., Devereaux, J.J., and Valiyaveetil, F.I. (2009b). Semisynthesis of K^+ channels. Methods in Enzymology *462*, 135–150.

Krishnan, M.N., Trombley, P., and Moczydlowski, E.G. (2008). Thermal Stability of the K^+ Channel Tetramer: Cation Interactions and the Conserved Threonine Residue at the Innermost Site (S4) of the KcsA Selectivity Filter. Biochemistry *47*, 5354–5367.

Kutluay, E., Roux, B., and Heginbotham, L. (2005). Rapid Intracellular TEA Block of the KcsA Potassium Channel. Biophysical Journal *88*, 1018–1029.

Lah, M.S., Palfey, B.A., Schreuder, H.A., and Ludwig, M.L. (1994). Crystal structures of mutant Pseudomonas aeruginosa p-hydroxybenzoate hydroxylases: the Tyr201Phe, Tyr385Phe, and Asn300Asp variants. Biochemistry *33*, 1555–1564.

Lee, J.Y., and Bang, D. (2010). Challenges in the chemical synthesis of average sized proteins: Sequential vs. convergent ligation of multiple peptide fragments. Peptide Science *94*, 441–447.

LeMasurier, M., Heginbotham, L., and Miller, C. (2001). KcsA: It's a potassium channel. J Gen Physiol *118*, 303–314.

Lenaeus, M.J., Vamvouka, M., Focia, P.J., and Gross, A. (2005). Structural basis of TEA blockade in a model potassium channel. Nat Struct Mol Biol *12*, 454–459.

Li, W., and Aldrich, R. (2004). Unique inner pore properties of BK channels revealed by quaternary ammonium block. J Gen Physiol *124*, 43–57.

Linn, K.M., Derebe, M.G., Jiang, Y., and Valiyaveetil, F.I. (2010). Semisynthesis of NaK, a Na^+ and K^+ conducting ion channel. Biochemistry *49*, 4450–4456.

Liu, Y., Holmgren, M., Jurman, M.E., and Yellen, G. (1997). Gated access to the pore of a voltage-dependent K^+ channel. Neuron *19*, 175–184.

Lockhart, D.J., and Kim, P.S. (1992). Internal stark effect measurement of the electric field at the amino terminus of an alpha helix. Science *257*, 947–951.

Lockhart, D.J., and Kim, P.S. (1993). Electrostatic screening of charge and dipole interactions with the helix backbone. Science *260*, 198–202.

Lockless, S.W., Zhou, M., and MacKinnon, R. (2007). Structural and thermodynamic properties of selective ion binding in a K^+ channel. PLoS Biol. *5*, e121.

Lodi, P.J., and Knowles, J.R. (1993). Direct evidence for the exploitation of an alpha-helix in the catalytic mechanism of triosephosphate isomerase. Biochemistry *32*, 4338–4343.

Long, S.B., Tao, X., Campbell, E.B., and MacKinnon, R. (2007). Atomic structure of a voltage-dependent K^+ channel in a lipid membrane-like environment. Nature *450*, 376–382.

Lu, T., Ting, A.Y., Mainland, J., Jan, L.Y., Schultz, P.G., and Yang, J. (2001). Probing ion permeation and gating in a K^+ channel with backbone mutations in the selectivity filter. Nat Neurosci *4*, 239–246.

Lu, W., Qasim, M.A., Laskowski, M., and Kent, S.B. (1997). Probing intermolecular main chain hydrogen bonding in serine proteinase-protein inhibitor complexes: chemical synthesis of backbone-engineered turkey ovomucoid third domain. Biochemistry *36*, 673–679.

Luescher, C., and Slesinger, P.A. (2010). Emerging roles for G protein-gated inwardly rectifying potassium (GIRK) channels in health and disease. Nat. Rev. Neurosci. *11*, 301–315.

Luzhkov, V., and Aqvist, J. (2001). K^+/Na^+ selectivity of the KcsA potassium channel from microscopic free energy perturbation calculations. Bba-Protein Struct M *1548*, 194–202.

Ma, J.C., and Dougherty, D.A. (1997). The Cation-pi Interaction. Chemical Reviews *97*, 1303–1324.

MacKinnon, R. (1991). Determination of the subunit stoichiometry of a voltage-activated potassium channel. Nature *350*, 232–235.

MacKinnon, R., and Yellen, G. (1990). Mutations Affecting TEA Blockade and Ion Channel Permeation in Voltage-Activated K^+ Channels. Science *250*, 276–279.

MacKinnon, R., Cohen, S.L., Kuo, A., Lee, A., and Chait, B.T. (1998). Structural conservation in prokaryotic and eukaryotic potassium channels. Science *280*, 106.

Mashl, R., Tang, Y., Schnitzer, J., and Jakobsson, E. (2001). Hierarchical approach to predicting permeation in ion channels. Biophysical Journal *81*, 2473–2483.

McDermott, A. (2009). Structure and Dynamics of Membrane Proteins by Magic Angle Spinning Solid-State NMR. Ann Rev Biophys *38*, 385–403.

Mehler, E. (1980). *Ab initio*, Quantum Chemical-Analysis of Non-Covalent Interactions Between Peptides as Modeled by Dimers and a Trimer of Formamide. J Am Chem Soc *102*, 4051–4056.

Menard, R., Plouffe, C., Laflamme, P., Vernet, T., Tessier, D., Thomas, D., and Storer, A. (1995). Modification of the Electrostatic Environment Is Tolerated in the Oxyanion Hole of the Cysteine Protease Papain. Biochemistry *34*, 464–471.

Meuser, D., Splitt, H., Wagner, R., and Schrempf, H. (1999). Exploring the open pore of the potassium channel from *Streptomyces lividans*. FEBS Lett *462*, 447–452.

Miesenböck, G. (2011). Optogenetic control of cells and circuits. Annu. Rev. Cell Dev. Biol. *27*, 731–758.

Miller, A.N., and Long, S.B. (2012). Crystal Structure of the Human Two-Pore Domain Potassium Channel K2P1. Science *335*, 432–436.

Miller, C. (2000). An overview of the potassium channel family. Genome Biol.

Minor, D.L.J. (2007). The neurobiologist's guide to structural biology: A primer on why macromolecular structure matters and how to evaluate structural data. Neuron *54*, 511–533.

Miranda, J.J.L. (2003). Position-dependent interactions between cysteine residues and the helix dipole. Protein Sci *12*, 73–81.

Mitchell, D.C. (2012). Progress in understanding the role of lipids in membrane protein folding. Biochim. Biophys. Acta *1818*, 951–956.

Montal, M.O., Iwamoto, T., Tomich, J.M., and Montal, M. (1993). Design, synthesis and functional characterization of a pentameric channel protein that mimics the presumed pore structure of the nicotinic cholinergic receptor. FEBS Lett *320*, 261–266.

Morais-Cabral, J.H., Zhou, Y., and MacKinnon, R. (2001). Energetic optimization of ion conduction rate by the K^+ selectivity filter. Nature *414*, 37–42.

Muir, T.W. (2003). Semisynthesis of proteins by expressed protein ligation. Annu Rev Biochem *72*, 249–289.

Muir, T.W., Sondhi, D., and Cole, P.A. (1998). Expressed protein ligation: a general method for protein engineering. Proceedings of the National Academy of Sciences *95*, 6705–6710.

Mullins, L. (1959). The penetration of some cations into muscle. The Journal of General Physiology *42*, 817–829.

Muñoz, V., and Serrano, L. (1994). Elucidating the folding problem of helical peptides using empirical parameters. Nat Struct Biol *1*, 399–409.

Muñoz, V., and Serrano, L. (1995). Elucidating the folding problem of helical peptides using empirical parameters. II. Helix macrodipole effects and rational modification of the helical content of natural peptides. Journal of Molecular Biology *245*, 275–296.

Muralidharan, V., and Muir, T.W. (2006). Protein ligation: an enabling technology for the biophysical analysis of proteins. Nat Meth *3*, 429–438.

Neyton, J., and Miller, C. (1988a). Discrete Ba^{2+} block as a probe of ion occupancy and pore structure in the high-conductance Ca^{2+} -activated K^+ channel. The Journal of General Physiology *92*, 569–586.

Neyton, J., and Miller, C. (1988b). Potassium Blocks Barium Permeation Through a Calcium-Activated Potassium Channel. The Journal of General Physiology *92*, 549–567.

Nicholson, H., Anderson, D.E., Dao-pin, S., and Matthews, B.W. (1991). Analysis of the interaction between charged side chains and the alpha-helix dipole using designed thermostable mutants of phage T4 lysozyme. Biochemistry *30*, 9816–9828.

Nicholson, H., Becktel, W.J., and Matthews, B.W. (1988). Enhanced protein thermostability from designed mutations that interact with alpha-helix dipoles. Nature *336*, 651–656.

Noren, C., Wang, J., and Perler, F. (2000). Dissecting the Chemistry of Protein Splicing and Its Applications. Angewandte Chemie International Edition *39*, 450–466.

Noskov, S., Bernèche, S., and Roux, B. (2004). Control of ion selectivity in potassium channels by electrostatic and dynamic properties of carbonyl ligands. Nature *431*, 830–834.

Oblatt-Montal, M., Yamazaki, M., Nelson, R., and Montal, M. (1995). Formation of ion channels in lipid bilayers by a peptide with the predicted transmembrane sequence of botulinum neurotoxin A. Protein Sci *4*, 1490–1497.

Palfey, B.A., Entsch, B., Ballou, D.P., and Massey, V. (1994). Changes in the catalytic properties of p-hydroxybenzoate hydroxylase caused by the mutation Asn300Asp. Biochemistry *33*, 1545–1554.

Patching, S.G. (2011). NMR structures of polytopic integral membrane proteins. Mol. Membr. Biol. *28*, 370–397.

Paulus, H. (2000). Protein splicing and related forms of protein autoprocessing. Annual Review of Biochemistry *69*, 447–496.

Payandeh, J., Scheuer, T., Zheng, N., and Catterall, W.A. (2011). The crystal structure of a voltage-gated sodium channel. Nature *475*, 353–358.

Perry, M., de Groot, M.J., Helliwell, R., Leishman, D., Tristani-Firouzi, M., Sanguinetti, M.C., and Mitcheson, J. (2004). Structural determinants of HERG channel block by clofilium and ibutilide. Mol. Pharmacol. *66*, 240–249.

Perry, M., Stansfeld, P.J., Leaney, J., Wood, C., de Groot, M.J., Leishman, D., Sutcliffe, M.J., and Mitcheson, J.S. (2006). Drug binding interactions in the inner cavity of HERG channels: molecular insights from structure-activity relationships of clofilium and ibutilide analogs. Mol. Pharmacol. *69*, 509–519.

Perutz, M.F., Gronenborn, A.M., Clore, G.M., Fogg, J.H., and Shih, D.T. (1985). The pKa values of two histidine residues in human haemoglobin, the Bohr effect, and the dipole moments of alpha-helices. Journal of Molecular Biology *183*, 491–498.

Ploegman, J.H., Drent, G., Kalk, K.H., and Hol, W.G. (1979). The structure of bovine liver rhodanese. II. The active site in the sulfur-substituted and the sulfur-free enzyme. Journal of Molecular Biology *127*, 149–162.

Powers, E.T., Deechongkit, S., and Kelly, J.W. (2005). Backbone-Backbone H-Bonds Make Context-Dependent Contributions to Protein Folding Kinetics and Thermodynamics: Lessons from Amide-to-Ester Mutations. Adv. Protein Chem. *72*, 39–78.

Presnell, S.R., and Cohen, F.E. (1989). Topological distribution of four-alpha-helix bundles. Proceedings of the National Academy of Sciences *86*, 6592–6596.

Ranatunga, K., Shrivastava, I., Smith, G., and Sansom, M. (2001). Side-chain ionization states in a potassium channel. Biophysical Journal *80*, 1210–1219.

Raunser, S., and Walz, T. (2009). Electron Crystallography as a Technique to Study the Structure on Membrane Proteins in a Lipidic Environment. Ann Rev Biophys *38*, 89–105.

Reitz, S., Cebi, M., Reiß, P., Studnik, G., Linne, U., Koert, U., and Essen, L.-O. (2009). On the function and structure of synthetically modified porins. Angewandte Chemie International Edition *48*, 4853–4857.

Richardson, J.S., and Richardson, D.C. (1988). Amino-Acid Preferences for Specific Locations at the Ends of Alpha-Helices. Science *240*, 1648–1652.

Rogers, N.K., and Sternberg, M.J. (1984). Electrostatic interactions in globular proteins. Different dielectric models applied to the packing of alpha-helices. Journal of Molecular Biology *174*, 527–542.

Roux, B. (2005). Ion conduction and selectivity in K^+ channels. Annu Rev Biophys Biomol Struct *34*, 153–171.

Roux, B., and MacKinnon, R. (1999). The cavity and pore helices in the KcsA K^+ channel: electrostatic stabilization of monovalent cations. Science *285*, 100–102.

Sali, D., Bycroft, M., and Fersht, A.R. (1988). Stabilization of protein structure by interaction of alpha-helix dipole with a charged side chain. Nature *335*, 740–743.

Sansom, M., Shrivastava, I., Bright, J., Tate, J., Capener, C., and Biggin, P. (2002). Potassium channels: structures, models, simulations. Biochimica Et Biophysica Acta-Biomembranes *1565*, 294–307.

Sarin, V.K., Kent, S.B.H., Tam, J.P., and Merrifield, R. (1981). Quantitative monitoring of solid-phase peptide synthesis by the ninhydrin reaction. Analytical Biochemistry *117*, 147–157.

Sánchez-Chapula, J.A., Navarro-Polanco, R.A., Culberson, C., Chen, J., and Sanguinetti, M.C. (2002). Molecular determinants of voltage-dependent human ether-a-go-go related gene (HERG) K^+ channel block. The Journal of Biological Chemistry *277*, 23587–23595.

Schmidt, D., Jiang, Q.-X., and MacKinnon, R. (2006). Phospholipids and the origin of cationic gating charges in voltage sensors. Nature *444*, 775–779.

Schnölzer, M., Alewood, P., Jones, A., Alewood, D., and Kent, S.B.H. (2007). *In Situ* Neutralization in Boc-chemistry Solid Phase Peptide Synthesis. Int J Pept Res Ther *13*, 31–44.

Schrempf, H., Schmidt, O., Kummerlen, R., Hinnah, S., Muller, D., Betzler, M., Steinkamp, T., and Wagner, R. (1995). A prokaryotic potassium ion channel with two predicted transmembrane segments from *Streptomyces lividans*. Embo J *14*, 5170–5178.

Schumaker, M.F., and MacKinnon, R. (1990). A simple model for multi-ion permeation. Single-vacancy conduction in a simple pore model. Biophys. J. *58*, 975–984.

Sengupta, D., Behera, R.N., Smith, J.C., and Ullmann, G.M. (2005). The alpha helix dipole: screened out? Structure *13*, 849–855.

Serrano, L., and Fersht, A.R. (1989). Capping and alpha-helix stability. Nature *342*, 296–299.

Sheridan, R.P., and Allen, L.C. (1980). The electrostatic potential of the alpha helix (electrostatic potential/alpha-helix/secondary structure/helix dipole). Biophys. Chem. *11*, 133–136.

Sheridan, R.P., Levy, R.M., and Salemme, F.R. (1982). alpha-Helix dipole model and electrostatic stabilization of 4-alpha-helical proteins. Proceedings of the National Academy of Sciences *79*, 4545–4549.

Shi, N., Ye, S., Alam, A., Chen, L., and Jiang, Y. (2006). Atomic structure of a Na^+- and K^+-conducting channel. Nature *440*, 570–574.

Shoemaker, K.R., Kim, P.S., York, E.J., Stewart, J.M., and Baldwin, R.L. (1987). Tests of the helix dipole model for stabilization of alpha-helices. Nature *326*, 563–567.

Söderberg, B.O., Sjöberg, B.M., Sonnerstam, U., and Brändén, C.I. (1978). Three-dimensional structure of thioredoxin induced by bacteriophage T4. Proceedings of the National Academy of Sciences *75*, 5827–5830.

Suessbrich, H., Schönherr, R., Heinemann, S.H., Lang, F., and Busch, A.E. (1997). Specific block of cloned *Herg* channels by clofilium and its tertiary analog LY97241. FEBS Lett *414*, 435–438.

Swenson, R. (1981). Inactivation of potassium current in squid axon by a variety of quaternary ammonium ions. The Journal of General Physiology *77*, 255.

Tao, X., Lee, A., Limapichat, W., Dougherty, D.A., and MacKinnon, R. (2010). A gating charge transfer center in voltage sensors. Science *328*, 67–73.

Tasaki, I., and Hagiwara, S. (1957). Demonstration of 2 Stable Potential States in the Squid Giant Axon Under Tetraethylammonium Chloride. J Gen Physiol *40*, 859–885.

Tate, C.G. (2001). Overexpression of mammalian integral membrane proteins for structural studies. FEBS Lett *504*, 94–98.

Trauner, D. (2008). Introduction: Chemical Approaches to Neurobiology. Chemical Reviews *108*, 1499–1500.

Uysal, S., Vásquez, V., Tereshko, V., Esaki, K., Fellouse, F.A., Sidhu, S.S., Koide, S., Perozo, E., and Kossiakoff, A. (2009). Crystal structure of full-length KcsA in its closed conformation. Proceedings of the National Academy of Sciences of the United States of America *106*, 6644–6649.

Valiyaveetil, F.I., Leonetti, M., Muir, T.W., and MacKinnon, R. (2006a). Ion Selectivity in a Semisynthetic K^+ Channel Locked in the Conductive Conformation. Science *314*, 1004–1007.

Valiyaveetil, F.I., MacKinnon, R., and Muir, T.W. (2002a). Semisynthesis and Folding of the Potassium Channel KcsA. J. Am. Chem. Soc. *124*, 9113–9120.

Valiyaveetil, F.I., Sekedat, M., MacKinnon, R., and Muir, T.W. (2006b). Structural and Functional Consequences of an Amide-to-Ester Substitution in the Selectivity Filter of a Potassium Channel. J Am Chem Soc *128*, 11591–11599.

Valiyaveetil, F.I., Sekedat, M., Muir, T.W., and MacKinnon, R. (2004a). Semisynthesis of a Functional K^+ Channel. Angew. Chem. *116*, 2558–2561.

Valiyaveetil, F.I., Sekedat, M.D., MacKinnon, R., and Muir, T.W. (2004b). Glycine as a D-amino acid surrogate in the K^+-selectivity filter. Proceedings of the National Academy of Sciences *101*, 17045–17049.

Valiyaveetil, F.I., Zhou, Y., and MacKinnon, R. (2002b). Lipids in the Structure, Folding, and Function of the KcsA K^+ Channel. Biochemistry *41*, 10771–10777.

van Duijnen, P.T., Thole, B.T., and Hol, W.G. (1979). On the role of the active site helix in papain, an *ab initio* molecular orbital study. Biophys. Chem. *9*, 273–280.

VanDriessche, G., Koh, M., Chen, Z., Mathews, F., Meyer, T., Bartsch, R., Cusanovich, M., and VanBeeumen, J. (1996). Covalent structure of the flavoprotein subunit of the flavocytochrome c: Sulfide dehydrogenase from the purple phototrophic bacterium Chromatium vinosum. Protein Sci *5*, 1753–1764.

Vergara, C., Alvarez, O., and Latorre, R. (1999). Localization of the K^+ Lock-In and the $Ba2^+$ binding sites in a voltage-gated calcium-modulated channel. Implications for survival of K^+ permeability. The Journal of General Physiology *114*, 365–376.

Vila-Perello, M., and Muir, T.W. (2010). Biological Applications of Protein Splicing. Cell *143*, 191–200.

Wada, A. (1976). The alpha-helix as an electric macro-dipole. Advances in Biophysics *9*, 1–63.

Wang, L., and Schultz, P. (2005). Expanding the genetic code. Angewandte Chemie International Edition *44*, 34–66.

Warwicker, J., and Watson, H.C. (1982). Calculation of the electric potential in the active site cleft due to alpha-helix dipoles. Journal of Molecular Biology *157*, 671–679.

Wiberg, K., and Laidig, K. (1987). Barriers to Rotation Adjacent to Double-Bonds .3. the C-O Barrier in Formic-Acid, Methyl Formate, Acetic-Acid, and Methyl Acetate - the Origin of Ester and Amide Resonance. J Am Chem Soc *109*, 5935–5943.

Witchel, H.J., Dempsey, C.E., Sessions, R.B., Perry, M., Milnes, J.T., Hancox, J.C., and Mitcheson, J.S. (2004). The low-potency, voltage-dependent HERG blocker propafenone--molecular determinants and drug trapping. Mol. Pharmacol. *66*, 1201–1212.

Wu, B., and Davey, C.A. (2010). Using Soft X-Rays for a Detailed Picture of Divalent Metal Binding in the Nucleosome. Journal of Molecular Biology *398*, 633–640.

Ye, S., Huber, T., Vogel, R., and Sakmar, T.P. (2009). FTIR analysis of GPCR activation using azido probes. Nat Meth *5*, 397–399.

Yellen, G. (1984a). Ionic permeation and blockade in Ca2+-activated K+ channels of bovine chromaffin cells. The Journal of General Physiology *84*, 157–186.

Yellen, G. (1984b). Relief of Na+ block of Ca2+-activated K+ channels by external cations. The Journal of General Physiology *84*, 187–199.

Yellen, G. (2002). The voltage-gated potassium channels and their relatives. Nature *419*, 35–42.

Yellen, G., Jurman, M., Abramson, T., and MacKinnon, R. (1989). Mutations Affecting Internal TEA Blockade Identify the Probable Pore-Forming Region of a K+ Channel. Biol Chem.

Yellen, G., Jurman, M.E., Abramson, T., and MacKinnon, R. (1991). Mutations affecting internal TEA blockade identify the probable pore-forming region of a K+ channel. Science *251*, 939–942.

Yohannan, S., Hu, Y., and Zhou, Y. (2007). Crystallographic Study of the Tetrabutylammonium Block to the KcsA K^+ Channel. Journal of Molecular Biology *366*, 806–814.

Zamponi, G.W., Doyle, D.D., and French, R.J. (1993). Fast lidocaine block of cardiac and skeletal muscle sodium channels: one site with two routes of access. Biophysical Journal *65*, 80–90.

Zhang, Q., Zhou, Y.-F., Zhang, C.-Z., Zhang, X., Lu, C., and Springer, T.A. (2009). Structural specializations of A2, a force-sensing domain in the ultralarge vascular protein von Willebrand factor. Proceedings of the National Academy of Sciences of the United States of America *106*, 9226–9231.

Zhou, H., Chepilko, S., Schütt, W., Choe, H., Palmer, L.G., and Sackin, H. (1996). Mutations in the pore region of ROMK enhance Ba^{2+} block. Am. J. Physiol. *271*, C1949–C1956.

Zhou, M., and al, E. (2004). A Mutant KcsA K+ Channel with Altered Conduction Properties and Selectivity Filter Ion Distribution. Journal of Molecular Biology *338*, 839–846.

Zhou, M., Morais-Cabral, J.H., Mann, S., and MacKinnon, R. (2001a). Potassium channel receptor site for the inactivation gate and quaternary amine inhibitors. Nature *411*, 657–661.

Zhou, M., Morgner, N., Barrera, N.P., Politis, A., Isaacson, S.C., Matak-Vinković, D., Murata, T., Bernal, R.A., Stock, D., and Robinson, C.V. (2011a). Mass spectrometry of intact V-type ATPases reveals bound lipids and the effects of nucleotide binding. Science *334*, 380–385.

Zhou, Y., and MacKinnon, R. (2003). The Occupancy of Ions in the K^+ Selectivity Filter: Charge Balance and Coupling of Ion Binding to a Protein Conformational Change Underlie High Conduction Rates. Journal of Molecular Biology *333*, 965–975.

Zhou, Y., and MacKinnon, R. (2004). Ion Binding Affinity in the Cavity of the KcsA Potassium Channel. Biochemistry *43*, 4978–4982.

Zhou, Y., Morais-Cabral, J.H., Kaufman, A., and MacKinnon, R. (2001b). Chemistry of ion coordination and hydration revealed by a K^+ channel-Fab complex at 2.0 Å resolution. Nature *414*, 43–48.

Zhou, Y., Xia, X.-M., and Lingle, C.J. (2011b). Cysteine scanning and modification reveal major differences between BK channels and Kv channels in the inner pore region. Proceedings of the National Academy of Sciences of the United States of America *108*, 12161–12166.